Université de Sherbrooke

Positron Emission Tomography (PET) for the early detection of sunitinib-induced cardiotoxicity

Written by
Gisela Marrero Cofino
Department of Nuclear Medicine and Radiobiology

Master's thesis presented to the Faculty of Medicine and Health Sciences
in view of obtaining a Master of Science (M.Sc) in
Nuclear Medicine and Radiobiology

Sherbrooke, Québec, Canada
December 2014

Members of the Jury
Dr. Roger Lecomte, Department of Nuclear Medicine and Radiobiology
Dr. Éric Turcotte, Department of Nuclear Medicine and Radiobiology
Dr. Benoit Paquette, Department of Nuclear Medicine and Radiobiology
Dr. Sheela Ramanathan, Department of Pediatrics

RÉSUMÉ

Le sunitinib est un inhibiteur de tyrosine kinase qui est utilisée comme agent anticancéreux. Bien que l'utilisation clinique du sunitinib représente une percée significative pour le traitement de certains cancers, ce médicament s'avère cardiotoxique chez plusieurs patients, une situation qui est problématique. Le sunitinib peut provoquer une hypertension, des arythmies, une chute de la fraction d'éjection ventriculaire gauche et une insuffisance cardiaque congestive qui peut être fatale. Le mécanisme responsable de la cardiotoxicité de sunitinib n'est pas encore bien compris. Comme plusieurs autres inhibiteurs des récepteurs de la tyrosine kinase, il se lie à un grand nombre de kinases et peut affecter de nombreux processus cellulaires. *In vivo*, les mécanismes responsables de la toxicité sont complexes et imprévisibles et une insuffisance cardiaque est parfois observée tôt pendant le traitement. La séquence des évènements menant à l'apparition d'une dysfonction cardiaque pendant le traitement n'est pas connue. Cela pose un problème important pour le diagnostic de complications cardiovasculaires avant qu'elles ne deviennent symptomatiques. Une identification précoce de ces événements néfastes serait très bénéfique pour le suivi du traitement au sunitinib. La tomographie d'émission par positrons (TEP) est une méthode reconnue pour l'évaluation du métabolisme et de la fonctionnalité du myocarde. Selon notre hypothèse de travail, une insuffisance cardiaque peut survenir rapidement pendant le traitement au sunitinib, elle est l'expression d'altérations structurelles et métaboliques au niveau du myocarde; ces modifications se produisent tôt pendant le traitement. Nous avons effectué une étude pour évaluer la faisabilité d'utiliser l'imagerie TEP pour la détection précoce de la cardiotoxicité induite par le sunitinib. La première étape a été de développer un modèle de cardiotoxicité chez des souris. L'induction de la cardiotoxicité s'est faite par administration orale pour une période de quatre semaines, soit de sunitinib 80mg/Kg/jour ou d'eau pour les souris contrôles. Le suivi inclut la mesure de la pression sanguine, l'évaluation des altérations biochimiques, l'expression de certains gènes et un examen histologique du myocarde. Un suivi par imagerie TEP a été effectué chaque semaine avec du ^{11}C-acétate et du ^{18}F-FDG afin d'évaluer le flux sanguin myocardique (MBF), le métabolisme oxydatif du myocarde incluant la consommation d'oxygène (MVO2), l'absorption du glucose (K_i), le taux métabolique oxydatif du glucose (MMRG) ainsi que la fraction d'éjection ventriculaire gauche (FEVG). Les résultats que nous avons obtenus par histopathologie, immunocoloration et microscopie électronique montrent que notre modèle est capable d'induire une cardiotoxicité. Nous avons également observé des évidences d'inflammation et de remodelage tissulaire à partir de l'étude de l'expression de certains gènes et de l'analyse de l'accumulation de collagène. Nous n'avons pas observé d'hypertension ni de lésions rénales. La TEP avec ^{18}FDG a montré une diminution rapide de la FEVG, une indication d'une dysfonction cardiaque qui a été classée comme insuffisance cardiaque de grade 2 à la fin de l'étude. Cependant, aucun signe de modifications du métabolisme cardiaque n'a été mis en évidence par TEP/^{18}FDG- ou TEP/^{11}C-acétate. Nos résultats laissent penser que l'apparition de la dysfonction contractile induite par sunitinib peut se produire en l'absence d'hypertension ou de dommages métaboliques manifestes. De nouvelles études avec des traitements plus longs permettraient peut être de mieux définir le début de la cardiotoxicité métabolique.

Mots-clés: Tomographie d'émission par positrons, sunitinib, cardiotoxicité, FEVG.

ABSTRACT

Sunitinib (Sutent®) is a multitargeted, small molecule receptor tyrosine kinase inhibitor used as an anti-cancer drug. It has increased the overall survival rate of metastatic renal cell carcinoma patients as well as the survival time of patients with pancreatic neuroendocrine tumors. Although the clinical use of sunitinib is a significant leap forward in the therapy of those cancers, its induction of cardiac toxicity in a substantial fraction of patients remains a critical problem. Sunitinib may cause hypertension, arrhythmias, drop of the left ventricular ejection fraction and congestive heart failure, fatal in some cases. These side effects are a frequent reason for interruption of its use. The mechanism(s) underlying sunitinib cardiotoxicity are not fully understood. Similar to other receptor tyrosine kinase inhibitors, it binds to a large number of cellular kinases, thus it can affect multiple cellular processes. *In vivo*, the pattern of toxicity is complex and unpredictable, with symptomatic heart failure sometimes observed early during treatment. The pattern of events preceding the onset of symptomatic cardiac dysfunction during treatment is not established. This represents a significant problem for the clinical diagnosis of cardiovascular complications before they become symptomatic. The identification and early detection of those events would be highly-beneficial for the clinical management of anti-cancer therapy with sunitinib.

Positron Emission Tomography (PET) is recognized for its ability to probe metabolic and functional aspects of myocardial function. Under the working concept that heart failure can occur early during sunitinib treatment, and may be sustained by early myocardial metabolic and structural alterations, we performed a study with the objective of assessing the use of PET for the early detection of sunitinib-induced cardiotoxicity. For this, we established a model of cardiotoxicity in C57BL/6 male mice given 80mg/Kg/day of sunitinib or water, orally for 4 weeks. General and cardiac toxicity were monitored by biochemical, microscopical (H&E, immunofluorescence and electron microscopy) as well as gene expression analyses and blood pressure measurements. PET scans were performed weekly using ^{11}C-acetate and ^{18}F-FDG to evaluated the myocardial blood flow (MBF), myocardial oxidative metabolism through the quantification of oxygen consumption (MVO_2), glucose uptake (K_i), myocardial metabolic rate of glucose (MMRG) and the left ventricular ejection fractions (LVEF).

We found that sunitibib was cardiotoxic as revealed by histopathology, immunostaining and electron microscopy. Signs of inflammation and tissue remodeling were found by gene expression analyses and collagen staining. No hypertension or renal damage were detected on the study. FDG-PET revealed an early decrease of the LVEF, indicative of cardiac dysfunction, which developed into grade-2 heart failure by the end of the study. However, no signs of alterations in cardiac metabolism were uncovered by FDG- or ^{11}C-acetate-PET. Our results hint that the onset of sunitinib-induced contractile dysfunction may occur in the absence of hypertension or overt metabolic damage and call for further studies with longer treatments to clearly mark the onset of metabolic cardiotoxicity.

Keywords: Positron emission tomography, sunitinib, cardiotoxicity, LVEF.

TABLE OF CONTENTS

LIST OF TABLES

LIST OF FIGURES

LIST OF ABBREVIATIONS

- AMPK: AMP-activated protein kinase
- ATP: Adenosine tri-phosphate
- C_{glu}: Mean plasma glucose
- cDNA: Reverse-transcribed complementary DNA
- CSF-1R: Colony-stimulating factor receptor type 1
- DAPI: 4',6-diamidino-2-phenylindole
- ECG: Echocardiogram
- EGFR: Epidermal growth factor receptors
- FDA: Food and drug administration
- FDG: 2-deoxy-2-[^{18}F]fluoro-D-glucose
- FGFR: Fibroblast growth factor receptors
- FOV: Field of view
- FLT3: Fms-like tyrosine kinase-3
- GB-PBS: 5% normal goat serum/0.5% bovine serum albumin in PBS
- H&E: Hematoxylin and eosin stain
- IGFR: Insulin-like growth factor receptor
- keV: Kilo electron volts
- K_i: FDG uptake constant
- KIT: Stem cell factor receptor
- LC: Lumped constant
- LV: Left ventricle
- LVEF: Left ventricular ejection fraction
- MET: Hepatocyte growth factor receptor
- MLEM: Maximum-likelihood expectation maximization
- MBF: Myocardial blood flow
- MMRG: Myocardial metabolic rate of glucose
- MPO-1: Myeloperoxidase-1
- MVO_2: Myocardial oxygen consumption
- N-K-ATPase: Sodium-potassium adenosine triphosphatase
- NO: Nitric oxide
- OCT: Optimal cutting temperature compound
- PBS: Phosphate-buffered saline
- PDGFRα and PDGFRβ: Platelet-derived growth factor receptors α and β
- PET: Positron emission tomography
- qPCR: Quantitative Polymerase Chain Reaction
- QTc: Corrected QT interval
- RCC: Renal cell carcinoma
- ROI: Regions of interest
- ROS: Reactive oxygen species
- RTK: Receptor tyrosine kinases
- SERCA2A: Sarco(endo)plasmic reticulum Ca^{2+}-ATPase
- SPECT: Single photon emission computed tomography
- T_3: Triiodothyronine

- TCA: Tricarboxylic acids cycle
- VEGFR1, VEGFR2 and VEGFR3: Vascular endothelial growth factor receptor 1, 2 and 3

1. INTRODUCTION

1.1. Sunitinib in the treatment of cancer

Receptor tyrosine kinases (RTK) are ubiquitous molecules that play multiple important roles in growth factor signaling (Schlessinger, 2014). The vast majority of RTK are formed by extracellular ligand-binding, trans-membrane and intracellular tyrosine kinase domains (Schlessinger, 2014). Normally, their cellular expression and activity are tightly controlled to ensure proper cellular homeostasis; however, deregulation of RTK function is a common occurrence in many types of human cancers (Schlessinger, 2014). Deregulation of RTK function may occur *via* several mechanisms including gain-of-function mutations, overexpression of the RTK or their ligands, abnormal autocrine or paracrine stimulation and chromosomal rearrangements leading to persistent activation of their function (Takeuchi and Ito, 2011). Aberrant stimulation of RTK function is largely of an oncogenic nature since almost invariably, it promotes survival and/or proliferation of tumor cells. Examples of RTK frequently altered or deregulated in cancer are the vascular endothelial growth factor receptors (VEGFR), epidermal growth factor receptors (EGFR), hepatocyte growth factor receptor (MET), fibroblast growth factor receptors (FGFR) and insulin-like growth factor receptor (IGFR) (Takeuchi and Ito, 2011).

Given their involvement in the development of malignancies, RTK have attracted a strong interest as targets in anti-cancer therapies and they currently account for approximately 20% of all drug discovery effort (Eschenhagen et al., 2011). Both, monoclonal antibodies (*eg*., trastuzumab and pertuzumab) and multiple small molecule compounds that interfere

with RTK function have been developed and are currently either in clinical use or in trials (Zhang et al., 2009). Most small molecule RTK inhibitors developed so far are ATP competitors (type 1 inhibitors), which recognize the active form of the kinase (Zhang et al., 2009). In contrast, type 2 inhibitors bind to the inactive conformation of the RTK, allosteric inhibitors bind outside the ATP-binding site and covalent inhibitors bind irreversibly to the active site, inactivating the kinase (Zhang et al., 2009).

Sunitinib malate (N-[2-(diethylamino)ethyl]-5-[(Z)-(5-fluoro-1,2-dihydro-2-oxo-3H-indol-3-ylidine)methyl]-2,4-dimethyl-1H-pyrrole-3-carboxamide), commercialized as Sutent by Pfizer, Inc. (New York) is a multitargeted, small molecule RTK type 1 inhibitor. It targets vascular endothelial growth factor receptors (VEGFR1, VEGFR2, and VEGFR3), platelet-derived growth factor receptors (PDGFRα and PDGFRβ), colony-stimulating factor receptor type 1 (CSF-1R), Fms-like tyrosine kinase-3 (FLT3) and stem cell factor receptor (KIT) (Mellor et al., 2011).

In January 2006, Sutent received accelerated approval from the FDA to be used in the treatment of metastatic renal cell carcinoma (RCC) patients and full approval for the treatment of gastrointestinal stromal tumor after disease progression on or intolerance to imatinib mesylate (Gleevec) (Goodman et al., 2007; Rock et al., 2007). Later on 2011, sunitinib was approved to treat progressive well-differentiated pancreatic neuroendocrine tumors in patients with unresectable, locally advanced, or metastatic disease (Raymond et al., 2011). In Canada, it was first approved by Health Canada in 2006 for the treatment of gastrointestinal stromal tumors (Health Canada, 2007).

Sunitinib is administered orally, typically in doses of 50 mg/day following cycles of 4 weeks-on/2 weeks-off treatment (Speed et al., 2012; http://www.sutent.com). It is used in the treatment of RCC, with response rates of 47% (Neuhaus et al., 2014). Before the advent of sunitinib, prognosis of RCC patients was poor; at time of diagnosis, 20% of patients presented a metastatic state with a median survival of 16 months and a 5-years survival rate lower than 10% (Neuhaus et al., 2014). The introduction of sunitinib has increased the overall survival rate in RCC patients to over two years (Motzer et al., 2009). In a recent study, progression-free survival time of patients with pancreatic neuroendocrine tumors was shown to be elevated from 5.5 to 11.4 months (Raymond et al., 2011).

1.2. Cardiac damage induced by sunitinib

The introduction of RTK inhibitors in clinical practice has been a significant leap forward in the therapy of cancer. However, a major drawback in the pharmacological use of RTK inhibitors is their side effects (Eckstein et al., 2014; Eschenhagen et al., 2011), especially those concerning cardiovascular safety (Eckstein et al., 2014; Force and Kolaja, 2011; Garcia-Alvarez et al., 2010; Mellor et al., 2011; Shah et al., 2013). Even during phase III clinical trials, sunitinib treatment showed side effects indicative of cardiac toxicity in a significant fraction of patients, specifically hypertension and fall of the left ventricular ejection fraction (LVEF) (Goodman et al., 2007; Motzer et al., 2007). The repercussions of these cardiovascular side effects are significant since in addition to be life-threatening, cardiac toxicity and dysfunction have a severe impact in the overall quality of life of affected patients, most strongly limiting their physical mobility and causing significant functional and emotional distress (Berg et al., 2014). In general, the quality of life of

patients with heart failure is poorer than that of their age-matched peers in the general population and that of patients suffering from other chronic diseases (Klocek and Czarnecka, 2013). Moreover, when present, the side effects require additional therapeutic management and may even lead to the discontinuation of sunitinib treatment (Hall et al., 2013).

Early after sunitinib incorporation to the clinics as a therapy for cancer, a series of studies confirmed cardiac toxicity as an important side effect. The retrospective study by Chu *et al*. (Chu et al., 2007) in imatinib-resistant metastatic gastrointestinal stromal tumor patients showed that 11% had a cardiovascular event, with 8% congestive heart failure. Within a group of 36 patients treated with the FDA-approved dose of sunitinib, 28% had LVEF drops higher than 10% and 47% of patients developed hypertension (Chu et al., 2007). An Italian retrospective study with patients treated for RCC showed that 9.7% developed grade-3 hypertension, and 18.9% suffered from some cardiac abnormality including 6.9% with grade-3 LVEF dysfunction and/or congestive heart failure (Di Lorenzo et al., 2009). Telli *et al.* found that 15% of patients developed symptomatic grade-3/4 heart failure (Telli et al., 2008), while a large study conducted by Richards *et al*. found an all-grade incidence of congestive heart failure of 4.1% among 6935 patients included in the study (Richards et al., 2011). A recent meta-analysis of 36 clinical trials of RTK inhibitors, 19 of which were conducted with sunitinib, clearly illustrates the magnitude of the problem (Qi et al., 2014). The most frequently reported cardiac effects of sunitinib usage are hypertension, decrease of the LVEF and heart failure.

Sunitinib can affect cardiac function indirectly; for example, clinical and sub-clinical hypothyroidism have been frequently observed during treatment, although the reported rates are very variable; from 4% to 27% (Cella et al., 2010; Faivre et al., 2007; Wolter et al., 2008). Sunitinib causes thyroid tissue injury, leading to thyroid tissue destruction, possibly by inducing capillary regression through inhibition of VEGF signaling (Kappers et al., 2011) or by other mechanisms that remain still unclear (Aparicio-Gallego et al., 2011). It is clear though that hypothyroidism correlates with cardiac risk (Biondi, 2007) as thyroid hormones are responsible for the regulation of multiple cardiac genes (Klein and Danzi, 2007). Hypothyroidism may impair cardiac contractility and increase systemic vascular resistance (Klein and Danzi, 2007).

Sunitinib constitutes the prototype "case study" for cardiac toxicity induced by RTK inhibitors. In spite of that, the mechanism(s) underlying its cardiotoxicity are not fully understood (Force and Kolaja, 2011; Hall et al., 2013). Sunitinib, as many other RTK inhibitors, binds to a large number of cellular kinases (Fabian et al., 2005; Karaman et al., 2008), thus it has the ability to affect multiple cellular processes. Sunitinib seems to possess both on-target and off-target side effects, related to its kinase-inhibition activity (Force and Kolaja, 2011). On-target side effects are based on the inhibition of kinases that could be beneficial from the perspective of oncology/angiogenesis but have a deleterious effect in cardiac physiology and metabolism. Off-target toxicity is due to non-selective inhibition of multiple kinases (and possibly non kinases) regardless of whether or not they contribute to tumor progression or survival, but that negatively impacts cardiac function (Force and Kolaja, 2011).

It is thought that the left ventricular (LV) dysfunction is the main cardiac adverse effect of sunitinib, resulting from cardiomyocyte toxicity aggravated by hypertension (Hutson et al., 2008). However, the evidence linking LV dysfunction with sunitinib-induced hypertension is still controversial (Mellor et al., 2011; Rini, 2007), although there is little room to doubt that hypertension, once present, would contribute to damage the heart. Hypertension results from a reduction of the microvessel density and vascular areas, developing an increase in peripheral vascular resistance (Inai et al., 2004). It has been demonstrated that the sunitinib-induced cardiotoxicity associates with depletion of coronary microvascular pericytes resulting in changes in the coronary microvasculature (Chintalgattu et al., 2013).

The massive energetic demand of the heart is met by the use of both fatty acids and glucose as the two main energy substrates (Neely et al., 1972; Stanley et al., 2005). Healthy hearts draw 65-70% of energy from the oxidation of long-chain fatty acids (Neely et al., 1972) but in certain pathological conditions such as ischemic injury, the myocardium responds by switching the preferential substrate to glucose (Jaswal et al., 2011), which is a less oxygen-demanding catabolic process (Ardehali et al., 2012). This adaptive response, if sustained, eventually affects the myocardial functional capacity, leading to heart failure (Dyck and Lopaschuk, 2006). There is solid indirect evidence indicating that sunitinib may generate myocardial metabolic distress; structural and functional mitochondrial abnormalities have been observed in patients, animal models and cultured cardiomyocytes exposed to sunitinib (Chu et al., 2007; French et al., 2010; Kerkela et al., 2009). Correspondingly, sunitinib treatment reduces the ATP concentration in cardiomyocytes (Hohenegger, 2012). However,

to our knowledge, direct measurements of myocardial metabolic functions in patients or animals treated with sunitinib have not been reported.

It has been proposed that the sunitinib-induced decline in LVEF is the result of cardiomyocyte damage and hypertrophy (Cohen et al., 2011). Recent studies point to sunitinib activation of the aryl hydrocarbon receptor as the mechanism underlying hypertrophy of cardiomyocytes (Maayah et al., 2014). An important aspect of sunitinib cellular toxicity is its inhibition of the AMP-activated protein kinase (AMPK), a central regulator of metabolic homeostasis and ATP utilization (Greineder et al., 2011; Schmidinger et al., 2008). AMPK can sense imbalance in the AMP/ATP ratio and upon activation, restore energetic balance by stimulation of catabolic pathways that enhance ATP generation and by shutting down processes that consume ATP (Rios et al., 2013). In addition to AMPK, sunitinib inhibits the ribosomal S6 kinase (RSK1) at therapeutically relevant concentrations (Hasinoff et al., 2008). RSK1 acts as a pro-survival factor through the inhibitory phosphorilation of the pro-apoptotic factor BAD (Hasinoff et al., 2008), thus its inhibition may explain the observed induction of apoptosis by sunitinib (Berridge et al., 2013; Chu et al., 2007).

In vivo, the pattern of toxicity induced by sunitinib seems extremely complex and unpredictable, with symptomatic heart failure observed as early as 22 days after the beginning of treatment (Witteles and Telli, 2012). So far, there is no precise information on the sequence and timing of events preceding the onset of symptomatic cardiac dysfunction

during sunitinib treatment. The identification and early detection of such events will be highly-beneficial for the clinical management of anti-cancer therapies with sunitinib.

1.3. Positron Emission Tomography (PET)

PET is a nuclear medical imaging modality (Divgi, 2009) whose principle consists in the simultaneous detection of two pairs of collinear gamma rays of 511 keV each. Those rays are emitted at the same time, under a relative angle of 180° to each other and are registered by opposing detectors in a ring scanner. The process of emission is called β^+ decay, in which photons are liberated after annihilation of a positron emitted from an unstable nucleus rich in protons (the radionuclide) and an electron of a nearby atom (Cherry, 2001; Ghosh et al., 2010). The detectors define a line of response with each true event of coincidence, in which the annihilation occurs somewhere along the line between the detectors (Anagnostopoulos et al., 2013). The line response is used to build multiple and sequential tomographic images which are then reconstructed three-dimensionally using a mathematical algorithm. The images are corrected for dead time, photon attenuation, random coincidences subtraction as well as scattered photons generated during the period of PET data acquisition. Then through the spatial distribution of the positron emitting radionuclide, also called radiotracer, and the appropriate kinetic analysis, it is possible to obtain quantitative measurements of biological parameters, suitable to provide insight into metabolic pathways *in vivo*, in real time (Chacko and Divgi, 2011).

PET on itself is a non-invasive technique that can be performed in a single experiment or in repeated studies on the same subjects (Lancelot and Zimmer, 2010). Radiotracers are

usually administered at nano or picomolar concentrations, in non-pharmacological doses, resulting in minimal or no interference with the biological process that is being studied (Divgi, 2009). In addition, the spatial resolution of clinical PET (4–7 mm) is better than other nuclear imaging techniques such as single photon emission computed tomography (SPECT), which has a spatial resolution of over 10 mm (Anagnostopoulos et al., 2013). The spatial resolution of preclinical PET using dedicated scanners reaches 1-2 mm (Chatziioannou, 2002).

Radiotracers used in PET aim to simulate natural molecules that form part of living organisms without altering their biochemical properties (Finn, 1999; Peterson and Gropler, 2010). Radiotracers can be produced in a cyclotron, a particle (protons or deuterons) accelerator (Lancelot and Zimmer, 2010). Radionuclides, considered as the "label" for PET radiotracers, can be incorporated into relevant biomolecules, sometimes by substituting the corresponding stable elements for their positron-emitter isotopes. For example, the stable ^{12}C can be substituted by ^{11}C; in addition, the native chemical elements in a molecular structure can be replaced by another element, as is the case of hydrogen replacement by ^{18}F in substrates of interest (van den Hoff, 2005). Some of the most commonly-used positron emitting radionuclides in PET scanning are: oxygen-15 (^{15}O), nitrogen-13 (^{13}N), carbon-11 (^{11}C) and fluorine-18 (^{18}F), with half-lives of 2, 10, 20 and 110 min, respectively.

1.4. The use of PET for the detection of cardiac damage

PET imaging is extensively used in cardiology (Klocke et al., 2003), it has mostly been used for the assessment of myocardial function, perfusion and metabolism (Ghosh et al.,

2010). In fact, PET has become the gold standard for noninvasive evaluation of myocardial perfusion and viability, thanks to its superior detection sensitivity and its spatial and temporal resolution in comparison to other nuclear techniques (Bengel et al., 2009; Gropler, 2013). General guidelines for the use of PET in clinical cardiology have been published by the American Society of Nuclear Cardiology (Dilsizian et al., 2009).

Healthy cardiac function depends on proper delivery of O_2 and oxidizable substrates to sustain the generation of enough quantities of ATP. Most cardiac diseases involving mechanical dysfunction are associated with energetic deficits frequently caused by disturbances in one or more metabolic steps of ATP synthesis (Carvajal and Moreno-Sanchez, 2003). In fact, alteration in the use of metabolic substrates is a biochemical hallmark of cardiac failure (Tuunanen et al., 2008). The most common functional assay done with PET is the detection of the LVEF but very often, functional PET is combined with myocardial metabolic analyses to provide information on metabolism changes under different physiological and pathological conditions (Anagnostopoulos et al., 2013). The typical metabolic parameters evaluated are either myocardial glucose uptake (K_i), myocardial metabolic rate of glucose (MMRG), myocardial blow flow (MBF) or myocardial oxygen consumption (MVO_2).

Several radiotracers that have been used in cardiac analyses are: 2-deoxy-2-[^{18}F]fluoro-D-glucose (FDG), ^{18} F-fluorothiaheptadecanoic acid (FTHA), ^{18} F-16-fluoro-4-thia-palmitate (FTP), oxygen-15 labeled water ($H_2{}^{15}O$), Rubidium-82 (^{82}Rb), ^{13}N-ammonia ($^{13}NH_3$), ^{11}C-glucose, ^{11}C-acetate and ^{11}C-palmitate (Bengel et al., 2009; Ghosh et al., 2010). In this study we utilized FDG and ^{11}C-acetate.

1.4.1. FDG

FDG is a FDA-approved glucose analogue (Bengel et al., 2009) and the most widely-used PET tracer, even in clinical practice (Grassi et al., 2012; Miele et al., 2008). FDG is transported into the myocyte, and converted into FDG-6-phosphate after phosphorylation by hexokinase, similar to the initial steps of glucose metabolism. Different from glucose-6-phosphate, this first step occurs in a unidirectional reaction because in the myocardium, the phosphatase for the reverse conversion is not present; therefore, ^{18}F-FDG-6-phosphate can not go back to ^{18}F-FDG (Ghosh et al., 2010). Also different from glucose, FDG-6-phosphate is not a good substrate for glycolysis or glycogen synthesis, then it becomes trapped in the myocytes, which provides a strong signal for imaging (Medical Advisory Secretariat, 2005).

Using FDG it is possible to evaluate the LVEF, K_i and MMRG. Detection of LVEF is the method of choice to evaluate cardiac toxicity in the clinic (Hesse et al., 2008). Due to its close relation to cardiac contraction, it is considered a contractile parameter (Borde et al., 2012). The decrease in LVEF has been postulated to be a direct result of cardiomyocyte injury (Cohen et al., 2011). LVEF values are obtained from synchronized PET acquisition images with the electrocardiogram-gated to the cardiac cycle to be finally calculated using computer algorithms.

Uptake of FDG by the myocardium has been used to reflect its degree of viability (Medical Advisory Secretariat, 2005). During energetic stress on the heart there is an increased glucose uptake that precedes and triggers left ventricular hypertrophy and cardiac severe

dysfunction (Young et al., 1999; Zhong et al., 2013). Increased FDG uptake can be observed in ischemic tissues, more so in mild to moderate ischemia (Egert et al., 1997; Ghosh et al., 2010; Tillisch et al., 1986), and also in heart failure (Bengel et al., 2009), increasing hypertrophy (Handa et al., 2007) and under dobutamine administration (Lautamaki et al., 2009). Excessive glucose uptake by the myocardium is associated with contractile dysfunction (Sen et al., 2013). However, decrease uptake of glucose can be present in situations of very severe ischemia (Ghosh et al., 2010) and decreased cardiac glucose/FDG uptake is a complicating issue consistently observed in diabetic patients (Israel et al., 2007; vom Dahl et al., 1993; Yokoyama et al., 2000).

K_i represents the net FDG influx constant (Sen et al., 2013) and its determination was the first application of cardiac metabolic imaging using FDG-PET (Russell III, 2009). Together with the levels of blood glucose (determined independently, usually by blood biochemistry), K_i is used to determine MMRG, which provides information on the rate of glucose oxidation. MMRG is increased as the initial physiologically adaptive response in the onset of heart failure, whereas as the disease progresses, the utilization of glucose declines (Ardehali et al., 2012). Reductions in MMRG have been observed in conditions of altered glucose transport (Carvajal and Moreno-Sanchez, 2003). FDG-PET has been previously used for cardiac metabolic studies in dogs (Herrero et al., 2002), rats (Charissa et al., 2009; Handa et. al., 2007; Murray et. al., 2006; Sen et. al., 2013) and mice (Herrero et al., 2004; Stegger et. al., 2009; Tantawy and Peterson, 2010; Zhong et al., 2013).

1.4.2. ^{11}C-acetate

^{11}C-acetate evaluates residual oxidative metabolism (Gargiulo et al., 2012), it is used to assess myocardial oxygen consumption (MVO_2) and myocardial blood flow (MBF). The simultaneous measurement of these parameters has been recognized as an advantage for this radiotracer (Klein et al., 2001), although its clinical application has been limited and its use remains mainly investigational (Ghosh et al., 2010). The initial tracer uptake is dependent on MBF (Timmer et al., 2010), which is closely linked to myocardial energy production (Tawakol et al., 2003). A sustained decreased in MBF has been found to cause chronic down regulation of contractile function (Di Carli et al., 2000). Quantification of MBF using ^{11}C-acetate has been in good agreement with MBF determined using $H_2{}^{15}O$ in a cohort of patients with hypertrophic cardiomyopathy, and in healthy subjects (Timmer et al., 2010). Moreover, comparisons between ^{13}N-ammonia and ^{11}C-acetate for the determination of MBF and MVO_2 in rats, have demonstrated good agreements (Bentourkia et. al., 2002). Recently, ^{11}C-acetate has been validated to meassure MBF and MVO_2 in a model of congestive heart failure in rats using a rest-stress protocol (Croteau et. al., 2012).

Normally, acetate undergoes activation by its conversion into acetyl-CoA and from there, depending on the cell type, it can be involved in either anabolic (fatty acid and cell membrane sysnthesis) or catabolic (through the tricarboxylic acid cycle (TCA) and oxidative phosphorylation to CO_2 and H_2O and thus producing energy) pathways (Grassi et al., 2012). ^{11}C-acetate is a tracer of rapid and avid uptake by the heart (Visser, 2001), where acetyl-CoA is quickly converted to energy (Grassi et al., 2012). The clearance of the ^{11}C in the form of $^{11}CO_2$ formed by the catabolism of the ^{11}C-acetate, is used to provide a measure

of the MVO_2, being a reflection of the activity of the TCA cycle, which is directly coupled to the oxidative phosphorylation (Arakawa et al., 2010; Hussain et al., 2009; Peterson and Gropler, 2010; Visser, 2001). MVO_2 is determined by cardiac energy demand (Brown et al., 1989) and it is closely coupled to the main determinants of systolic function, contractile state and wall stress (Knaapen et al., 2007). MVO_2 reductions have been reported in patients with impaired left ventricular function (Schwaiger and Wolpers, 1990) and during ischemia (Peterson and Gropler, 2010). However MVO_2 has also been found to increase during the progression of heart failure (Ardehali et al., 2012).

2. HYPOTHESIS AND OBJECTIVES

Based on the accumulated knowledge from previous studies, in which alterations of myocardial substrate metabolism precede the contractile dysfunction in several cardiac conditions (Doenst et. al., 2010; Evans and Clarke, 2012; Zhong et. al., 2013), and given that contractile dysfunction is a frequent side effect of sunitinib that can appear in the first weeks of treatment (van den Brom et al., 2009; Witteles and Telli, 2012), we hypothesize that PET would be a useful tool to determine cardiac metabolic changes early during sunitinib treatment, which may contribute to understand and diagnose the onset of cardiac toxicity. A detailed characterization of alterations in substrate metabolism in the early stages of sunitinib treatment may provide insights about the pattern of cardiac pathophysiology generated by this drug, which can have a significant predictive value in clinical practice, for the early diagnosis and follow up of cardiac events.

The objetive of this work is to determine if PET can be use as a tool for the early detection of sunitinib-induced cardiotoxicity. For this, we will establish a model of sunitinib cardiotoxicity in male C57BL/6 mice administered with 80mg/Kg of sunitinib or water by oral gavage, in a treatment schedule of 5 days-on/two days-off, for 4 weeks. ^{11}C-acetate- and FDG-PET will be used to detect cardiac metabolic and functional alterations during treatment with sunitinib. ^{11}C-acetate will be specifically used to study the myocardial blood flow (MBF) and myocardial oxidative metabolism through the quantification of oxygen consumption (MVO_2), while FDG will be utilized to determine glucose uptake (K_i), the myocardial metabolic rate of glucose (MMRG) and the left ventricular ejection fraction

(LVEF) from the cardiac-gated FDG images to evaluate myocardial contractile function. Several other methods (such as microscopy and gene expression analyses) will be included to assess the presence of general toxicity and cardiotoxicity and to reliably demonstrate the presence of cardiac pathophysiology. These tests will be also extremely important to support the findings obtained with PET.

3. MATERIALS AND METHODS

3.1. Sunitinib preparation

Sunitinib (99% purity) was purchased from Euroasian Chemicals Pvt. Ltd (Mumbai, India). To prepare the stock solution for administrations, sunitinib was disolved in sterile water (Baxter Corporation, ON) at a final concentration of 11.4 mg/mL, by agitation in a reciprocal shaker bath (VWR Scientific, ON) at 37°C for 30 min, protected from light. The solution was separated in aliquots, protected from light and stored at 4°C until use.

3.2. Animals

Twelve weeks-old male C57BL/6 mice were obtained from Charles River (St-Constant, QC), animals were maintained under a standard 12 h light/dark cycle with free access to food (Rodent Laboratory Chow 5001, Purina, St. Louis, MO) and water, at a constant temperature of 22°C and 50% humidity. Upon arrival, the animals were let to acclimatize to the new environment for at least one week before the beginning of the experiments. Since male C57BL/6 are highly aggressive towards each other, they were each housed in individual cages. Following the acclimation period, the mice were randomly distributed per group, identified by ear clipping and the individual information on the cage. A code number was assigned to each animal. All the animal protocols were approved by the Animal Research Ethics Committee, Faculty of Medicine and Health Sciences, Université de Sherbrooke.

3.3. Experimental procedures

In addition to the evaluation of cardiotoxicity by PET, the experimental design included several tests to assess the presence of general toxicity and cardiotoxicity upon sunitinib treatment. Those were intended to reliably demonstrate the existence of cardiac pathophysiology from a biological point of view, and to support the interpretation of PET results. The tests employed covered various biochemical, molecular and histological parameters. An overall view of the experimental design is shown in Figure 1.

3.3.1. Sunitinib dosage and administration

Animals were given 80mg/Kg of sunitinib or water by oral gavage, at mornings, in a volume of 10 ml/Kg. Treatment schedule consisted in sunitinib administration for 4 weeks (5 days of treatment followed by 2 days off, each week), according to previous studies (Hui et al., 2011; Murray et al., 2003; Pili et al., 2013). Previous to administration, sunitinib and vehicle were incubated for 10 min at 37°C with agitation in a reciprocal shaker bath protected from light. After the administration, the animals were closely observed for a period of 1 hour. The mice were monitored daily for signs of discomfort or symptoms of toxicity. Several parameters were routinely recorded, such as tail and eyes appearance, diarrhea, blood in feces, palmar or plantar swelling and arching of the spine, indicative of pain

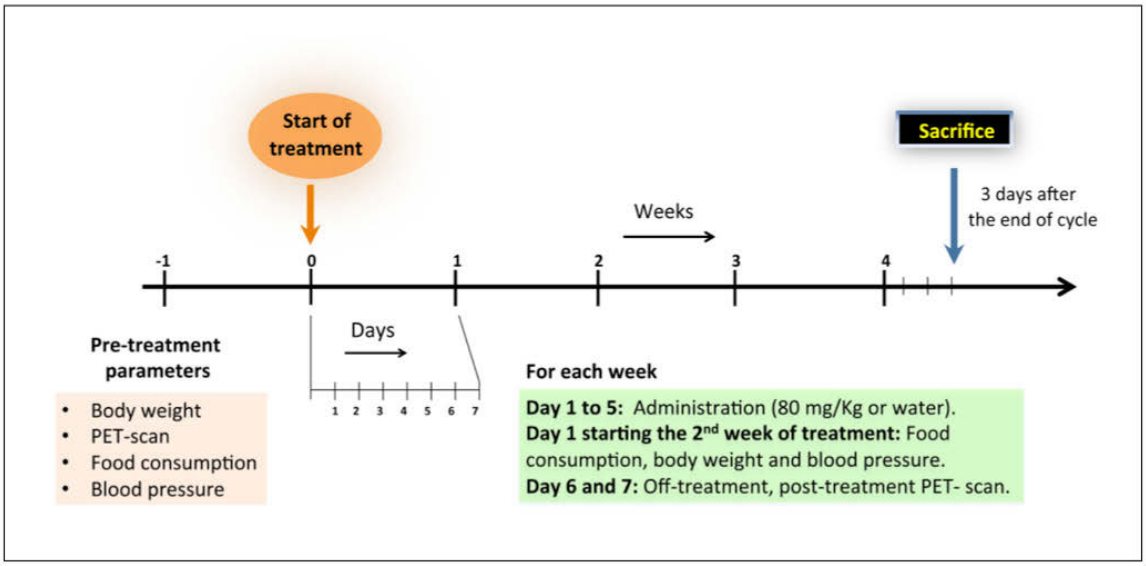

Figure 1. Treatment and data collection schedule of the experiments.

3.3.2. Body weight and food consumption

Body weight and food consumption were used as sensitive indicators of general toxicity of sunitinib treatment. Weight data was also use to adjust the volume of administration at the beginning of each week of treatment. The body weight was recorded using a precision weighing balance (Mettler Navigator ^{TM}) at day 0 and then once per week, at day 1 of each week. Food consumption was evaluated once per week at day 0 and during treatment, at day 1 of each week. Because mice have nocturnal habits and they consume most of the food during their active night hours (Ritskes-Hoitinga, 2004), food consumption was measured during the night. The day of evaluation, all the food was removed from the cages at 7:00 pm and a fixed, pre-weighted amount of chow (usually 8-9 g) was placed in each individual cage. Next day at 10:00 am (15 hours later), the remaining food was carefully recovered, weighted, and recorded for each individual mouse. The amount of food consumed per mouse during the fixed period was calculated by the difference in grams between the initial and the final weight of food collected, and expressed as gram of food consumed per gram of body weight. The average of food intake was calculated for each group per week of the study.

3.3.3. Urine biochemistry

Urine biochemical analyses were performed as an indication of renal damage, a known side effect of sunitinib treatment in cancer patients (Jha et al., 2013; Takahashi et al., 2012). At day 0 and at day 7 of each week of treatment, the mice were picked up gently and induced to urinate by bladder massage. One drop of urine was collected and applied to the reaction

test pad of a Siemens Multistix® 10SG reagent strip, according to the manufacturer's instructions. These biochemical test strips are able to detect blood in urine.

3.3.4. Blood pressure

Systolic and diastolic blood pressures were recorded at day 0 of the experiment and at day 7th of each *week* of treatment, using a tail-cuff Method (Daugherty et al., 2009) and a CODA-6 apparatus (Kent Scientific, Torrington, CT). Briefly, the animals were anesthetized under atmosphere of isoflurane via an induction chamber at a concentration of 2 % volume and 1.5 L/min oxygen flow, then the isoflurane was reduced to 1-1.5% volume and 1.5 L/min oxygen delivered through a nose cone, and maintained like this for the rest of the procedure. This concentration of isoflurane is sufficient to ensure that the mice do not wake up during the blood pressure test. To prevent hypothermia during the procedure, the animals were warmed with a heating pad (UltraHeat™ Standard Dry Heating Pad). Lubricant ophthalmic ointment (Refresh Lubricant Eye Ointment Lacri-Lube) was applied to the eyes immediately after the mice were anesthetized, to prevent cornea dryness. The tail was threaded through the occlusion cuff of the CODA-6 and the cuff was gently slid as close to the base of the tail as possible. Tail temperature was monitored with an infra-red thermometer by pointing it to the tail base area. Once the temperature was stabilized between 35-37 °C, readings of systolic and dyastolic pressures were taken using a detection time of 20 seconds with lecture intervals of 5 seconds. The first five consistent readings were recorded and averaged for each animal.

3.3.5. PET imaging

PET imaging was done at day 0 of the experiment and at day 6th and 7th of each week of treatment. PET scans were performed using a LabPET4, (Sherbrooke avalanche photodiode small animal scanner)–based small animal positron emission tomography with a field of view (FOV) of 3.75 cm and a LabPET8 Triumph, dual modality PET/computed tomography scanner (Gamma Medica-IDEAS Inc., Sherbrooke, Quebec, Canada) with a FOV of 7.5 cm. Both scanners have demonstrated similar imaging definition and spatial resolution (Bergeron et al., 2009; Bergeron et al., 2014). The scanners were calibrated by imaging of a cylindrical phantom that approximates the size of a mouse (24.8 ml, 26-mm diameter × 47-mm axial length) filled with water containing a known quantity (≈15 MBq) of 2-deoxy-2-[^{18}F]fluoro-D-glucose (FDG).

3.3.5.1. Radiochemicals

The radiotracers used were ^{11}C-acetate and FDG, produced in a TR-19 cyclotron (ACSI, Vancouver, Canada) at the cyclotron facility of the Department of Nuclear Medicine and Radiobiology, Sherbrooke Molecular Imaging Center, Université de Sherbrooke, following the procedures described in Authier *et al*. (Authier et al., 2008) and Paquette *et al*. (Paquette et al., 2012).

3.3.5.2. Animals preparation

Immediately before the scans, the animals were subjected to anesthesia with isoflurane at 2.5% vol and 1.5 L/min oxygen flow in an induction chamber. Following the induction phase, the isoflurane was reduced and maintained at 1-1.5% vol and 1-1.5 L/min oxygen in

a constant flow delivered through a nose cone. This percentage of isoflurane has a minimal effect on cardiac function, compared to other volatile anesthetics (Zhou et al., 2005). To prevent hypothermia during the procedure, the animals were warmed with a heating pad. Lubricant ophthalmic ointment was applied to protect the eyes from dryness. Blood glucose levels were measured with a Precision Xtra glucometer (Abbott, UK) following the manufacturer's instructions. Briefly, a small drop of blood was obtained by puncturing the distal section of the tail and the blood sample was deposit it into the test strip and read.

For intravenous injection of the radiotracers a 30-gauge needle was connected to an intradermic polyethylene nontoxic catheter (PE10, inner diameter 0.28mm, outer diameter 0.61mm (Becton Dickinson) and filled with heparinized saline (0.53 UI Heparine sodium injection USP (Sandoz, Canada) per mL saline solution (sodium chloride injection USP 0.9%, Hospira Healthcare Corporation, Montreal) to prevent blood clotting. The catheter was then inserted into the caudal vein. Echocardiogram (ECG) signals were registered throughout the procedure using subcutaneous needle electrodes (SA Instrument Inc., NY) inserted in the right foreleg and the left hindpaw. The respiration was measured with a small pneumatic pillow sensor (SA Instrument Inc., NY) placed under the mouse thorax while the cutaneous temperature was registered by a small thermister probe (SA Instrument Inc., NY). The mice were promptly transferred to the PET scanners in the supine position and gently restrained to the scanner bed. During the scans, the animals were maintained under anesthesia (isoflurane 1.5% vol and 1.5L/min oxygen) and at a controlled temperature of 36 °C. The mouse was positioned with the heart in the middle of the FOV, with the aid of a Doppler probe (0.64 cm [1/4 in.], 9 MHz; Parks Medical Electronics).

3.3.5.3. ^{11}C-acetate and FDG PET imaging protocols

The imaging protocols used to explore whether PET can detect alterations in the oxidative metabolism and myocardial function during a four-weeks sunitinib treatment in this murine model are shown in Figure 2. ^{11}C-acetate was specifically used to study the myocardial blood flow (MBF) and myocardial oxidative metabolism through the quantification of oxygen consumption (MVO_2). FDG was utilized to determine glucose uptake (K_i), the myocardial metabolic rate of glucose (MMRG) and the left ventricular ejection fractions (LVEF) from the cardiac-gated FDG images; these parameters are indicators of myocardial glucose utilization and myocardial function. Doses of each radiotracer were prepared in a work station, equipped with a Capinter dose calibrator CRC-25R (Capinter Inc., NJ). All the radioactive manipulations were done following the University of Sherbrooke radioprotection guidelines.

Since ^{11}C-acetate has a shorter half live than FDG (20.4 min and 110 min, respectively), the PET scans were started with a ^{11}C-acetate dynamic data acquisition with a pre-determined time of 21 minutes. One minute after the start of list mode data acquisition, a dose of 50±10 MBq of ^{11}C-acetate in 0.05 ml of 0.9% NaCl was administered intravenously at a flow of 0.1 ml/min using an injection pump (Lomir BioMedical Inc., Montreal). A manual saline flush (~0.05-0.06 ml over a period of 30 seconds) was applied immediately after the end of the radiotracer injection. Ten minutes after the end of the ^{11}C-acetate dynamics, a second list mode data acquisition of 46 minutes was started. One minute after the start (at minute 32), a dose of 15±5 MBq of FDG in 0.05 ml of 0.9% NaCl at a flow of 0.1 ml/min was

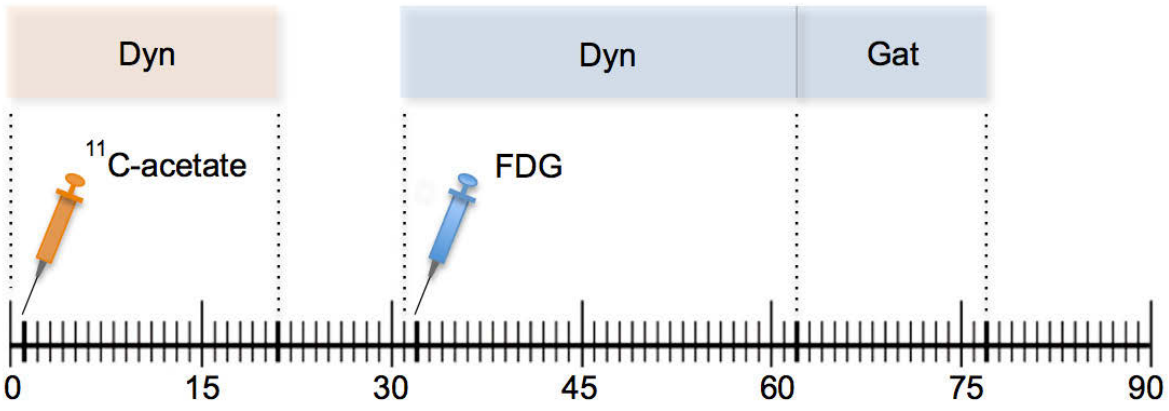

Figure 2. ^{11}C-acetate and FDG-PET imaging protocol (0 to 77 minutes). Dyn: list-mode dynamic acquisition. Gat: ECG-gated dynamic acquisition mode.

injected intravenously using an injection pump. A manual saline flush of ~0.05-0.06 ml over a period of 30 seconds was again applied immediately after the end of the FDG injection. Once the dynamics were completed, the animals were returned to their cages for recovery with free access to food and water. To prevent hypothermia during the recovery from anesthesia a heating pad was placed under the cage, covering approximately 50% of the bottom of the cage area.

3.3.5.4. Image reconstructions

For the analysis of the cardiac parameters (MVO_2, MBF and MMRG), ^{11}C-acetate and FDG PET images were reconstructed on a 92 x 92 x 128 matrix and on a 92 x 92 x 64 matrix for the emission list-mode data recorded from LabPET 8 and LabPET4, respectively, with a common voxel size of 0.5 x 0.5 x 0.59675 mm^3 using the maximum-likelihood expectation maximization (MLEM) algorithm with 15 iterations (Selivanov et al., 2000). For each analysis, a series of frames was independently chosen for each radiotracer; 29-frame sequences were taken for ^{11}C-acetate as follow: 1 x 1 min, 12 x 10 s, 11 x 30 s and 5 x 150 s and 32 frames for FDG, distributed as 1 x 1 min, 12 x 15 s, 9 x 30 s, 5 x 150 s and 5 x 300 s.

The last 15-minutes frame of the cardiac FDG gated PET data acquired in the list-mode was also reconstructed into eight electrocardiogram gates on the basis of R-R intervals (Croteau et al., 2003) using MLEM algorithm with 35 iterations to calculate the left ventricular ejection fraction. The data from the first minute of acquisition, previous to the radiotracers injection, was used to evaluate the residual activity from the previous injection

or any accidental coincidences. The mean activity estimated from this frame in a delayed time window was removed from all the decay-corrected subsequent frames of the emission sinogramas before data analysis.

3.3.5.5. Quantitative image analysis, PET variables

Images were analyzed using the "in house" Sherbrooke LabTEP image analysis software. For quantitative evaluation using a kinetic modeling of both radiotracers, regions of interest (ROI) were manually drawn in the transaxial planes over the myocardium and in the center of the blood pool of the left ventricle. A third ROI was drawn for the FDG in the liver, as previous studies have shown that the exponentially decaying part of time activity curves are very similar for the arterial blood and the liver, allowing the use of the liver input curve to estimate the later blood clearance phase. Therefore, a hybrid input curve was generated using left ventricle and liver input curves for the FDG as described by Tantawy and Peterson (Tantawy and Peterson, 2010). Such hybrid input curve is the approach recommend by these authors to calculate the MMRG, rather than the use of the left ventricle input curve alone or the arterial input function generated from manual arterial blood sampling, as previously reported (Tantawy and Peterson, 2010). ROI were applied to each time frame of the PET images, and the average radioactivity concentration was computed to obtain the tissue time-activity curves. All time-activity curves were corrected for radionuclide decay.

MBF and MVO_2 were quantified from blood and myocardial time–activity curves generated from PET images of ^{11}C-acetate. The curves were fitted with the PetKm software

(PET Kinetic Modeling, University of Sherbrooke) (Bentourkia M., Univ of Sherbrooke, personal communication) and analyzed using a three-compartment kinetic model to obtain values for K_1 (ml/g/min) and K_2 (ml O_2/min/100 g myocardial tissue), representing MBF and MVO_2, respectively.

For the calculation of the MMRG the FDG myocardial and hybrid input curves were fitted with PetKm software. The Patlak graphical analysis was chosen for the kinetic modeling. The interval of frames 19^{th}-30^{th} from FDG dynamic data, corresponding to the time period of minutes 7^{th}-36^{th} was taken. The early–time data representing the exchange of radiotracer between blood and myocardium were not used (Herrero et al., 2004). The mean plasma glucose (C_{glu}) levels (in mg/dl) taken before each PET imaging sesion were used for the calculations, and a value of 1.0 was assumed for the Lumped constant (LC) of the myocardium. The K_i obtained (FDG uptake constant) was then used to calculate MMRG through the equation: MMRG (μmol/g/min) = K_i C_{glu}/LC (Zhong et al., 2013).

To calculate the LVEF the pixel size of the images was transformed to approximate the mouse heart size to human dimensions, using the XMedCon program (http://xmedcon.sourceforge.net/). Reorientation and cardiac data analysis were performed with the Corridor4DM software from Segami Oasis (Columbia, MD), as previously described (Croteau et al., 2003).

3.3.6. Animal tissue collection

Three days after the last scan, animals were weighted and euthanized by treatment with isoflurane (Abbott Laboratories, ON) via an anesthesia chamber at a concentration of 5 % volume and 1.5 L/min oxygen flow) followed by cervical dislocation. The hearts were collected, rinsed with 0.9% saline solution, weighted in an analytical balance (Toledo XS, Mettler Toledo) and immediately dissected longitudinally and placed in the appropriate buffers depending on the future application.

3.3.7. Histological analysis and immunofluorescent microscopy

One half of the hearts was fixed in buffered formalin (10% formaldehyde, 33mM NaH_2PO_4, 46 mM Na_2HPO_4) for 24 h at room temperature, transferred to 70% ethanol and embedded in paraffin blocks at the pathology service of the Centre hospitalier universitaire de Sherbrooke (CHUS). In addition, parts of several samples were fixed in 3.5% paraformaldehyde and frozen-embedded in OCT (TissueTek/VWR) for immunofluorescent microscopy. Sections 5 µm thick were mounted on slides and either stained with hematoxylin & eosin (H&E) by the pathology services of the CHUS or used for detection of myocardial interstitial fibrosis, by staining with Masson's trichrome for collagen, performed at Wax-it Inc. Histology Services, Vancouver, Canada. Histological images were obtained using a Nanozoomer 2.0 slide scanner (Hamamatsu Photonics K. K., Japan) and visualized and processed with the NDP Viewer software (Hamamatsu Photonics K. K., Japan). Pathological damage to the hearts was evaluated by Dr. Marie Odile Benoit-Biancamano, Department of Pathology and Microbiology, (Univ. of Montreal).

Frozen, 5 μm thick sections were generated using a Cryostat (Leica 3050) and used for immunofluorescence staining, performed as described (Guttman et al., 2006). Briefly, thawed sections were treated for 5 minutes in 0.2% Triton X-100 in phosphate-buffered saline (PBS); this was followed by three ten-minute washes with PBS. The tissues were blocked for 20 minutes with 5% normal goat serum/0.5% bovine serum albumin in PBS (GB-PBS) and then incubated with a rabbit anti-mouse myeloperoxidase-1 (MPO-1) (1:200, Ab-1, NeoMarkers RB 373-AD) overnight at 4°C in GB-PBS containing 0.1% Tween 20. The next day, the slides were washed three times for 10 minutes in 0.5% BSA/0.1% Tween 20 in PBS and incubated with a fluorescent goat anti-rabbit antibody conjugated to Alexa-488, 1:1000 dilution (Molecular Probes, CA) for 2 hours at room temperature. The slides were washed as before and coverslips were mounted using ProLongGold with 4',6-diamidino-2-phenylindole (DAPI) (Molecular Probes), to stain the cell nuclei. Fluorescence was visualized using an Olympus IX81 microscope.

3.3.8. Transmission electron microscope

Fragments of the left ventricular myocardium from the heart apex were fixed in 2.5% glutaraldehyde in 0.1M sodium cacodylate buffer for 12 hours. After two rinses in 0.1M cacodylate buffer (pH 7.3) for 5 minutes, specimens were post-fixed for 90 min with 1% osmium tetroxide in cacodylate buffer. Tissues were rinsed twice in cacodylate buffer and dehydrated in increasing ethanol concentrations (70, 85, 90, and 3 x 100%) followed by immersion in propylene oxide three times for 5 minutes. Infiltration was conducted in a 1:1 mixture of propylene oxide and epoxy resin (Epon 812) for 1 hour, followed by 2 x 1-hour and one overnight infiltration steps in 100% resin. Samples were placed into uniquely

labeled molds in 100% resin and polymerized in a 65°C oven for 48 h. Longitudinally oriented sections of tissue between 70-80 nm thick were cut from the blocks using a Leica ultramicrotome, contrasted with 2% uranyl acetate and 3% lead citrate. The grids were examined at 80 keV in a Hitachi H-7500 transmission electron microscope equipped with a 16-megapixel AMT TR160 digital camera controlled by an Advanced Microscopy Techniques software. All reagents were purchased from Electron Microscopy Sciences (Cedarlane, ON).

3.3.9. Gene expression analyses

Gene expression analyses were performed by quantitative PCR (qPCR) on reverse-transcribed products (cDNA) prepared from total RNA isolated from the heart's ventricular apex of mice randomly selected from each group. Sections of approximately 10 mg were excised from the left ventricle (LV) immediately after euthanizing the animals and placed in RNALater (Qiagen) to preserve RNA integrity. The samples were incubated overnight at 4°C and transferred next day to -80°C until use. Total RNA was purified using the RNAEasy kit (Qiagen) according to the manufacturer's instructions. Briefly, the tissues were separately homogenized in Safe-lock 2 ml tubes (Eppendorf) containing 350 µl of RLT buffer with one sterile 2-mm diameter tungsten bead, using a Mixer Mill MM400 (Retsch, Germany) at a shaking frequency of 25/second, for 4 minutes. The homogenates were then centrifuged at 15000 x g for 5 minutes and the supernatant was mixed with 350 µl of 70% ethanol and loaded into the kit's columns. The columns were spun in a microfuge at 10000 x g for 1 minute, the flow-through was discarded and the column was washed with 700 µl of RWI buffer, followed by 2 washes with 500 µl of RPE buffer, by

centrifugation as described above. The RNA was eluted from the columns by addition of 30 µl of RNAse-free water and centrifugation for 1 minute at 10000 x g. RNA concentrations were determined by optical density measurement at 260 nm using a Nanodrop spectrophotometer (Thermo Scientific).

The cDNAs were prepared by reverse transcription of total RNA using the Quantitech reverse transcription kit from Qiagen, following the manufacturer's instructions. Briefly, 500 ng of total RNA were cleaned of contaminating genomic DNA by treatment with 2 µl of gDNA-wipe out solution for 2 minutes at 42°C. The cDNAs were synthesized by addition of a mix containing the random primers, buffer and reverse-transcriptase (RT) enzyme followed by incubation for 30 minutes at 42°C. At the end of the cDNA synthesis step, the RT was inactivated by treatment for 3 minutes at 95°C and the 20 µl reactions were taken to a final volume of 100 µl with RNAse-free water.

The qPCR reactions were done in 96-well plates (Axygen) using the iQ™ SYBR® Green Supermix from Biorad and an Eppendorff Real Plex-2 qPCR machine, in a final volume of 10 µl per reaction. The reaction mixes consisted in 1 µl of cDNA, 1 µl of the gene-specific mix of forward and reverse primers (2 µM each), 3 µl of water and 5 µl of the 2 x qPCR mix. PCR conditions were: 10 minutes at 95°C to activate the enzyme followed by 40 cycles of: 95 °C denaturing for 30 seconds, 60°C annealing for 30 seconds and 72 °C extension for 30 seconds. Fluorescence readings were taken during the extension part of the cycles. At the end of each qPCR run, a melting curve analysis of the qPCR products was carried out to monitor the specificity of the amplifications. Relative transcript levels were

calculated using the delta Cq method corrected for primer efficiencies (Pfaffl, 2001) and expressed as the relative expression of the sunitinib-treated group with respect to the control (water-treated) group. The list of genes analyzed and the sequences of the primers for each gene are shown in Table 1.

3.3.10. Statistical analyses

Data processing and statistical analyses were done with GraphPad Prism 6 (GraphPad Software, Inc., San Diego, CA). All values are expressed as group means ± standard error of the mean. Statistical comparisons were performed using Student's t-test.

Table 1. The genes analyzed in this study and the qPCR primers. Relevant functions are given for each gene product.

Gene	Acc. No.	Product	Primers	Function
Inflammation				
Tnf	NM_013693.3	Tumor necrosis factor alpha	CCACCACGCTCTTCTGTCTAC AGGGTCTGGGCCATAGAACT	Cytokine, inflammation
Nos2	NM_010927.3	Nitric oxide synthase 2, inducible	CGCTTTGCCACGGACGAGA AGGAAGGCAGCGGGCACAT	Inflammation
Il6	NM_031168.1	Interleukin 6	GAGGATACCACTCCCAACAGACC AAGTGCATCATCGTTGTTCATACA	Cytokine, inflammation
Il1b	NM_008361.3	Interleukin 1 beta	ACGGACCCCAAAAGATGAAG TTCTCCACAGCCACAATGAG	Cytokine, inflammation
Il18	NM_008360.1	Interleukin 18	GCCTCAAACCTTCCAAATCAC GTTGTCTGATTCCAGGTCTCC	Cytokine, inflammation
Cxcl1	NM_008176.3	Chemokine (C-X-C motif) ligand 1 (KC)	ACCCAAACCGAAGTCATAGC TCTCCGTTACTTGGGGACAC	Chemokine, inflammation
Hypertrophy/Remodeling				
Col1a1	NM_007742.3	Collagen, type I, alpha 1	CTCCCAGAACATCACCTATCA ACTGTCTTGCCCCAAGTTCCG	Remodeling
Cyp1a1	NM_009992.4	Cytochrome P450, family 1, subfamily a, polypeptide 1	CTGGATGCCTTCAAGGACTTG TGTCCTGACAATGCTCAATGAG	Marker of hypertrophy
Areg	NM_009704.3	Amphiregulin	ATCTTTGTCTCTGCCATCATCC GTCCCGTTTTCTTGTCGAAGC	Remodeling
Tgfb1	NM_011577.1	Transforming growth factor, beta 1	TGACGTCACTGGAGTTGTACGG GGTTCATGTCATGGATGGTGC	Inflammation/Remodeling
Fgf21	NM_020013.4	Fibroblast growth factor 21	AATCCTGGGTGTCAAAGCCTC ACTGGTACACATTGTAACCGTC	Cardiac protection
Mitochondrial function				
Ucp2	NM_011671.4	Uncoupling protein 2 (mitochondrial, proton carrier)	ACAGCCTTCTGCACTCCTG GGCTGGGAGACGAAACACT	Mitochondrial function
Ucp3	NM_009464.3	Uncoupling protein 3 (mitochondrial, proton carrier)	GGATGCCTACAGAACCATCG TTGTGATGTTGGGCCAAGT	Mitochondrial function
Cox4i1	NM_009941.2	Cytochrome c oxidase subunit IV isoform 1	TCACTGCGCTCGTTCTGAT CGATCGAAAGTATGAGGGATG	Mitochondrial respiration
Cox5b	NM_009942.2	Cytochrome c oxidase subunit Vb	GTGGTGTCCCCACTGATGA TGAAGCTGCCTTTGGAGGTA	Mitochondrial respiration
Uqcrc1	NM_025407.2	Ubiquinol-cytochrome c reductase core protein 1	CTCAACAGACATTACAAAGCCC ACGGCATCTTCTTCATACACTC	Mitochondrial respiration

Table 1... cont

Energy metabolism				
Slc2a4	NM_009204.2	Solute carrier family 2 (facilitated glucose transporter), member 4 (Glut4)	GTGACTGGAACACTGGTCCTA CCAGCCACGTTGCATTGTAG	Glucose transporter
CD36	NM_001159558.1	CD36 antigen	TTGTACCTATACTGTGGCTAAATGAG CTTGTGTTTTGAACATTTCTGCTT	Fatty acid uptake
Pdk4	NM_013743.2	Pyruvate dehydrogenase kinase, isoenzyme 4	GCCAATTTCTCGTCTCTACGC TGACTTGTTAAAGACTGGGAGC	Metabolic regulator
Slc27a1	NM_011977.3	Solute carrier family 27 (fatty acid transporter), member 1	GGTTGACGGTGGTACTGCGC GTAGCGGCAGATTTCACCTATG	Fatty acid uptake
Pgc1a	NM_008904.2	Peroxisome proliferative activated receptor, gamma, coactivator 1 alpha	CCCTGCCATTGTTAAGACC TGCTGCTGTTCCTGTTTTC	Transcriptional control
Ppara	NM_011144.6	Peroxisome proliferator activated receptor alpha	CGGGAACAAGACGTTGTCAT CAGATAAGGGACTTTCCAGGTC	Transcriptional control
Ppard	NM_011145.3	Peroxisome proliferator activator receptor delta	AGAACACACGCTTCCTTCCA CCGACATTCCATGTTGAGG	Transcriptional control
Cpt1b	NM_009948.2	Carnitine palmitoyltransferase 1b, muscle	CATCCCAGGCAAAGAGACA AAGCGACCTTTGTGGTAGACA	Lipid transport
Acadm	NM_007382.5	Acyl-Coenzyme A dehydrogenase, medium chain	TGTCGAACACAACACTCGAAA CTGCTGTTCCGTCAACTCAA	Lipid oxidation
Housekeeping gene				
Rplp0	NM_007475.5	Ribosomal protein, large, P0 (36B4)	TCTGGAGGGTGTCCGCAAC CTTGACCTTTTCAGTAAGTGG	

4. RESULTS

The objective of this work was to evaluate the feasibility of ^{11}C -acetate- and FDG-PET imaging for the early detection of cardiotoxicity induced by sunitinib treatment. To address this, we treated male C57BL/6 mice with sunutinib at a dose of 80mg/Kg/day following a schedule of administration of 5 days per week, for 4 weeks. The selection of male mice was based on previous studies in which males showed higher susceptibility to hypertrophy and heart failure than females. Females can develop a relative protection from the occurrence of cardiovascular illnesses, a phenomenon that has been found not only in animals but also in humans (Fliegner et al., 2010; Gurgen et al., 2011; Sari et al., 2011).

Sunitinib dosing in cancer patients is typically 50mg/day, administered in 6-week treatment cycles of 4 weeks on/2 weeks off, as recommended by demonstrated clinical efficacy for advanced solid tumors (Faivre et al., 2006). We employed a dose of 80 mg/Kg/day based on several considerations: (*i*) the half-life of sunitinib in normal human volunteers has proven to be approximately 25-fold higher than that in mice (Chintalgattu et al., 2013; Hipp et al., 2008) therefore, higher doses are required for mice in order to obtain similar drug exposures as those achieved in humans; (*ii*) 80 mg/Kg/day induce a substantial and optimal antitumor effect in murine models (Ebos et al., 2007/; Hui et al., 2011); and (*iii*) high doses of sunitinib have been used in multiple preclinical studies in mice, either in single-dose administrations of 80, 120, and 160 mg/Kg (Haznedar et al., 2009; Lim et al., 2010; Welti et al., 2012), in repeat-dose administrations of 80 mg/Kg (Pili et al., 2013) and 120

mg/Kg/day for 7days (Welti et al., 2012) and also 80 mg/Kg/day for 21days (Murray et al., 2003) and up to 4 and 5 weeks in other models (Haznedar et al., 2009).

We decided to perform a 4-weeks treatment period to resemble a typical cycle of clinical sunitinib administration schedule, with the difference that instead of 7 days per week, the administration was adjusted to 5 days per week, as done in previous studies (Hui et al., 2011; Murray et al., 2003; Pili et al., 2013). For this decision, we also took into account the clinical evidence of the occurrence of cardiac adverse effects during the first 4-weeks cycle of treatment (Chu et al., 2007; de Boer et al., 2010; Khakoo et al., 2008; Mellor et al., 2011; Steingart et al., 2012).

4.1. Biological evaluation of general toxicity induced by sunitinib

Based on the reported incidence of several adverse effects during sunitinib administration in humans, the treated animals were observed daily to detect signs of general toxicity. We monitored for gastrointestinal problems such as diarrhea or bloody stools, lesions of the skin (desquamation, blisters and callus formation in areas subjected to pressure, such as the paws and foot pads) as well as hair depigmentation (Aparicio-Gallego et al., 2011; Neuhaus et al., 2014; Schwandt et al., 2009). Other events such as anorexia, weight loss and hematuria, also reported in the literature (Eisen et al., 2012; Quintyne et al., 2013; Schwandt et al., 2009), were evaluated once per week by food consumption and body weight measurements, while the presence of blood in urine was determined by a biochemical test.

During the daily and individual observation of the animals, a change in the color of the stools was evident in the treated group from the beginning of the study. The feces became yellowish with respect to the controls, but no diarrhea, bloody stools or lesions of the skin were observed in any of the two groups throughout the experiment. The treated animals show signs of inactivity that started the second week of treatment, which progressively increased during the course of the study. A slight hair depigmentation in the group under sunitinib treatment was noted by the 4th week. Urine biochemical analyses performed for each individual mouse didn't show any indication of blood in the urine, suggesting that the administration schedule and dose of sunitinib used did not induce significant renal damage.

The analysis of body weight (Figure 3) revealed that the control group consistently gained weight during the study, from an average of 27 g at week 0 to 29.8 g at the end of the study. However, the treated group failed to show any increase in weight. The differences between the two groups became statistically significant at the 2nd week of treatment and by the 3rd and 4th week were highly significant. In addition, the amount of food consumed by each animal in a 15-hour time period, decreased in the group treated with sunitinib (Figure 4) starting the first week of treatment and was most remarkable after a sudden and statistically significant drop observed at the 3rd week. These results indicate that sunitinib administration at 80mg/Kg causes anorexia and weight faltering in C57 BL6 adult male mice.

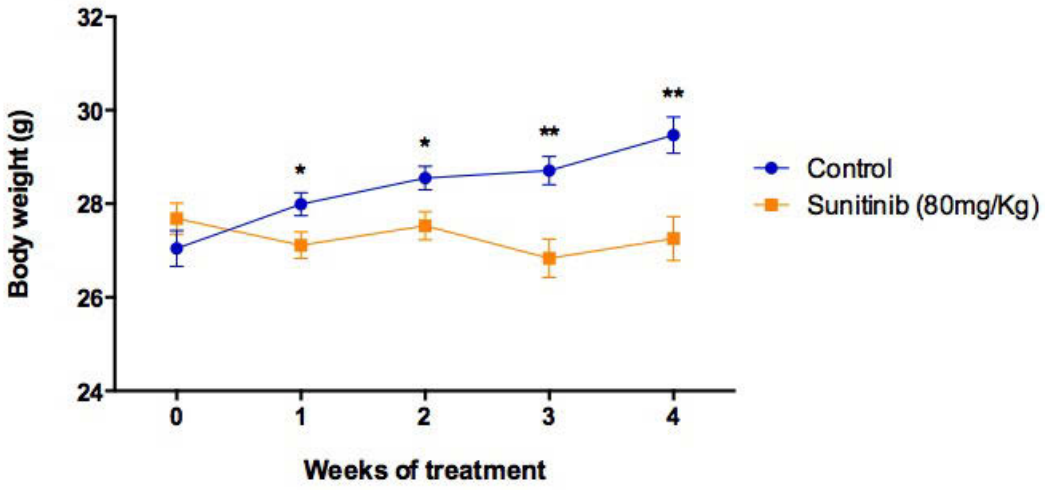

Figure 3. Body weight of C57BL6 male mice at 0 (pre-treatment), 1, 2, 3 and 4 weeks of treatment with sunitinib 80mg/Kg. The graph shows the means and standard errors. The asterisks denote statistical significant differences between the sunitinib-treated and control groups as determined by Student's t-test, (*) $p < 0.05$) and (**) $p < 0.01$).

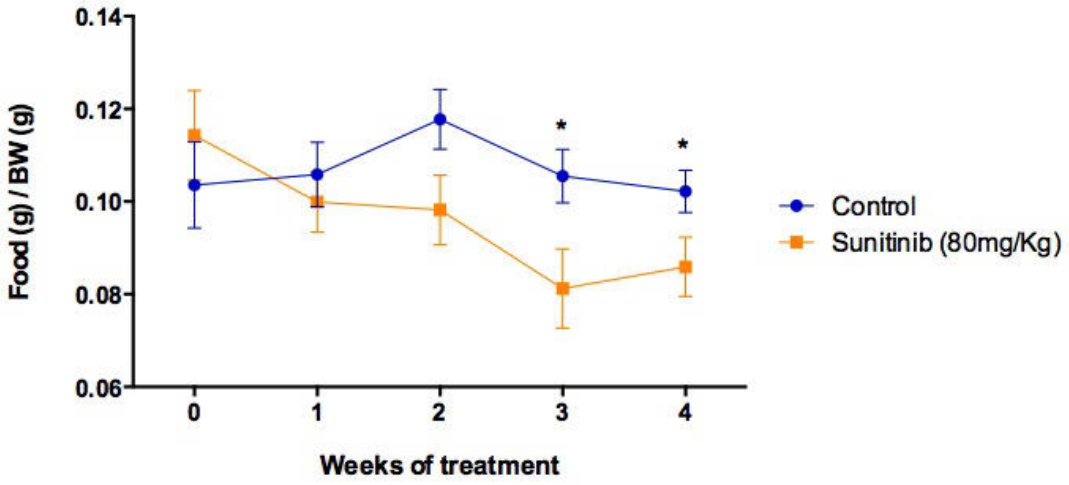

Figure 4. Food consumption of C57BL6 male mice at 0 (pre-treatment), 1, 2, 3 and 4 weeks of oral administration of sunitinib 80 mg/Kg. Food consumption (Food (g)/ BW(g)) is expressed as the ratio between food intake in a 15-hours period *vs* the body weight (BW) of the animal. The graph shows the means and standard errors. The asterisks denote statistical significant differences between the sunitinib-treated and control groups as determined by Student's t-test, (*) $p < 0.05$).

4.2. Biological evaluation of cardiac toxicity induced by sunitinib

Significant cardiovascular side effects have been often reported as a consequence of the mechanisms of action of many anti-cancer agents (Eschenhagen et al., 2011), and sunitinib is not the exception. Cardiac adverse effects of sunitinib treatment vary in severity from asymptomatic prolongation of the QTc (the heart rate-corrected time between the start of the Q wave and the end of the T wave in the heart's electrical cycle) (Dasanu et al., 2012) and hypertension to myocardial infarction and sudden death (Schmidinger et al., 2008).

Hypertension is considered a mechanism by which RTK inhibitors therapy can cause left ventricular systolic dysfunction, heart failure, ischemia and infarction (Dasanu et al., 2012; Hutson et al., 2008; Shah et al., 2013). Therefore, detection of hypertension is an indicator for intervention against cardiac toxicity during RTK inhibitors treatment. Because RTK inhibitors can cause dramatic and somewhat unpredictable increases in blood pressure early in treatment, the National Cancer Institute clinical trial protocols recommend monitoring blood pressure weekly during the first cycle of RTK inhibitor therapy and then at least every 2 to 3 weeks for the duration of treatment (Steingart et al., 2012). It has been reported that sunitinib can induce significant increases in systolic and diastolic blood pressures, even within the first cycle (4 weeks) of treatment (Chu et al., 2007; Mellor et al., 2011; Shah et al., 2013). Given this precedent, we monitored blood pressure during the experiment. The analysis of systolic and diastolic blood pressures recorded before the beginning of the experiment, and at day 7^{th} of each week of treatment using a tail-cuff method, did not differ between the 2 groups (Figure 5).

A

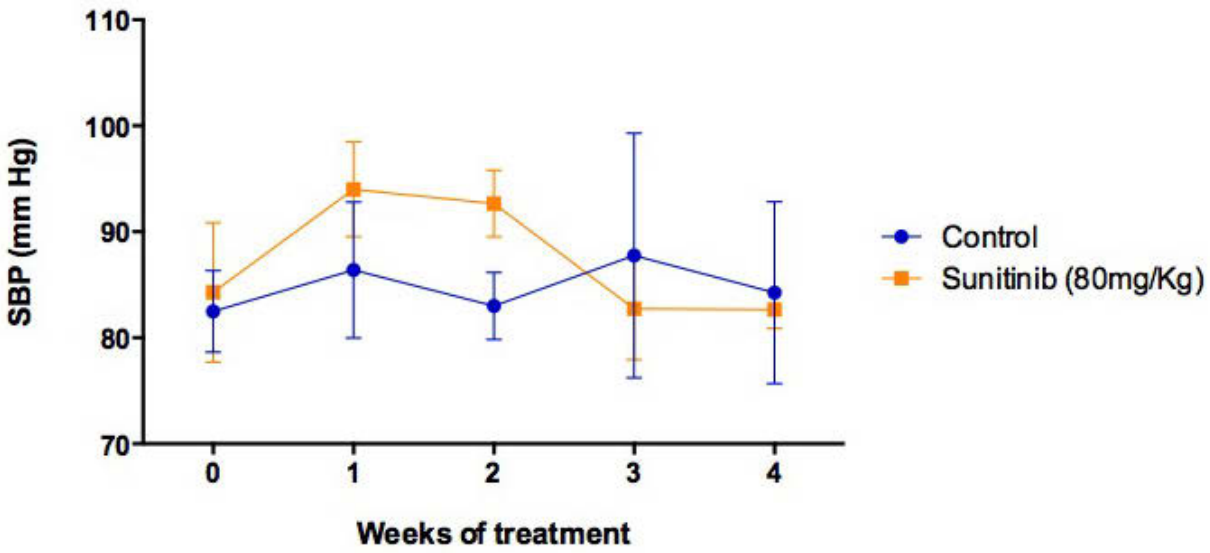

B

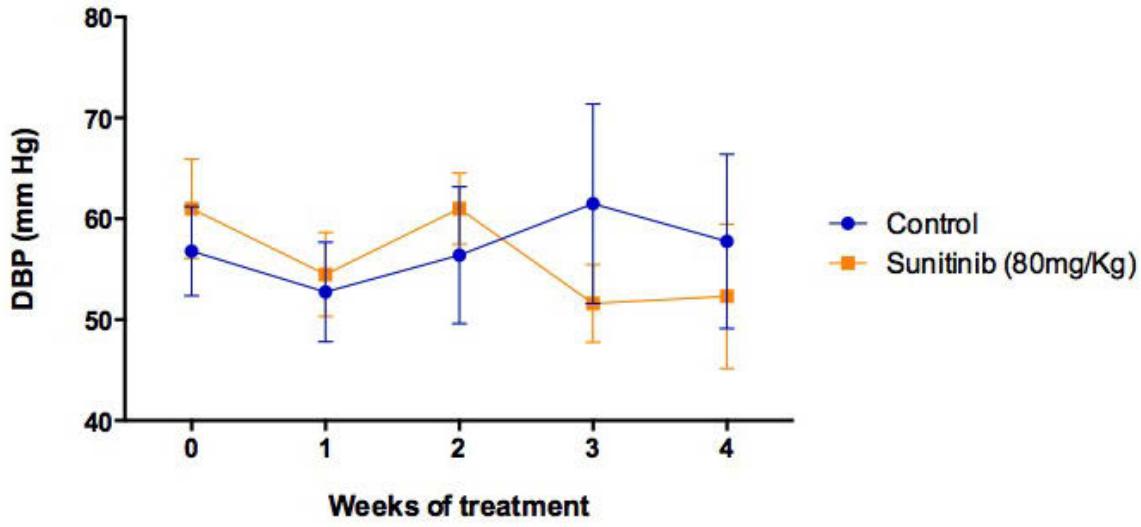

Figure 5. Systolic (A) and diastolic (B) blood pressure of C57BL6 male mice at 0 (pre-treatment), 1, 2, 3 and 4 weeks of treatment with sunitinib 80mg/Kg. The graphs show the means and standard errors. SBP: Systolic blood pressure; DBP: Diastolic blood pressure.

Histological staining of 5 μm-thick heart sections with hematoxylin and eosin (H&E) was used to investigate the cardiac tissues of both groups, with the objective of documenting the occurrence of myocardial histopathological changes as a consequence of sunitinib treatment. The analysis of H&E-stained tissues under a light microscope showed only moderate pathology in some of the sunitinib-treated animals (Figure 6). Mild fibroplasia accompanied by hemosiderophages, consistent with chronic microhemorrhage, was observed, as well as abundant myofiber vacuolation and signs of early muscle degeneration presented by cloudy swelling possibly indicating intracellular edema.

The histopathological findings showing tissue damage suggested the possibility of an ongoing inflammatory process. Inflammation can be triggered in response to a wide range of homeostatic insults, which include tissue injury (Chovatiya and Medzhitov, 2014). Based on this, we evaluated the expression of a battery of genes known to be involved in the inflammatory response in the heart under various conditions of myocardial homeostatic stress (Aoyagi and Matsui, 2011; Hedayat et al., 2010) (Table 1). The analysis of relative mRNA levels for a group of inflammatory genes in the left ventricle of sunitinib-treated mice, by qPCR (Figure 7), showed statistically significant upregulation of the genes coding for the pro-inflammatory factors TNFα (tumor necrosis factor), NOS2 (inducible nitric oxide synthase), IL1β (interleukin 1 beta) and CXCL1 (chemokine X-ligand 1, also known as KC in mice). However, a surprisingly different response was observed for the *Il6* (interleukin 6) gene, which was significantly downregulated in animals under sunitinib treatment. In addition, no significant change was detected in the transcript levels of the *Il18*

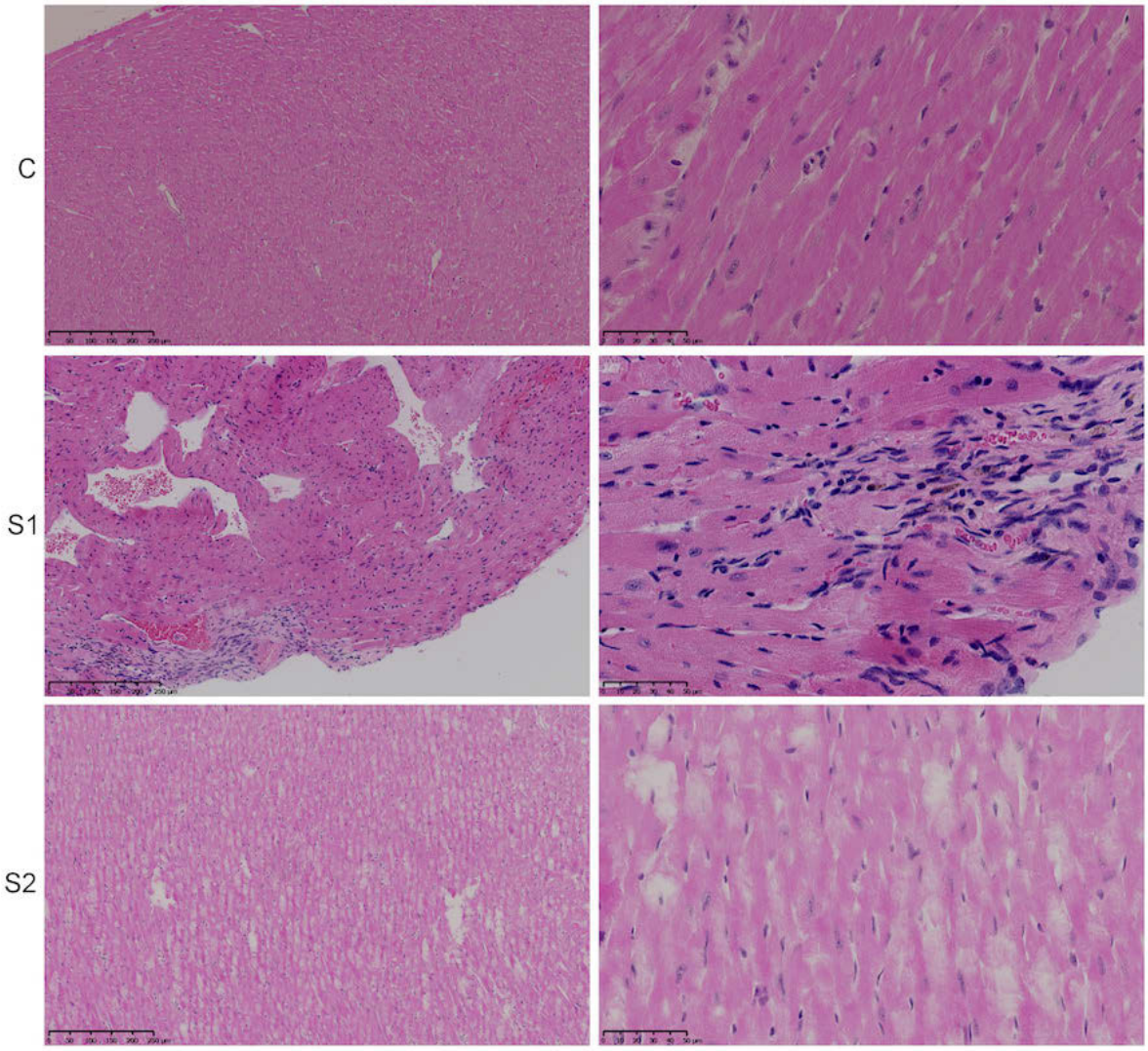

Figure 6. H&E staining of cardiac tissue from representative C57BL/6 male mice orally administered with vehicle (C) or sunitinib 80 mg/Kg for 4 weeks (S1 and S2). Arrows in S1 indicate a zone of fibroplasia and the presence of hemosiderophages. Vacuolation and intracellular edema are present in S2 as white areas in the myocardium. Scale bars are 250 μm (left panel) and 50 μm (right panel).

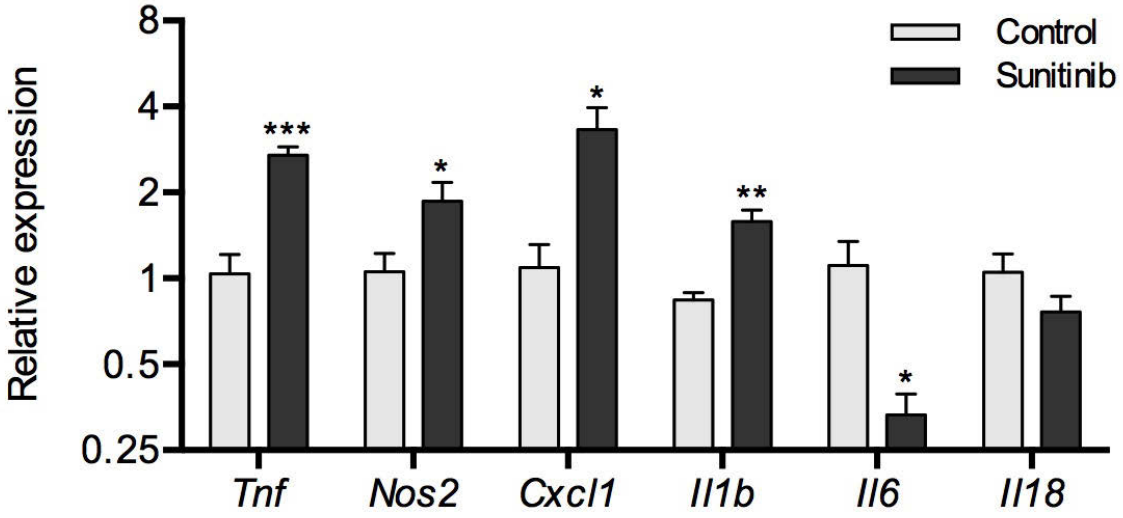

Figure 7. Relative transcript levels of inflammation-related genes in the left ventricle of C57BL/6 male mice after 4 weeks of treatment with water (control) or sunitinib 80mg/Kg. The data was generated by qPCR; the graph shows the means and standard errors. The genes evaluated were tumor necrosis factor alpha (*Tnf*), inducible nitric oxide synthase (*Nos2*), chemokine (C-X-C motif) ligand 1 (*Cxcl1*), interleukin 1 beta (*Il1b*), interleukin 6 (*Il6*) and interleukin 18 (*Il18*). The asterisks denote statistical significant differences between the sunitinib-treated and control groups as determined by Student's t-test, (*) $p < 0.05$); (**) $p < 0.01$); (***) $p < 0.001$.

(interleukin 18) gene (Figure 7). The local increase in the transcript levels of this group of pro-inflammatory genes strongly suggests the presence of an underlying inflammatory process in the left ventricle of sunitinib-administered animals.

CXCL1 is a chemokine that is a potent chemoattractant for neutrophils; it promotes their extravasation and infiltration in tissues. Neutrophils are the first inmmune cells that accumulate in damaged tissues (Amanzada et al., 2014), and under certain conditions, they can also actively contribute to the onset and perpetuation of injury (Seely et al., 2003). In addition neutrophil infiltration of the myocardium has been previously observed after tissue damage for example, in models of ischemia reperfusion injury (Ao et al., 2009). The increase in the relative expression of the *Cxcl1* gene suggested the possibility of neutrophil recruitment to the myocardium of the animals treated with sunitinib. In fact, immunofluorescent microscopy of heart tissue sections (Figure 8), using an antibody against myeloperoxidase-1 (MPO-1, a marker of neutrophils) revealed a clear increase on the number of neutrophils in the hearts of sunitinib- treated animals with respect to the controls. This finding supports the idea that an active injury/inflammatory process is occurring in the myocardium of the sunitinib-treated mice.

Myocardial hypertrophy and fibrosis have been reported to occur as a consequence of sunitinib administration (Chintalgattu et al., 2013; Chu et al., 2007; Kerkela et al., 2009; Maayah et al., 2014). While the onset of hypertrophy is the result of adaptive changes in the myocardium as a compensatory response to stress (Frey et al., 2004), fibrosis results

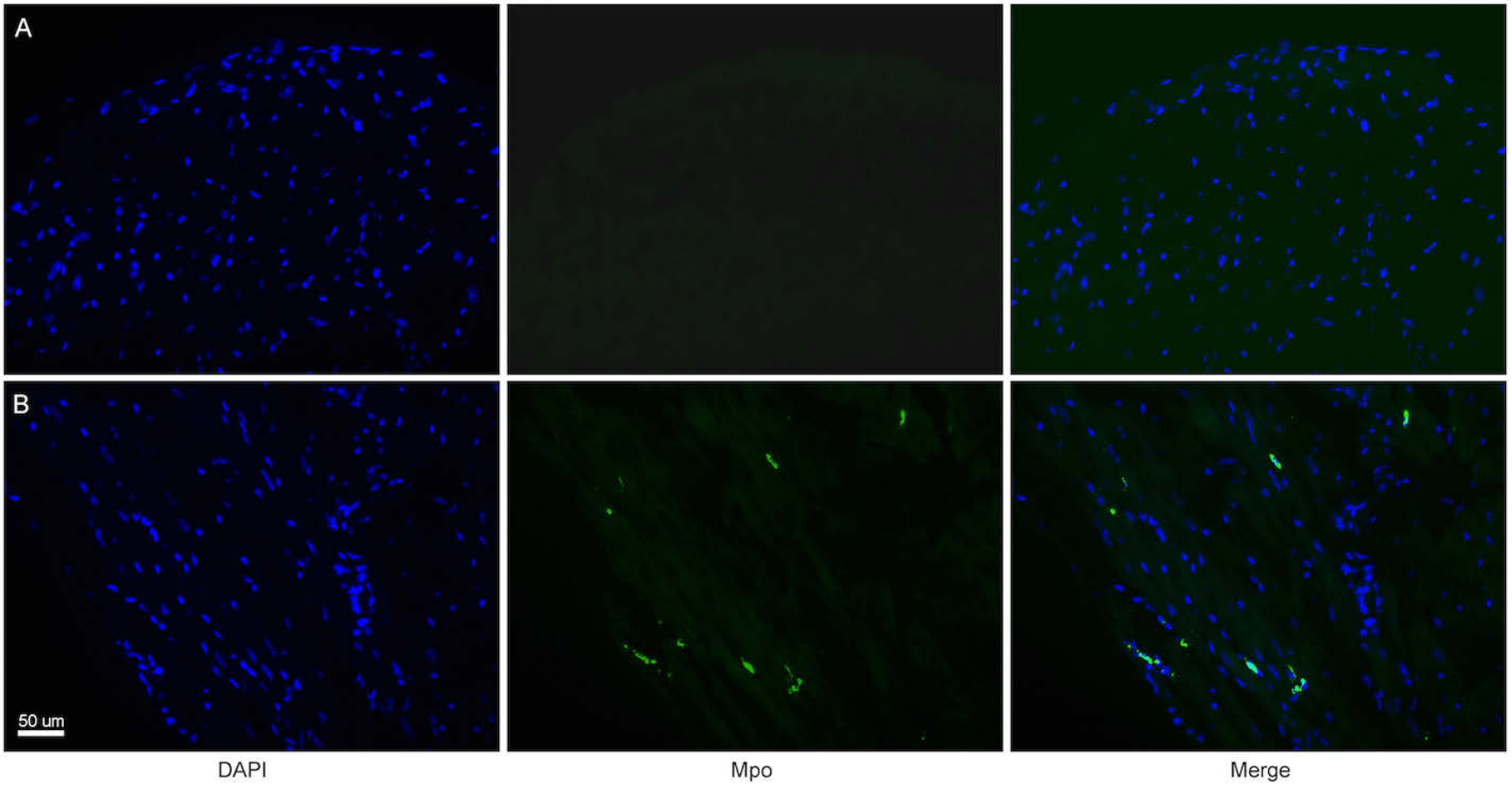

Figure 8. Neutrophil staining of heart sections of sunitinib-treated with 80mg/Kg and control C57BL6 male mice. Frozen sections (5 μm) were immunostained with an anti-myeloperoxidase 1 (MPO-1) antibody. Neutrophils are stained green and cell nuclei blue (DAPI), panel A: untreated controls; panel B: sunitinib-treated. Scale bar is 50 μm.

from excessive accumulation of extracellular matrix components (mostly collagen) typically triggered by tissue injury and remodeling (Fan et al., 2012). Both, hypertrophy and fibrosis are associated to myocardial dysfunction and disease (Fan et al., 2012; Frey et al., 2004). An analysis of the heart weights, individually normalized against the total body weight, showed no differences between the sunitinib- and the vehicle-treated animals (Figure 9), demonstrating the absence of overt myocardial mass increase. The expression of *Cyp1a1*, a gene overexpressed in sunitinib-induced hypertrophy (Maayah et al., 2014), was moderately upregulated almost reaching statistically significance (Figure 10). In contrast, the expression of *Fgf21*, a member of the fibroblast growth factors family produced by cardiomyocytes, which protects against cardiac hypertrophy (Planavila et al., 2013), was slightly (but non-significantly) decreased. Taken together, these results may be interpreted as an indication of an early-stage hypertrophy process.

Masson's trichrome staining of cardiac sections (Figure 11) revealed a mild but clear interstitial accumulation of collagen fibers in the myocardium, indicative of emerging fibrosis as a result of the sunitinib treatment. In keeping with this, the expression of the collagen type I alpha 1 gene (*Col1a1*) was upregulated (Figure 10). The amphiregulin gene (*Areg*), an epidermal growth factor receptor ligand mitogenic for fibroblasts which has been previously implicated in fibrosis (Perugorria et al., 2008; Shoyab et al., 1989; Zhou et al., 2012), was also significantly upregulated (Figure 10). However, we were unable to detect any change in the expression of transforming growth factor beta (*Tgfb1*), a major driver of fibrosis in the heart and other tissues (Fan et al., 2012).

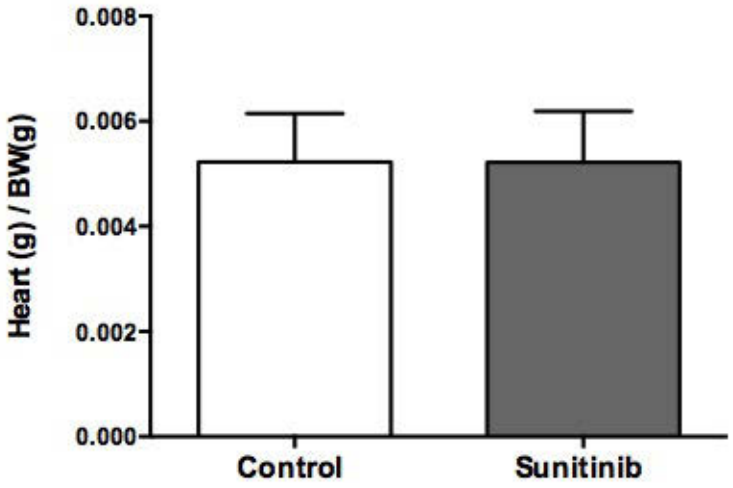

Figure 9. Relative weights of C57BL6 male mice hearts after 4 weeks of oral administration with water or sunitinib 80 mg/Kg. Relative heart weights (Heart (g)/BW(g)) are expressed as the ratio between heart weight *vs* the body weight (BW) of the animal. The graph shows the means and standard errors.

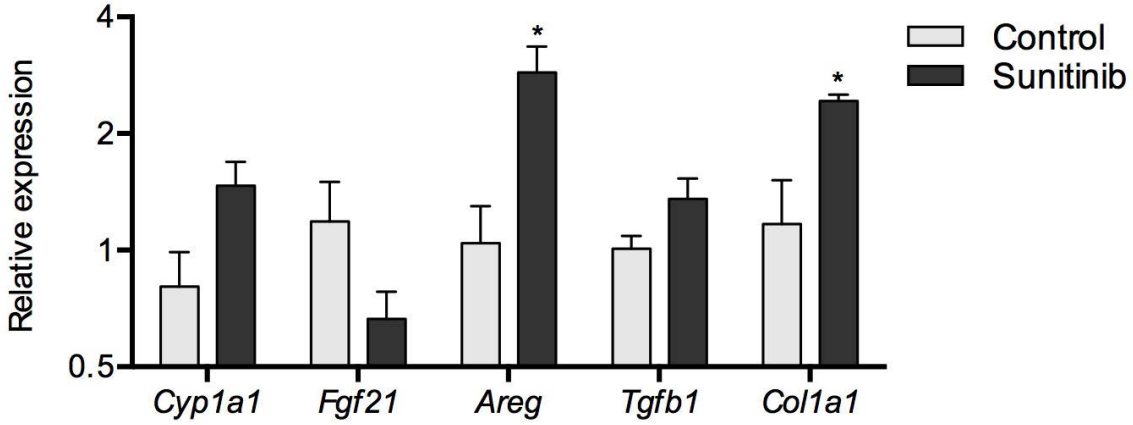

Figure 10. Relative transcript levels of hypertrophy- and remodeling-related genes in the left ventricle of C57BL/6 male mice after 4 weeks of treatment with water (control) or sunitinib 80mg/Kg. The data was generated by qPCR; the graph shows the means and standard errors. The genes evaluated were cytochrome P450, family 1, subfamily a, polypeptide 1 (*Cyp1a1*), fibroblast growth factor 21 (*Fgf21*), amphiregulin (*Areg*), transforming growth factor beta 1 (*Tgfb1*) and collagen type I alpha 1 (*Col1a1*). The asterisks denote statistical significant differences between the sunitinib-treated and control groups as determined by Student's t-test, (*) $p < 0.05$.

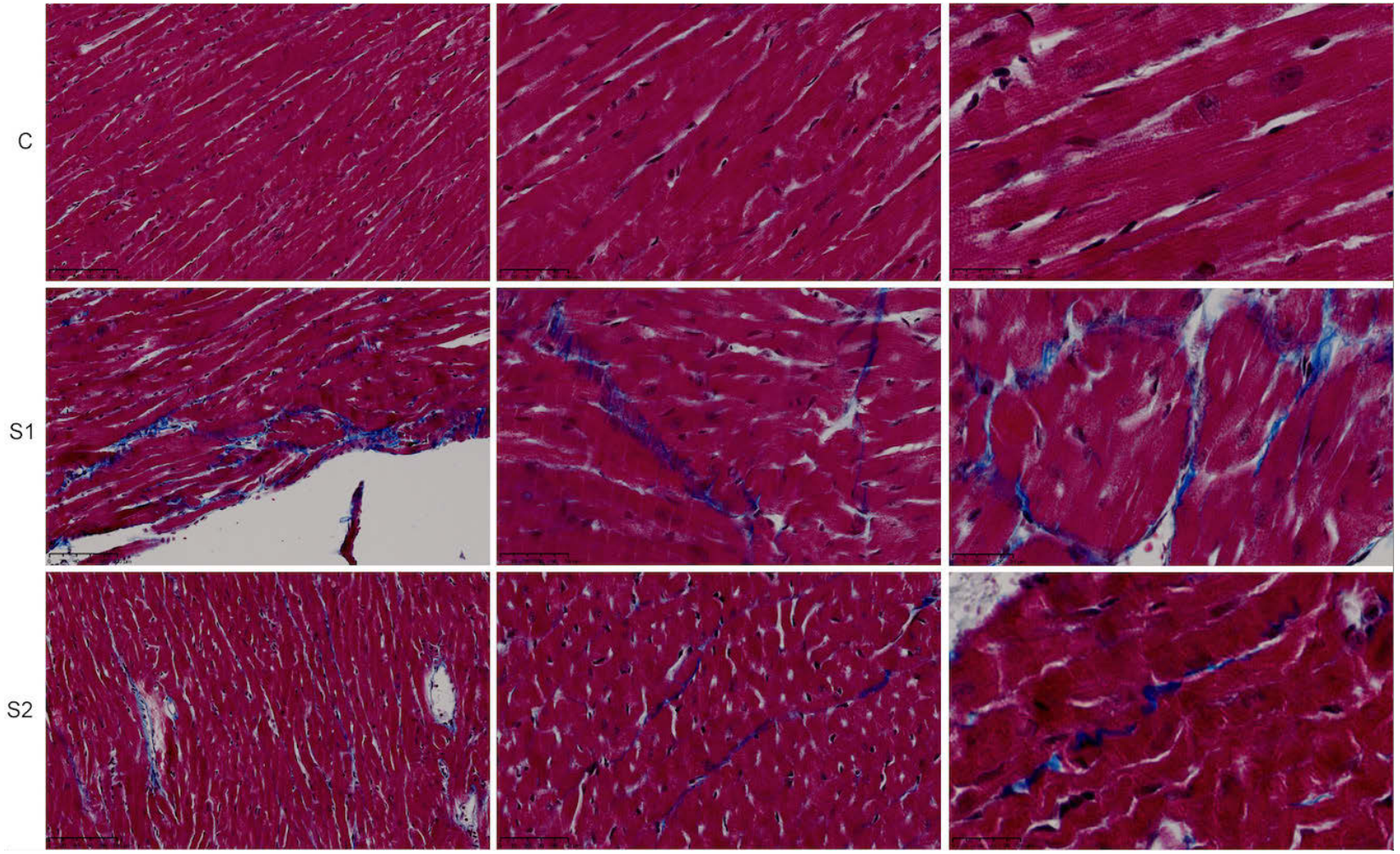

Figure 11. Masson's trichrome staining of cardiac tissue from representative C57BL/6 male mice orally administered vehicle (C) or sunitinib 80 mg/Kg for 4 weeks (S1 and S2). Collagen accumulation appears stained in blue. Scale bars are 100 μm (left panel), 50 μm (central panel) and 25 μm (right panel).

Mitochondrial dysfunction has a well-known role in cell and tissue injury, inflammation and remodeling (Kumar et al., 2013). Previous studies performed in humans, mice and cultured cardiomyocytes have reported that sunitinib induces mitochondrial damage (Kerkela et al., 2009; Monsuez et al., 2010). This is an specially important aspect of the deleterious effects of sunitinib, not only due to the toxic nature of mitochondrial injury but also because of the crucial role of the mitochondria in the coordination and functioning of cellular energy metabolism, to which the heart is particularly sensitive (Finck, 2007; Jaswal et al., 2011; Scolletta and Biagioli, 2010). Defects in mitochondrial biogenesis and function are thought to underlie energetic alterations in cardiovascular pathophysiology (Rimbaud et al., 2009; van Bilsen et al., 2004).

Ultrastructural analysis of left ventricular sections by transmission electron microscopy showed clear signs of cardiomyocyte damage in sunitinib-treated animals. Figure12 shows the appearance of empty cytoplasmic spaces between cardiac myofibrils as well as altered mitochondria with ruptured membrane and partial loss of mitochondrial matrix. In addition, Figure 13 shows the appearance of septae in the mitochondria, an event typically seen in skeletal and cardiac muscle injury (Duncan and Shamsadeen, 1991). Although myofibrils were well oriented and the sarcomere were properly defined (Figure 14A), we observed numerous degenerated, swollen mitochondria with reduced or vanished matrix and effaced cristae (Figure 14B) as well as an abundance of intra-mitochondria membranes whorls. Numerous sarcoplasmatic lipid droplets were also detected, in close contact with adjacent mitochondria (Figure 15).

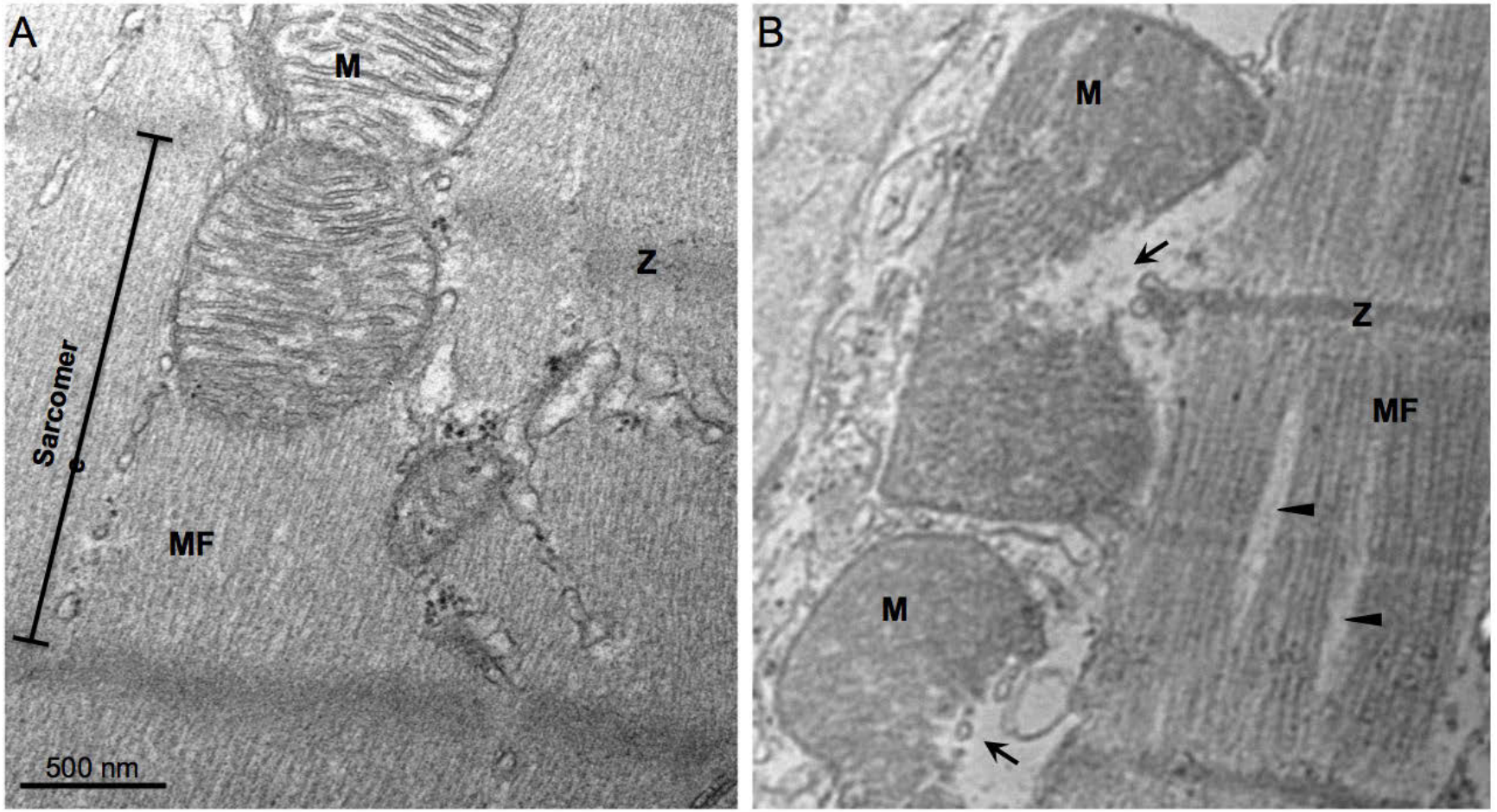

Figure 12. Transmission electron micrograph of the left ventricle of C57BL6 male mice after 4 weeks of treatment with water (A) or sunitinib 80mg/kg (B). Mitochondria (M), myofibrils (MF), Z line (Z). The arrows indicate broken mitochondria with reduced or vanished matrix and disrupted crests. Arrow heads show cytoplasmic voids between the cardiac myofibrils.

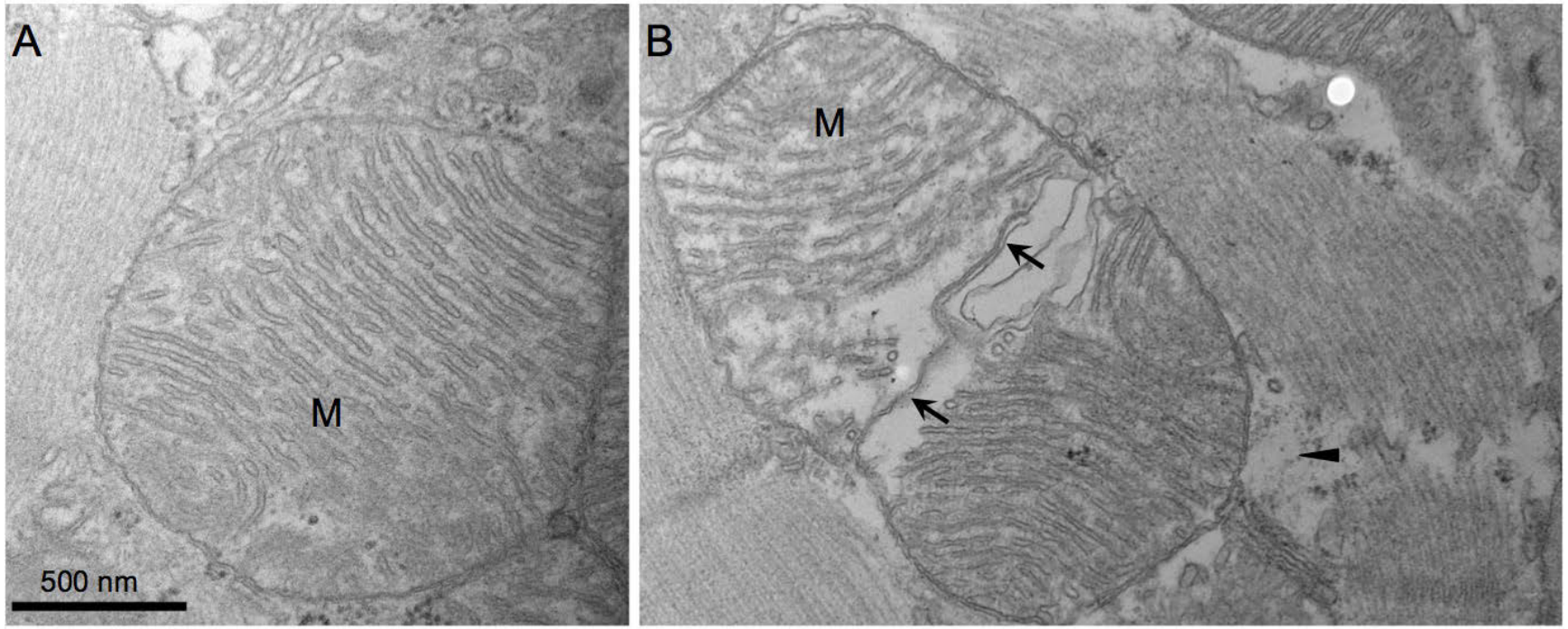

Figure 13. Transmission electron micrograph of the left ventricle of C57BL6 male mice after 4 weeks of treatment with vehicle (A) or sunitinib 80mg/kg (B). Mitochondria (M). The arrows indicate a mitochondrial septum. Arrow head shows a zone of cytoplasmic loss.

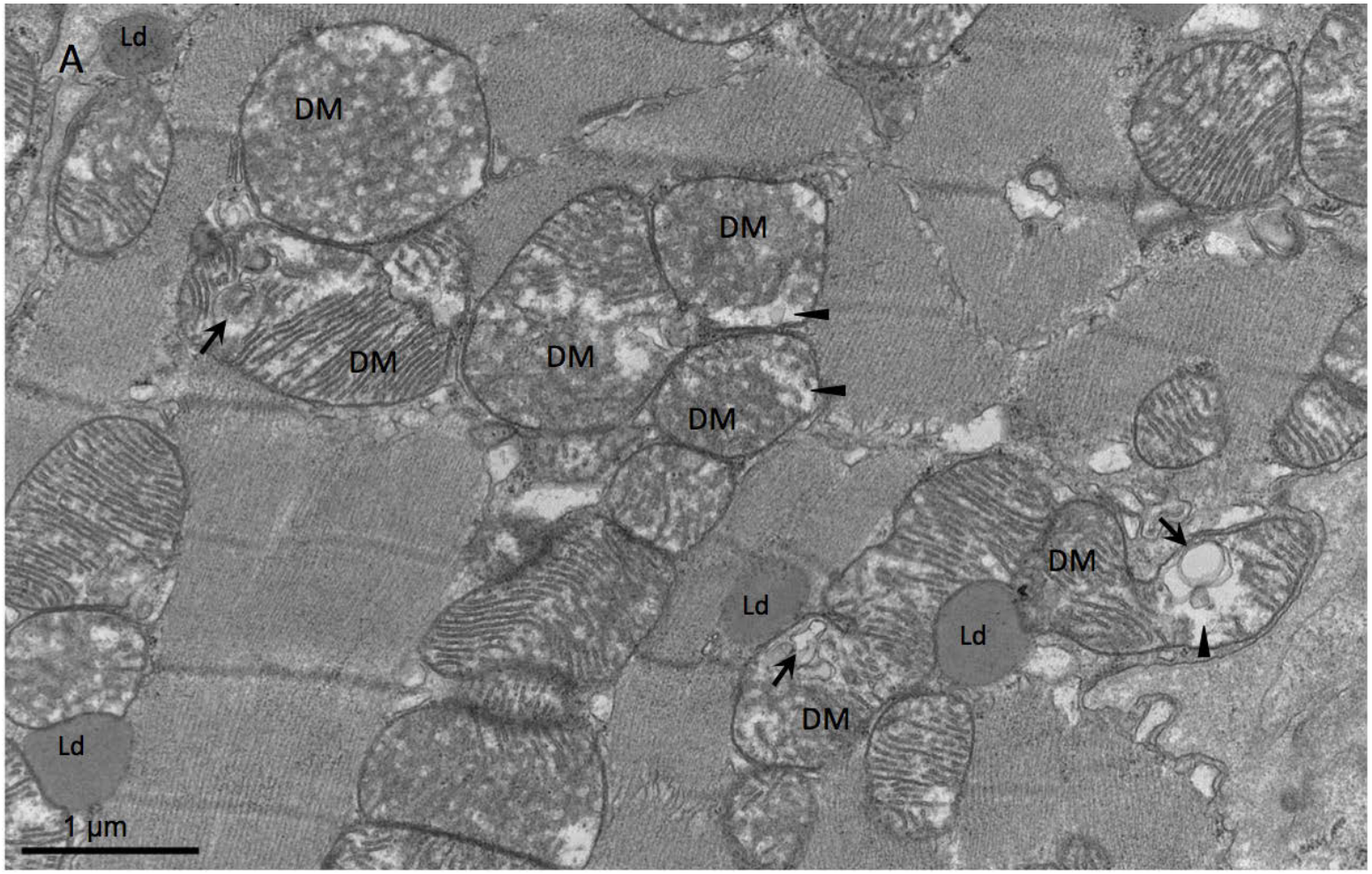

Figure 14A. Transmission electron micrograph of left ventricle from C57BL6 male mice after 4 weeks of treatment with sunitinib 80mg/kg. Degenerating mitochondria (DM) and lipid droplets (Ld) are indicated. The arrows indicate intra-mitochondria membrane whorls. Arrow heads point to vanished mitochondrial matrix.

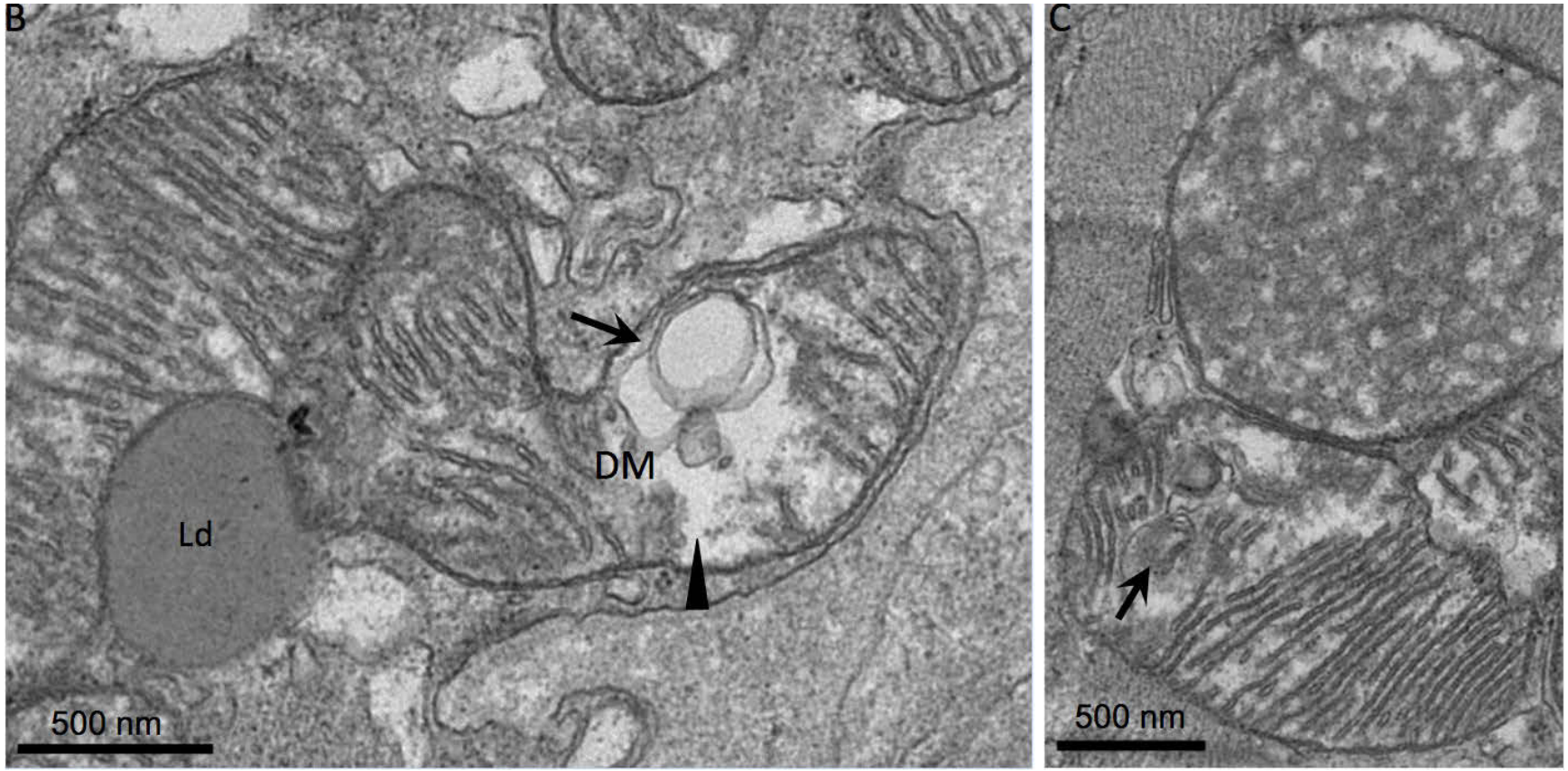

Figure 14B-C. Transmission electron micrograph of the left ventricle of C57BL6 male mice after 4 weeks of treatment with sunitinib. Degenerating mitochondria (DM) and lipid droplets (Ld) are indicated. The arrows indicate intra-mitochondria membrane whorls. Arrow heads point to regions of vanished mitochondrial matrix.

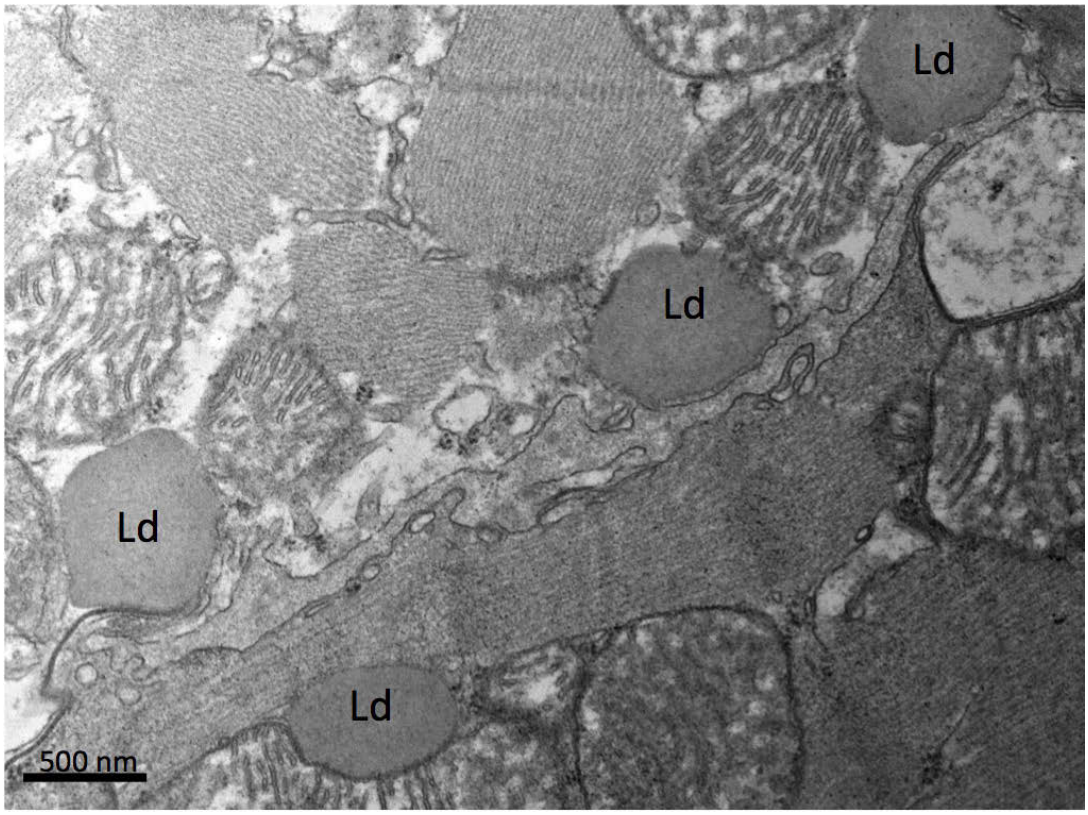

Figure 15. Transmission electron micrograph of left ventricle of C57BL6 male mice after 4 weeks of treatment with sunitinib. Lipid droplets (Ld) are indicated.

The ultrastructural mitochondrial alterations revealed by transmission electron microscopy indicated the possibility of generalized mitochondrial dysfunction in sunitinib-treated animals. Since perturbations of cardiac energy metabolism are a significant factor in cardiac myopathies (Finck, 2007), we evaluated the relative expression of a selected group of genes involved in cellular and mitochondrial function and energy metabolism (Table 1). We targeted genes coding for important components of the mitochondrial electron transport chain complexes III and IV, fatty acids transport and oxidation as well as proteins involved in cellular glucose transport and metabolism. In addition, several transcription factors with described key roles in the control of substrate metabolism were also studied.

The gene expression analyses in Figure 16 show no changes in the relative expression of *Cox4i1*, *Cox5b* and *Uqcrc1*, involved in mitochondrial respiration, suggesting that expression of those genes was insensitive to our 4-weeks sunitinib treatment. However, the expression of *Ucp2* and *Ucp3* decreased in treated animals, reaching significant levels for *Ucp3*. These genes code for the uncoupling proteins 2 and 3 respectively, which are members of the anion carrier proteins superfamily present in the inner mitochondrial membrane and which regulate mitochondrial membrane potential, and therefore, ATP synthesis and reactive oxygen species (ROS) production (Laskowski and Russell, 2008; Perrino et al., 2013). Reduction in the levels of UCP3 can lead to exacerbated ROS production and cardiomyocyte damage (Perrino et al., 2013).

Out of the genes tested involved in substrate metabolism (Figure 17) neither the glucose

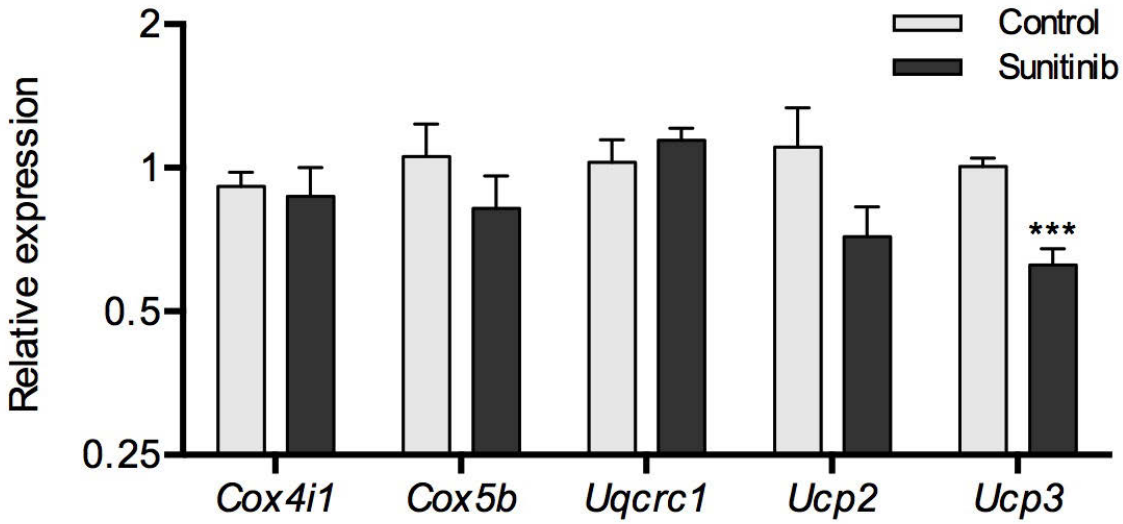

Figure 16. Relative transcript levels of mitochondrial genes in the left ventricle of C57BL/6 male mice after 4 weeks of treatment with water (control) or sunitinib 80mg/Kg. The data was generated by qPCR; the graph shows the means and standard errors. The genes evaluated were cytochrome c oxidase subunit IV isoform 1 (*Cox4i1*), cytochrome c oxidase subunit Vb (*Cox5b*), ubiquinol-cytochrome c reductase core protein 1 (*Uqcrc1*), uncoupling protein 2 (*Ucp2*) and uncoupling protein 3 (*Ucp3*). The asterisks denote statistical significant differences between the sunitinib-treated and control groups as determined by Student's t-test, (***) $p < 0.001$.

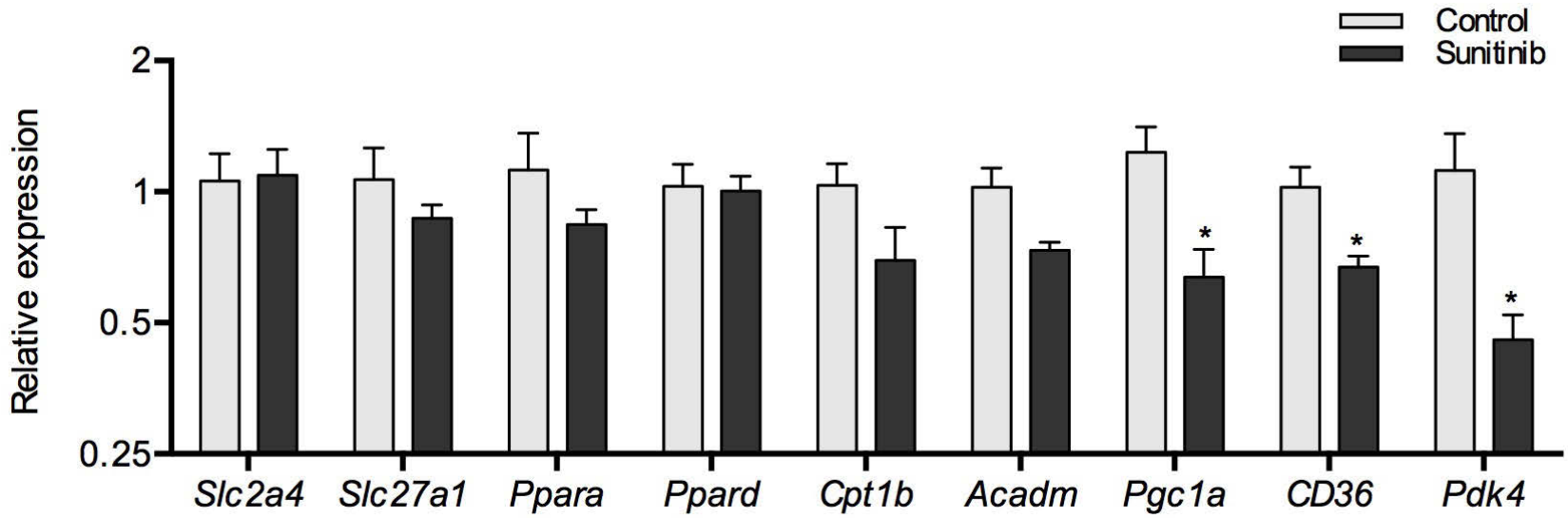

Figure 17. Relative transcript levels of metabolism-related genes in the left ventricle of C57BL/6 male mice after 4 weeks of treatment with water (control) or sunitinib 80mg/Kg. The data was generated by qPCR; the graph shows the means and standard errors. The genes evaluated were solute carrier family 2 (facilitated glucose transporter), member 4 (*Slc2a4*), solute carrier family 27 (fatty acid transporter), member 1 (*Slc27a1*), peroxisome proliferator activated receptor alpha (*Ppara*), peroxisome proliferator activator receptor delta (*Ppard*), peroxisome proliferative activated receptor, gamma, coactivator 1 alpha (*Pgc1a*), carnitine palmitoyltransferase 1b (*Cpt1b*) acyl-Coenzyme A dehydrogenase, medium chain (*Acadm*), CD36 antigen (*Cd36*) and pyruvate dehydrogenase kinase, isoenzyme 4 (*Pdk4*). The asterisks denote statistical significant differences between the sunitinib-treated and control groups as determined by Student's t-test, (*) $p < 0.05$).

transporter *Slc24a* (Glut4), the fatty acid transporter *Slc27a1* nor the peroxisome proliferator activated receptors alpha and delta (*Ppara* and *Ppard*) showed any expression changes. *Cpt1b* and *Acadm* were moderately (but non-significantly) downregulated. CPT1B is the main long-chain fatty acid transporter in cardiomyocyte's mitochondrial external membrane and is the rate-limiting step in mitochondrial β-oxidation (He et al., 2012). *Acadm* codes for MCAD, an acyl-coenzyme A dehydrogenase essential for the oxidation of medium-chain fatty acids (Spiekerkoetter and Wood, 2010). Only *Pgc1a*, *CD36* and *Pdk4* displayed an statistically significant alteration of expression. PGC1alpha is a co-activator of transcription that is fundamental for the selection of substrate utilization in the heart and has been found downregulated in heart failure in humans and animal models (Aubert et al., 2013). CD36 is a fatty acid transporter responsible for 40-60% of the cellular fatty acid uptake and a reduction on its cellular level can lead to the preferential use of glucose as a source of energy (Guzzardi and Iozzo, 2011). PDK4 (pyruvate dehydrogenase kinase 4) inhibits the conversion of pyruvate to acetyl-CoA and promotes the utilization of fatty acids as energy source. Conversely, if PDK4 levels are decreased, the use of glucose over fatty acids can be favored (van Bilsen et al., 2004).

These gene expression analyses suggest that the cardiac metabolism of fatty acids is being negatively affected in the sunitinib-treated group possibly promoting the occurrence of a metabolic switch in energy substrate utilization. That, together with the induction of tissue damage, inflammation and mitochondrial injury, indicate that the sunitinib treatment schedule and dosage used in the mouse model described here generated cardiac toxicity.

4.3. Evaluation of sunitinib-induced cardiac toxicity using PET

Alterations in myocardial function and energy metabolism are distinctive caracteristics of multiple cardiac diseases (Gropler, 2013; Herrero et al., 2007; Tokarska-Schlattner et al., 2006). Among the most common perturbations recognized in the course of heart disease are decreases of the LVEF and modifications in the usage of glucose or fatty acids as the main energy substrate (Jaswal et al., 2011). To explore the ability of PET to detect those signs of cardiotoxicity in our animal model, we performed ^{11}C-acetate and FDG PET imaging at days 0 and at days 6th or 7th of each week of treatment. ^{11}C-acetate was used to estimate MVO_2 as a reflection of the overall oxidative metabolism given the close connection between the tricarboxylic acid and oxidative phosphorylation (Peterson and Gropler, 2010). MVO_2 is a fundamental indicator of systolic functions such as heart rate, contractile state, and wall stress (Knaapen et al., 2007). We also utilized ^{11}C-acetate to measure the MBF, as a strong correlation between the relative uptake of ^{11}C-acetate with the relative MBF has been described (Jiji et al., 2012; Klein et al., 2001), and changes in MBF are associated with important perturbations in cardiac metabolism (Di Carli et al., 2000).

K_1 and K_2 values, representing MBF and MVO_2, respectively, were extracted using a three compartment kinetic analysis applied to PET ^{11}C-acetate dynamics. There were no statistically significant differences between treated animals with the pre-treatment values (Figure 18), except an unexplained difference for MVO_2 between pretreatment and scan 1. Furthermore, no differences in MBF and MVO_2 were observed between controls and animals treated with sunitinib during the 4 weeks of the study (Figure 18). These results

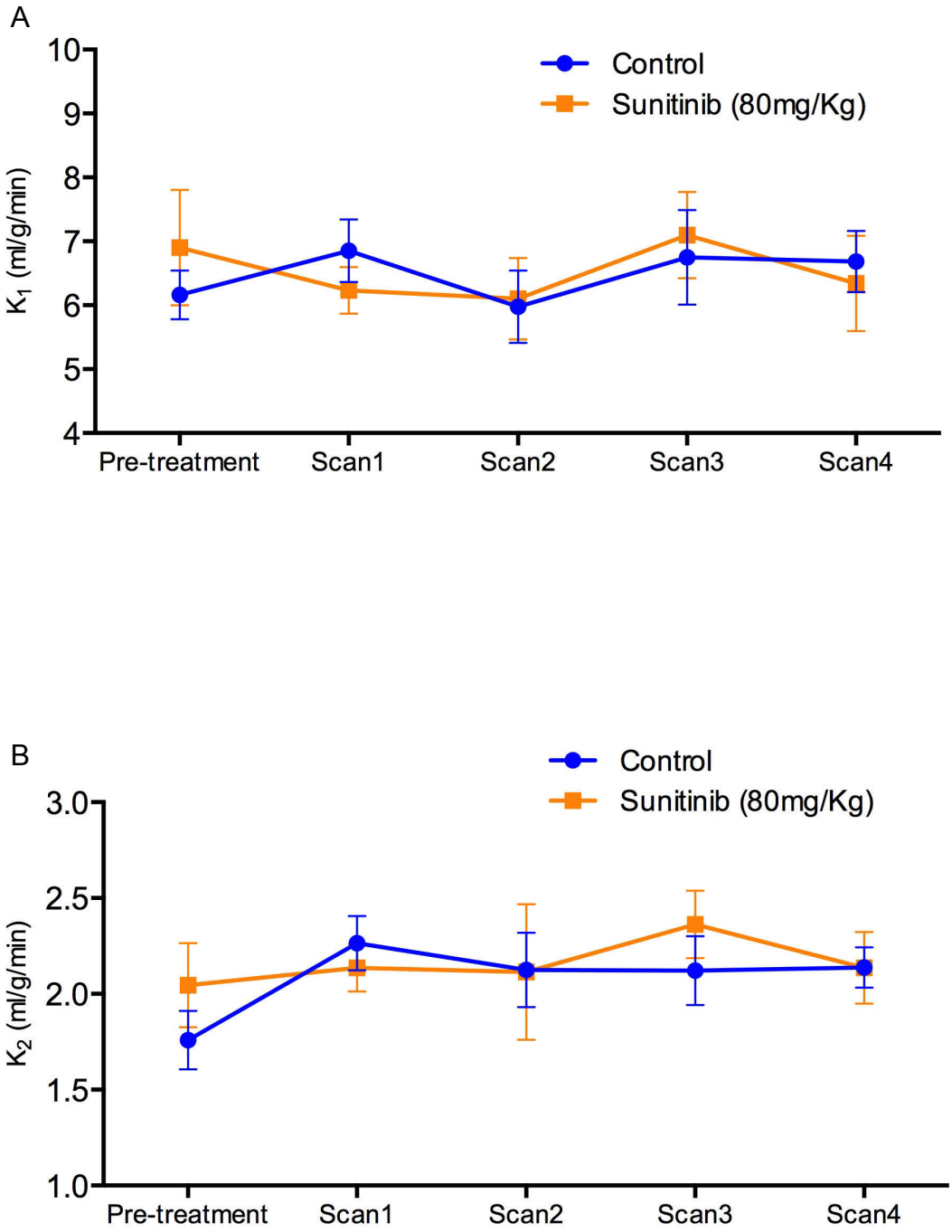

Figure 18. (A) Myocardial blow flow values (MBF) expressed as K_1 and (B) myocardial oxygen consumption (MVO_2) represented as K_2. Both variables were estimated from a three compartment kinetic analysis for ^{11}C-acetate obtained from C57BL6 male mice at pre-treatment and scans done each of four weeks of treatment with sunitinib (80mg/Kg). The graphs show the means and standard errors.

indicate either that there are not detectable perturbations in myocardial perfusion (K_1) and oxygen consumption (K_2), or that the PET protocol used in this study is unable to detect them.

The FDG influx constant (K_i) was determined by PET, as a measurement of myocardial glucose uptake. The mean K_i values obtained using Patlak analysis are shown in Figure 19. No significant differences were found either between pre- and post-treatment neither between control and sunitinib-treated groups. These results suggest that there are not detectable changes in myocardial glucose uptake as a consequence of the sunitinib treatment schedule used in our study.

Non-radioactive blood glucose levels are required to calculate the MMRG (Zhong et al., 2013). Blood glucose levels were determined by glucometer measurements right before the PET scans, the values obtained are shown in Figure 20. No differences were detected between the two groups or within each group. The values of K_i and blood glucose were used to calculate MMRG using Patlak analysis. The result shown in Figure 21 demonstrate that there are no significant differences in the metabolic rate of glucose between the controls and the sunitinib-treated animals.

In the clinical monitoring of cardiotoxicity and heart failure, the LVEF is used as the initial indicator of left ventricular dysfunction (Witteles et al., 2011). PET imaging in a syncronized dynamic gated acquisition with FDG was used to measure LVEF. Figure 22

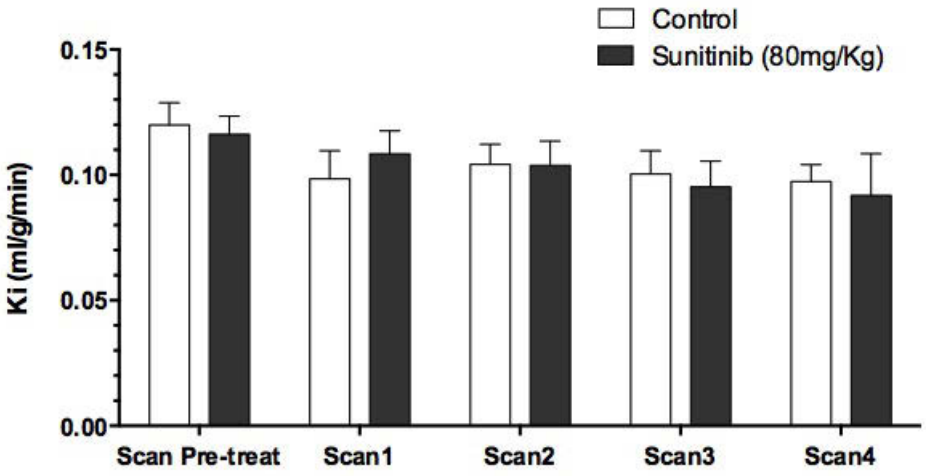

Figure 19. Myocardial FDG uptake (*K*i) for control and sunitinib-treated (80mg/Kg) C57BL/6 male mice. Data was obtained at pre-treatment and scans done each of four weeks of treatment with sunitinib. The graph shows the means and standard errors.

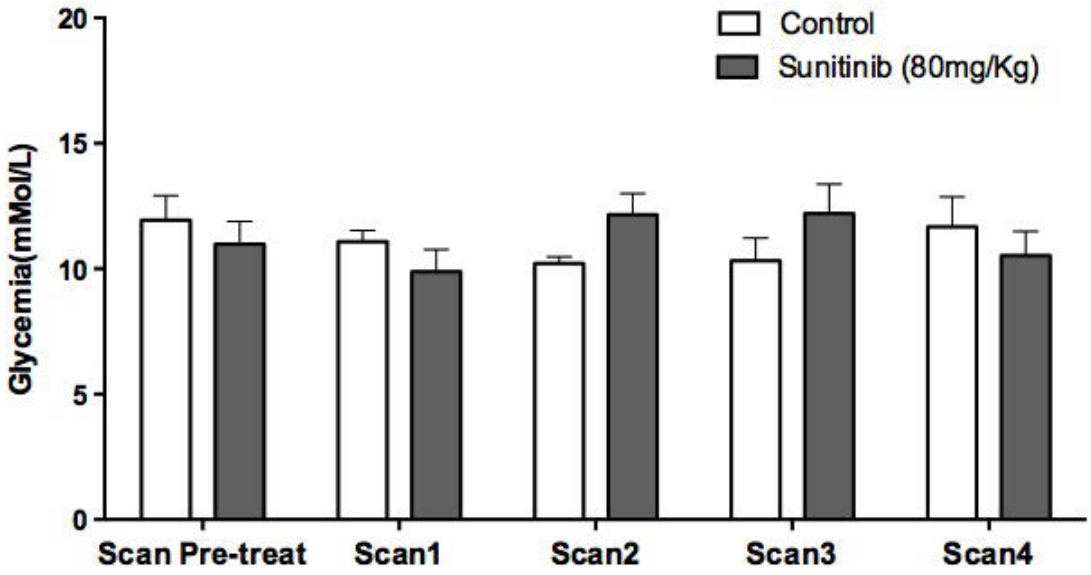

Figure 20. Blood glucose levels for control and sunitinib-treated (80mg/Kg) C57BL/6 male mice. Data was obtained at pre-treatment and scans done each of four weeks of treatment with sunitinib. The graph shows the means and standard errors.

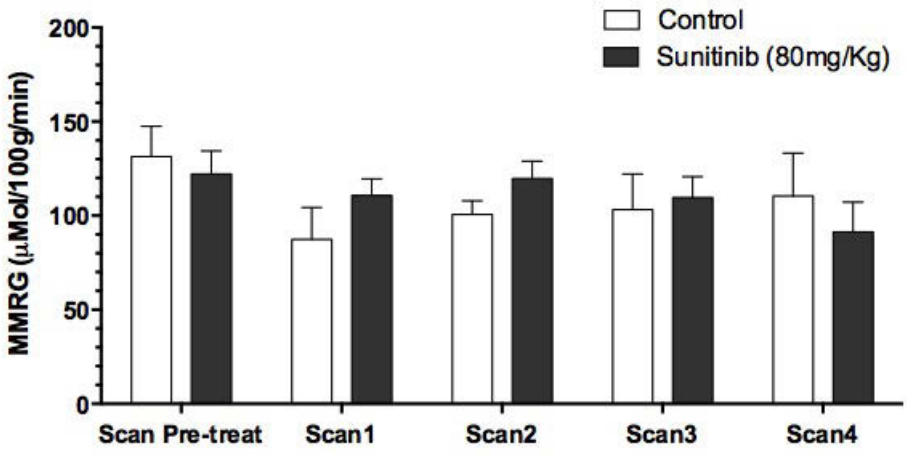

Figure 21. Myocardial metabolic rate of glucose (MMRG) for control and sunitinib-treated (80mg/Kg) C57BL/6 male mice. Data was obtained at pre-treatment and scans done each of four weeks of treatment with sunitinib. The graph shows the means and standard errors.

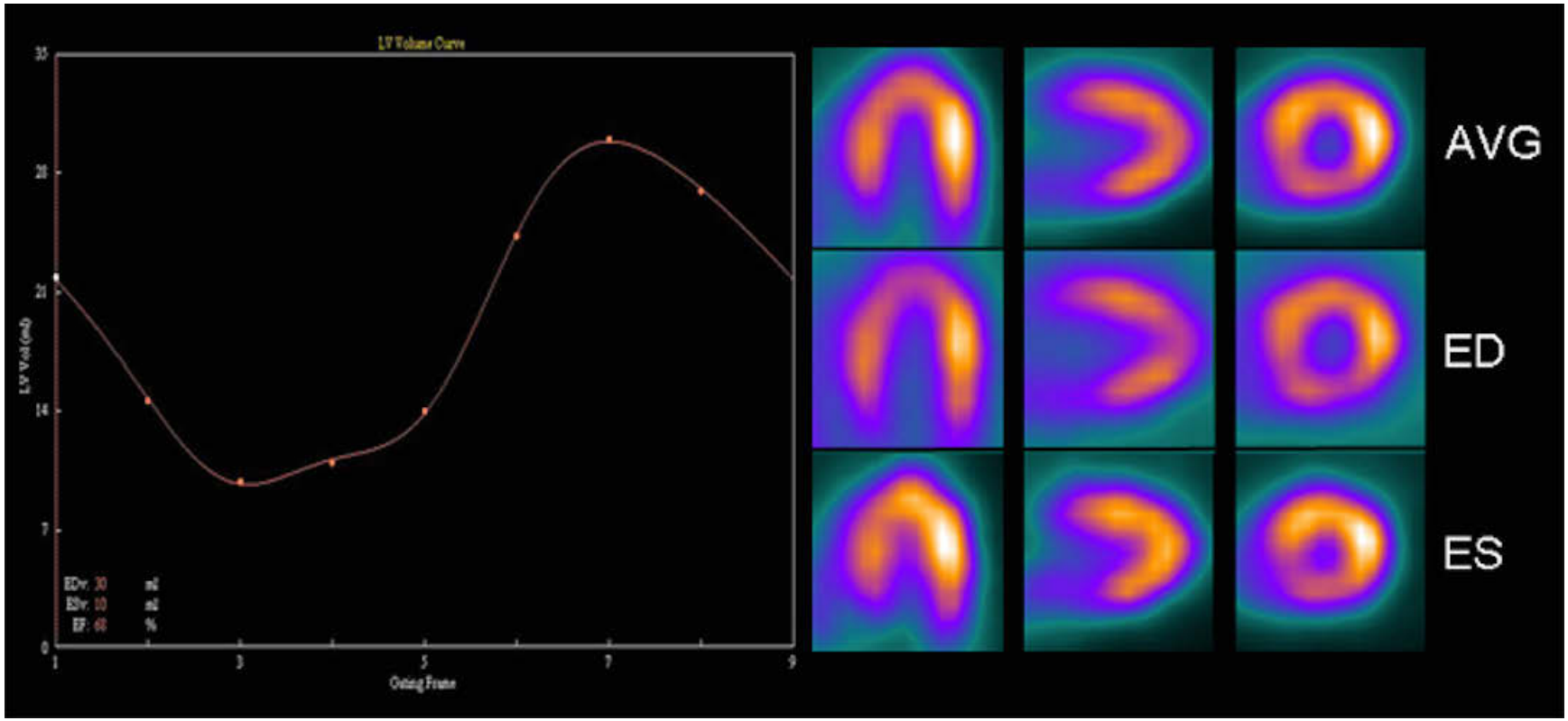

Figure 22. Cardiac images of C57BL6 male mice treated with sunitinib 80 mg/kg, 30 minutes after intravenous administration of 13.3 MBq of FDG. The images shown were obtained from a synchronized acquisition with the mouse electrocardiogram signal. AVG = average; ED = end of diastole; ES = the end of systole.

shows the cardiac images obtained with a sequence of images synchronized into eight electrocardiogram gates for a representative mouse from the sunitinib-treated group. The data obtained in these curves are used to generate the ejection fraction values. The pre-treatment LVEF values fell within the range reported for mice in previous studies (Lightfoot et al., 2010; Stegger et al., 2009; Zhong et al., 2013) and did not differ between the two groups (Figure 23). Throughout the experiment, the LVEF values were stable in the control group and no significant differences were found when compared against the pre-treatment values (Figure 23). However, sunitinib-treated mice showed a significant and progressive decrease in LVEF with respect to the control group, starting the first week of treatment. The average LVEF fell from a pretreatment value of 74.43 ± 0.9 % to 63.60 ± 2.0% at the end of the fourth week of treatment with a maximum drop of 10.83 %. These results reveal that the sunitinib treatment used in this study cause cardiac toxicity evidenced by a significant reduction in the LVEF and detectable by FDG-PET imaging.

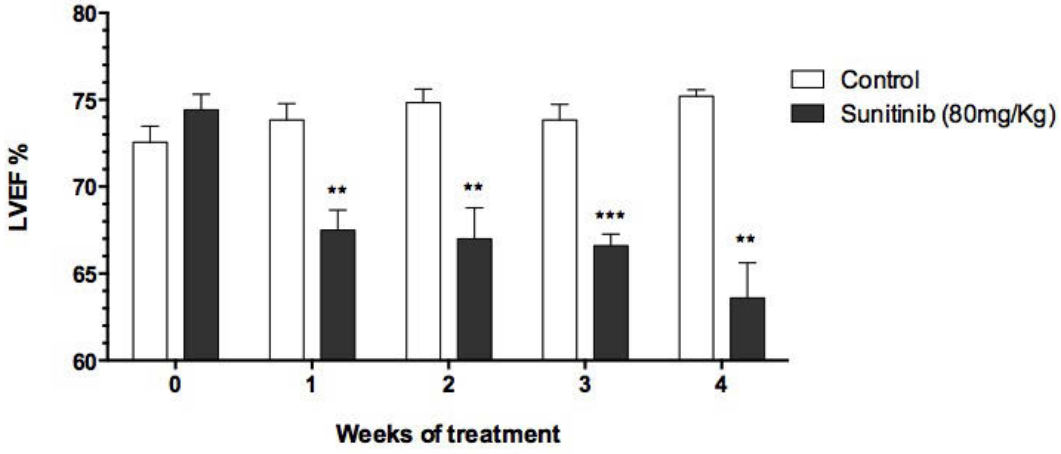

Figure 23. Left ventricle ejection fraction (LVEF) of C57BL6 male mice at 0 (pre-treatment), 1, 2, 3 and 4 weeks of treatment with sunitinib 80mg/Kg. LVEF were obtained by cardiac PET imaging in a syncronized dynamic gated with FDG. The graph shows the means and standard errors. The asterisks denote statistical significant differences between the sunitinib-treated and control groups as determined by Student's t-test, (*) $p < 0.05$), (**) $p < 0.01$) and (***) $p < 0.001$).

5. DISCUSSION

Cardiovascular diseases and cancer are the two leading causes of death by non-communicable diseases in high-income countries (World Health Organization). In Canada, they accounted for 49.6% of all deaths in 2011 (Statistics Canada, 2014). Ironically, many therapies that offer a higher chance of survival to cancer patients, have the side effect of a significant risk for cardiac toxicity and the development of cardiac clinical conditions. As heart failure is the ultimate fate of cardiac damage, this is an important complicating aspect of anti-cancer therapies, for which a solution is urgently needed.

Sunitinib has been a succesful anti-cancer drug, however, it can induce symptomatic grade 3 or 4 heart failure as early as 22 days after the initiation of treatment (Telli et al., 2008). In fact, cardiac damage is the top-second reason for interruption of sunitinib treatment (Witteles and Telli, 2012). In spite of significant efforts, it is not yet fully understood what renders some patients at risk of cardiac toxicity while others are rather unaffected (Abdel-Aziz, 2011). The biological complexity of cardiac physiology and metabolism pose a tremendous challenge for the detection of toxicity before it becomes symptomatic. In this regard, PET remains as one of the best monitoring alternatives due to its non-invasive nature and its recognized ability to probe metabolic aspects of myocardial function (Ong et al., 2014). However, PET protocols to detect early signs of toxicity and predict or avoid symptomatic heart damage are far from optimal in clinical practice.

In this study, we explored the use of ^{11}C-acetate and FDG PET for the early detection of cardiac metabolic and functional alterations during treatment with sunitinib. We utilized a mouse model of short-term sunitinib administration, which we characterized for several biological parameters, along with the ability of PET to detect changes in myocardial blood flow, oxygen consumption, glucose uptake, glucose utilization and left ventricular ejection fraction. Our PET results showed no significant changes in myocardial blood flow, oxygen consumption, glucose uptake or glucose utilization but we detected a significant and progressive reduction in the LVEF.

5.1. Cardiac contractile dysfunction

In this study, the LVEF fell since the first week of treatment, with a maximum drop of 10.83% at week four. Decreases of LVEF values have been recorded in 8-33% of patients treated with sunitinib (Blasi et al., 2012; Di Lorenzo et al., 2009; Mellor et al., 2011; Monsuez et al., 2010; Rainer et al., 2012; Richards et al., 2011; Steingart et al., 2012; Zambelli et al., 2011). A rapid onset of LV dysfunction (as the one observed by us) has been reported, sometimes with inconstant reversibility (Mellor et al., 2011; Monsuez et al., 2010), possibly explained by the two weeks off-treatment built into each cycle of four weeks-on/two weeks-off regularly used in the clinics. Although no specific guidelines have been established regarding LVEF drops, the clinical definition of cardiotoxicity produced by the Cardiac Review and Evaluation Committee that supervised the trastuzumab clinical trials (Seidman et al., 2002) has become the *de facto* standard (Albini et al., 2010; Gillespie et al., 2011; Wells and Lenihan, 2010). It considers a fall of LVEF to under a 55% absolute level, or a 10% decline as indicators of drug-induced cardiac toxicity (Seidman et al.,

2002). Moreover, according to new criteria of common terminology for adverse events recommended by Stanford Cardiology, a LVEF drop between 10%-19% is considered as left ventricle sytolic dysfuction and grade 2 heart failure (Witteles et al., 2011). Our results at the fourth week of treatment showing a decrease of over 10% in the LVEF are then indicative of cardiac toxicity after only one cycle of treatment.

The mechanisms of sunitinib-associated left ventricular dysfunction are not fully known. It is thought that it results from direct cardiomyocyte toxicity (Cohen et al., 2011) exacerbated by hypertension (Hutson et al., 2008). However, not all the patients that develop left ventricular dysfunction suffer from hypertension (Force and Kolaja, 2011), thus this association has been challenged and remains controversial (Mellor et al., 2011; Rini, 2007). Nevertheless, high blood pressure has been reported in multiple studies of sunitinib treatment (Chu et al., 2007; Di Lorenzo et al., 2009; Mellor et al., 2011); such hypertension is seen as the result of the anti-angiogenic effect of the drug, which ultimately leads to a decrease in capillary density and an increase of peripheral vascular resistance (Aparicio-Gallego et al., 2011; de Boer et al., 2010; Inai et al., 2004). Some authors have suggested that the etiology of hypertension may be also related to direct sunitinib renal toxicity and dysfunction, as hematuria (blood in the urine, reflective of renal damage) and nephrotic syndrome have been reported during therapy with sunitinib (Mori et al., 2010; Takahashi et al., 2012; Zhu et al., 2009). This is probably aggravated in patients with renal cell carcinoma (a patient population to which sunitinib is commonly administered) since they present a high (65.6%) prevalence of renal dysfunction.

Throughout our study, we did not detect blood in the urine, suggesting that the sunitinib dose and administration schedule used here did not induced significant renal damage in mice. We did not find blood pressure differences between treated and control groups, even though there was a significant LVEF drop. This suggests that (at least in our mouse model) there is not a clear relationship between hypertension and LVEF decrease. Similar results have been reported in some studies in humans (Chu et al., 2007; Telli et al., 2008) and a previous study using C57BL/6 mice treated with sunitinib at 40 mg/kg/day during 3 weeks, which failed to show any elevation of blood pressure that could be associated with cardiac dysfunction (Chintalgattu et al., 2013).

5.2. Cardiac tissue injury

LVEF is a functional parameter that can be affected by structural tissue damage. The histological assessment of our cardiac tissue samples showed only moderate pathological changes, which may nonetheless, be contributing to dysfunction. The nature of myocardial tissue injury during RTK inhibitor treatments has been poorly investigated and remains largely undefined (Schmidinger et al., 2008). Some data with RTK inhibitors that have been cardiotoxic in the clinic have shown no evidence of cardiac tissue damage in studies with animals, using routine histological examination (Yang and Papoian, 2012). On the other hand, heart lesions such as myocardial vacuolation and pericardial inflammatory infiltrates have been noted in rat models (French et al., 2010; Maayah et al., 2014; Mellor et al., 2011). We found mild fibroplasia with hemosiderophages, consistent with chronic microhemorrhage as well as abundant myofiber vacuolation and signs of early muscle degeneration with possible intracellular edema. Clear signs of inflammation and tissue

remodeling were also found, evidenced by the elevation of local gene expression of pro-inflammatory mediators, the infiltration of neutrophils into the cardiac tissue, the upregulation of genes involved in tissue remodeling and wound healing, and the deposition of collagen.

Inflammation is a protective mechanism that can be triggered by tissue injury, including in sterile conditions (Chovatiya and Medzhitov, 2014). It leads to the secretion of pro-inflammatory mediators such as TNFα, IL1β, nitric oxide (NO), *etc*; these mediators have been shown to be relevant in the context of heart damage (Hedayat et al., 2010). TNFα (whose gene we found upregulated) has been implicated in tissue damage (Yang et al., 2013) and reduction of cellular ATP (Spector et al., 2007), and it plays a key role in depression of myocardial contractility (Hedayat et al., 2010). IL1β (also upregulated in our study) exacerbates contractile dysfunction in synergism with TNFα, by promoting calcium leak from the sarcoplasmic reticulum, and together with other proinflammatory cytokines, induces the expression *Nos2* and the production of NO by cardiac myocytes (Bracey et al., 2013; Hedayat et al., 2010). Interestingly, the expression of IL6, a cytokine previously reported to both improve and deteriorate cardiovascular performance (Hedayat et al., 2010), is downregulated. The reason(s) for *Il6* downregulation and the potential biological significance of it are unclear.

The increased expression of several pro-inflammatory factors can help explaining the structural (tissue injury) and functional (decreased LVEF) damage seen in our sunitinib-treated animals. In fact, since the postulation of the "cytokine hypothesis" by Seta *et al.* in

1996 (Seta et al., 1996), the role of inflammation in heart damage has been well established and it is widely viewed today as a central contributor to the pathogenesis and progression of heart failure (Hedayat et al., 2010). Injury and inflammation are inextricably linked and typically trigger a remodeling response characterized by extracellular matrix deposition. If sustained, this response may evolve into fibrosis, which represents a major pathophysiological trait of harmful left ventricular remodeling and constitute a hallmark feature of the hypertrophic response (Aoyagi and Matsui, 2011; Strayer and Rubin, 2014).

The vast majority of cells in the heart are fibroblasts (Aoyagi and Matsui, 2011), they are also the main source of cardiac fibrillar collagen. Alterations in collagen abundance, isoforms, cross-linking patterns and recycling have been shown to play a key role in cardiac remodeling and progressive LV dysfunction (Hedayat et al., 2010), possibly by increasing muscle stiffness and interfering with systolic contraction and diastolic relaxation, as well as impairing diffusion of oxygen and nutrients (Ho et al., 2014; Strayer and Rubin, 2014). Fibrosis can also lead to remodeling of electrical conduction pathways in the heart, which is a major factor in the pathogenesis of cardiac arrhythmias (*e.g.*, atrial fibrillation and ventricular tachycardia), which are some of the cardiac adverse effects reported by sunitinib treatment in humans (Bello et al., 2009; Strayer and Rubin, 2014). We observed an increase in *Col1a1* gene expression and interstitial collagen deposition, a typical feature of myocardial injury (Lipshultz et al., 2013). Accompanying these, the expression of *Areg*, an EGFR ligand involved in the response to tissue mechanical loading in cardiomyocytes, fibroblasts, and vascular smooth muscle (Ye et al., 2013) was upregulated, as well as *Cyp1a1*, a marker of hypertrophy (Maayah et al., 2014), whereas

Fgf21, a cardio-protective fibroblast growth factor (Planavila et al., 2013), was downregulated. Surprisingly, the expression of the gene coding for TGFB1, a recognized factor in the development of fibrosis (Fan et al., 2012), was only slightly upregulated.

The results from FDG-PET clearly demonstrated that in the model used in this study, there is a significant fall of the LVEF detectable from the first week of treatment with sunitinib, which did not correlate with hypertension or renal damage. The microscopy and gene expression analyses performed here suggest that an emerging fibrosis/hypertrophy process is underway after four weeks of treatment but we are lacking data for the first weeks. The larger decrease on the LVEF at week four strongly suggests that these alterations are actively contributing to LV dysfunction at that time. However, given the time required for the development of fibrosis and hypertrophy, we believe it unlikely that they are major factors to LV dysfunction at the early phases of treatment.

In contrast to fibrosis and hypertrophy, the direct pharmacological effect of sunitinib over the activity of a wide range of cellular processes is more immediate. Sunitinib is known to cause hypothyroidism as early as 2 weeks after initiation of treatment (Collinson et al., 2011; Girardi et al., 2010; Kappers et al., 2011). The resulting reduction of triiodothyronine (T_3) levels impacts the expression of cardiac sodium-potassium adenosine triphosphatase (Na-K-ATPase) (Kamitani et al., 1992; Schmidinger, 2013) which may render the cardiomyocytes unable to maintain an adequate ionic balance leading to progressive intracellular water accumulation, cell swelling, vacuolation and damage. Also, the reduction of T_3 can lead to myocardial systolic and diastolic dysfunction by affecting the

expression of the sarco(endo)plasmatic reticulum cardiac ion pump SERCA2A (Ca^{2+}-ATPase exchanger), which regulates cardiac contraction and relaxation by controlling the intracellular concentration of Ca^{2+} (Force and Kolaja, 2011; Muller et al., 2003; Schmidinger, 2013). As we did not evaluate these parameters, we can not provide an assessment of whether they were contributing factors to the observed LV dysfunction.

5.3. Cardiac metabolism

Sunitinib inhibits the AMP-activated protein kinase (AMPK), a central regulator of cellular metabolism and ATP utilization (Greineder et al., 2011; Schmidinger et al., 2008). In the presence of sunitinib, ATP binding to AMPK is blocked and therefore it is unable to transfer ATP to substrates, interfering with the activation of energy-conserving mechanisms and aggravating energy depletion (Kerkela et al., 2009). ATP concentration has been previously found significantly reduced in cardiomyocytes exposed to sunitinib (Hohenegger, 2012). This is hardly surprising considering the inhibition of AMPK and the profound structural and functional mitochondrial abnormalities uncovered in patients and in treated cardiac cells in culture (Kerkela et al., 2009). Compelling evidence suggests that increased mitochondrial damage and dysfunction are a common denominator in cardiovascular disease development (Ballinger, 2005). The mitochondrial alterations reported in the literature include swelling, loss of normal architecture, disruption of cristae, cavitation of matrix and increased number of electron-dense matrix deposits (French et al., 2010; Kerkela et al., 2009; Montaigne et al., 2012). We found similar mitochondrial injuries in samples from sunitinib-treated animals after four weeks of treatment, which

support the notion of cellular and mitochondrial damage and it is suggestive of abnormalities in cardiac energy metabolism.

Perturbation of cardiac energy metabolism has multiple consequences including a reduction in the capacity and efficiency of mitochondrial respiration and ATP production (Aubert et al., 2013). We found a decrease in the expression of the uncoupling proteins *Ucp2* and *Ucp3*, two critical enzymes directly involved in mitochondrial ATP production, Ca^{2+} uptake and fatty acid utilization (Essop et al., 2004; Laskowski and Russell, 2008; Perrino et al., 2013; Safari et al., 2014). UCPs levels are decreased by the known cardiotoxic drug doxorubicin (Perrino et al., 2013) and are often reduced in heart failure in humans and animal models (Laskowski and Russell, 2008). The lower expression of *Ucp2* and *Ucp3* may be an indication of decreased ATP production in sunitinib-treated hearts.

Myocardial metabolism has the ability to switch from utilization of its main substrate (long-chain fatty acids, (Kuge et al., 2008; Neely et al., 1972)) to glucose in response to myocardial injuries such as hypertrophy, ischemia and heart failure (Jaswal et al., 2011). While this metabolic switch initially serves an adaptive function, long-term inhibition of the major source of energy leads to an energetic compromised heart with diminished functional capacity and eventually, progression to heart failure (Dyck and Lopaschuk, 2006)**.** The expression profile of mitochondrial and metabolic genes that we observed in the sunitinib-treated mice hints to some defect in the metabolism of fatty acids as *Cd36*, *Pdk4* and *Pgc1a* genes were significantly downregulated, and other relevant genes (*Cpt1b*, *Acadm*) showed a slight, non-significant decrease. Although these results should be taken

with caution because we tested only a fraction of the relevant genes and studied regulation only at the transcriptional level, there is a trend to a lower expression that could be indicative of emerging fatty acid metabolic defects. This interpretation is further supported by the correspondence of our observations with published results showing that the adaptive switch of the injured heart to a preferential use of glucose aiming to maximize efficiency, is characterized by the downregulation of pyruvate dehydrogenase kinase isoforms (PDKs), uncoupling proteins (UCPs) and carnitine palmitoyltransferase-1 (CPT-1) (Ardehali et al., 2012).

However, we did not find indications by FDG-PET of an increase in glucose consumption, (MMRG) as it should have been expected. To determine MMRG, the blood glucose levels and K_i are required. Neither K_i nor the levels of blood glucose showed any change, for any group. An increase in K_i was anticipated because it has been reported to occur in the presence of contractile dysfunction (Sen et al., 2013). Furthermore, the relative expression of *Slc2a4* (GLUT4), a regulator of glucose uptake and the major glucose transporter isoform in the heart (Heather et al., 2013; Postic et al., 1994; Santalucia et al., 1999; Santalucia et al., 1992) was also expected to increase because substrate transport across the sarcolemma is the first regulated step in cardiomyocyte substrate metabolism (Heather et al., 2013) and the expression of this glucose transporter has been found increased when myocardial glucose utilization is promoted (Hamblin et al., 2009). Conversely, a reduced glucose uptake has been related with decrease levels of *Slc2a4* (Murray et al., 2006). Nonetheless, the *Slc2a4* gene was not upregulated in the animals under sunitinib administration, supporting the PET observation of a lack of increase in glucose utilization.

Moreover, we did not find changes in MVO_2 or MBF, which typically accompany the slowing down of cardiac fatty acid metabolism. Oxygen consumption is related to energy expenditure, (the amount of energy consumed from the substrate) (Guitierrez and Theodorou, 2012) and the ability of the heart to match oxygen supply to demand is a fundamental principle of myocardial flow regulation (Tawakol et al., 2003). Given our findings of a lowered LVEF in the treated group, and considering previous demonstration that the contractile state of the myocardium determines MVO_2 (Schwaiger and Wolpers, 1990), we predicted a reduction of MVO_2. It was asumed that sunitinib-induced contractile dysfunction (shown by decreased LVEF) would correlate with a metabolic switch with lower MVO_2 levels reflecting distortions in the oxidative metabolism but paradoxically, MVO_2 and MBF levels did not change with sunitinib treatment.

The reasons for these findings are unclear. The treatment used in this study was clearly toxic to animals as shown by hypoactivity, lower body weight and lower food consumption, all previously reported effects of sunitinib (Hipp et al., 2008; Tanaka et al., 2011). In addition, the histopathology, immunostaining and electron microscopy showed clear signs of structural cardiac damage. The fact that PET was able to reveal LVEF drops but failed to uncover any changes in MMRG, MVO_2 or MBF indicates the possibilities that those changes are not present or escaped detection by PET, as performed in this study. Our findings resemble what is known in cardiology as "stunned myocardium", a postischemic condition characterized by contractile dysfunction with normal perfusion and normal FDG uptake (Medical Advisory Secretariat, 2005). Stunning is a reversible condition that precedes the more severe "hibernating myocardium"; in hibernation, there is reduced

perfusion, contractile dysfunction, alteration of structural proteins and metabolism, cytoskeleton disorganization, myofilaments loss and sarcomeric instability (Anagnostopoulos et al., 2013; Medical Advisory Secretariat, 2005). Continuous or repetitive stunning can lead to hibernation and differentiating between them is complicated because they may coexist (Medical Advisory Secretariat, 2005). It can be speculated that early during treatment, sunitinib induces cardiac stunning and as the treatment progresses stunning evolves to a more severe and distinctive damage that involves clear metabolic dysfunction. This is a reasonable scenario, given our results and the fact that sunitinib induces the generation of oxygen radicals and disturbances of cellular Ca^{2+} homeostasis (Rainer et al., 2012), which are also considered the most plausible molecular bases of cardiac stunning (Bolli and Marban, 1999).

Yet, another revealing finding supports the idea of perturbations in the metabolism of fatty acids. Normally, cardiac myocytes do not accumulate lipid droplets, reflecting a finely-regulated equilibrium between lipid uptake and oxidation (Ge et al., 2012; Goldberg et al., 2012; van Herpen and Schrauwen-Hinderling, 2008). However, when the rates of uptake, synthesis and utilization are mismatched, the excess lipid is stored in cytoplasmic droplets (Goldberg et al., 2012; Olofsson et al., 2009). Impairment of cardiac fatty acid oxidation leads to intracellular lipid accumulation, which eventually becomes cytotoxic (Finck, 2007; Goldberg et al., 2012). Cardiac lipid accumulation, especially long-chain fatty acids, has been associated with contractile dysfunction (Abel, 2011; Fountoulakis et al., 2005; Park et al., 2007). Intracellular lipid deposit has been documented in heart biopsies from patients

treated with imatinib, another RTK inhibitor (Kerkela et al., 2006). We reported here that sunitinib induces accumulation of cytosolic lipid droplets in cardiomyocytes.

Being a multi-targeted RTK inhibitor, sunitinib binds to multiple cellular kinases (Fabian et al., 2005; Karaman et al., 2008) and has the potential to be cytotoxic in many different ways, in fact, it is thought that it has both on-target and off-target side effects (Force and Kolaja, 2011). That, together with our results, opens the possibility that the onset of LV dysfunction induced by sunitinib may occur in the absence of overt myocardial metabolic perturbation, at least at early stages of treatment. We performed treatment for only four weeks, thus it is possible that metabolic alterations had just begun to emerge and a longer treatment is required for them to be significant in this mouse model.

The biochemical mechanisms underlying the cardiotoxicity of RTK inhibitors remain poorly understood (Hall et al., 2013). Energy metabolism perturbations are widely accepted as major drivers of contractile dysfunction and heart failure (Huss and Kelly, 2005; Turer et al., 2010), but they are not considered the only cause of it. Other factors such as abnormalities in excitation-contraction coupling (arrhythmias, considered as one of the most serious immediate cardiac functional abnormalities), perturbations in the physiology of Ca^{2+}, and alterations in the synthesis and concentration of reactive nitrogen and oxygen species, which may lead to cellular damage, can also play a role (Berridge et al., 2013; Dasanu et al., 2012; Davies et al., 1996; Giordano, 2005; Hare and Stamler, 2005), more so considering that sunitinib for example, induces the generation of oxygen radicals and disturbances of cellular Ca^{+2} homeostasis (Rainer et al., 2012).

In summary, using FDG-PET, we documented early LV dysfunction (shown by a drop in the LVEF) in a mouse model of 5 days-on/two days-off sunitinib administration of 80 mg/Kg/day for four weeks. LV dysfunction did not correlate with hypertension, neither with changes in MMRG, MVO_2 or MBF during the time of the study, as determined by FDG- and ^{11}C-acetate-PET. Our results illustrate the biological complexity of the myocardial damage induced by sunitinib and highlight the need of further studies to understand its molecular bases and devise effective ways for its early detection.

6. CONCLUSIONS

Sunitinib is typically administered to patients in repeated cycles of 4 weeks-on/two weeks-off treatment, at doses of 50 mg/day. Administration is done every day during the 4 weeks on treatment. Cardiac damage has been observed in patients at different time points of the therapy, this together with the poor understanding of the pattern of events leading to toxicity, makes the prediction of whether and when the treatment will become cardiotoxic extremely difficult. Here we demonstrate that sunitinib administration of 80 mg/kg/day during 5 days per week, for 4 weeks caused cardiac toxicity in C57BL6 male mice, which makes it a useful model for the *in vivo* study of the mechanisms leading to the onset of cardiac damage.

In our model, sunitinib administration triggered LV dysfunction as early as one week after the beginning of treatment. This dysfunction was detected by FDG-PET and was manifested by a significant decrease of the LVEF, with a relative drop of more than 10% at the 4^{th} week of treatment. According to current classifications to evaluate drug-induced cardiac toxicity, this damage can be classified as grade-2 heart failure, which would indicate the need for further intervention during sunitinib clinical use.

Contractile dysfunction is almost invariably associated with perturbations in myocardial metabolism that cause defects in ATP production and lead to energetic stress. These defects can be reflected as changes in glucose metabolism, fatty acid metabolism and oxidative metabolism, which can be investigated using PET. Under the hypothesis that during

sunitinib treatment metabolic derrangements will precede contractile dysfunction, we evaluated changes in glucose metabolism (glucose uptake and MMRG) and oxidative metabolism (MVO_2) along with cardiac perfusion (MBF), as an approach to uncover any pattern of early alterations that could provide clues about the onset of toxicity. However, we did not detect changes in those metabolic parameters, as evaluated with FDG and ^{11}C-acetate PET, suggesting that LV dysfunction can arise in the absence of overt metabolic damage early during sunitinib treatment.

Other analyses revealed structural cardiac damage such as mild histopathological alterations and collagen deposition after 4 weeks of treatment with sunitinib. In addition, electron microscopy showed ultrastructural mitocondrial injury and deposition of cytoplasmic lipid droplets in the cardiomyocytes. The degree and frequency of these alterations suggest that they are just emerging at week 4 but this interpretation needs to be confirmed experimentally by similar analyses at early time points of the treatment. In addition, we found evidences of myocardial inflammation and remodeling by gene expression analyses and immunofluorescence, which may be interpreted as a reflection of tissue injury.

In summary, we have established a working model of sunitinib cardiac toxicity in mice; our study indicates that a 4-weeks treatment with sunitinib at 80mg/Kg/day in male C57BL/6 mice is sufficient to induce early left ventricular dysfunction that eventually progresses to grade-2 heart failure. We also showed that the early LV dysfunction does not correlate with overt alterations in cardiac glucose and oxidative metabolism detectable by FDG- and ^{11}C-

acetate-PET. Gene expression analyses and intracellular lipid droplets accumulation, detected at the end of the study, point to some defect in long-chain fatty acids utilization by the myocardium but this possibility needs to be addressed experimentally in separate studies.

7. PERSPECTIVES

The results presented here suggest that the 4-weeks treatment with sunitinib with the dose and schedule used did not trigger an overt metabolic damage neither a switch in substrate utilization detectable by ^{11}C-acetate and FDG-PET. Interestingly, we have been unable to find any published work reporting the occurrence of such a metabolic switch during sunitinib treatment. Since this is the first time that we use this model of sunitinib cardiotoxicity, we consider that a full characterization of the model is a critical step for future studies. We recommend several variations that can be applied alone or in combination, to explore the occurrence of metabolic, structural and functional toxicity and better characterize the nature of sunitinib-induced damage.

Based on the assumption that the histopathological and mitochondrial damage, and the changes in gene expression observed after four weeks of treatment are in the early stages, we recommend to extend the time of treatment as performed here for 1-2 more weeks and evaluate the same parameters. This may provide a clear indication regarding the timeline of appearance of metabolic derangements in this model. Also, an administration schedule of 7 days/week (which eliminates the 2 days-off/week used in this study) can be assayed as it is known that early stage damage by sunitinib may be reversible (Mellor et al., 2011; Monsuez et al., 2010).

An important aspect of the full characterization of the model will be the incorporation of in-depth gene expression and/or functional metabolic studies, as well as histopathological

assessments starting from the first week of treatment. These could be done either independently or in parallel with PET measurement of cardiac function and metabolic flux but in any case, they are decisive to generate independent data on sunitinib toxicity and to facilitate a better interpretation of any metabolic phenotype uncovered by PET. One key issue not addressed in our study is the monitoring of tyroid hormones (T_3 and T_4) levels. As discussed above, hypothyroidism is a known side effect of sunitinib and could be an important contributor to cardiac dysfunction by mechanisms not directly related to energy generation. Thyroid function can be evaluated by blood biochemistry, it can provide important information regarding contractile dysfunction that can ultimately complement PET results.

Cardiac PET using ^{11}C-acetate evaluates oxidative metabolism. However it is unable to provide direct data on fatty acids β-oxidation. This is a particularly interesting question given our results showing changes of expression in critical genes involved on fatty acids metabolism, and the accumulation of intracytoplasmic lipid droplets, which suggest the existence of alterations in the metabolism of long-chain fatty acids. To generate such data, a radiotracer such as ^{11}C-palmitate could be used; the kinetics of this long-chain fatty acid analog is identical to native, unlabeled palmitate thus it can provide direct information on β-oxidation (Heather et al., 2006; Peterson and Gropler, 2010; Tuunanen et al., 2008). These studies can be done in combination with the use of perhexiline, a potent inhibitor of carnitine palmitoyltransferase-1 (CPT-1) and carnitine palmitoyltransferase-2 (CPT-2) (Kennedy et al., 2000) as a positive control. Perhexiline shifts the metabolism from the use

of free fatty acids to glucose utilization (Barba et al., 2009; Lee et al., 2005) thus it can provide a clear signature of defective fatty acids metabolism.

8. ACKNOWLEDGEMENTS

I would like to thank my supervisor Dr. Roger Lecomte for allowing me to complete my Master's thesis in his lab. Also my co-supervisor Dr. Éric Turcotte for his help. My special thanks to Jacques Rousseau, Michel Paquette and Otman Sarrhini for their great contribution to this work.

I wish to thank Jean-François Beaudoin and Maxime Paillé for their technical support. I would also like to express my sincere appreciation to Dr. Guillaume Grenier, Vanessa Couture, Dr. Sheela Ramanathan, Dr. Subburaj Ilangumaran, Marian Mayhue, Dr. Diwarkar Bobbala and Alberto Villalobos, from the Immunology group at the CRCHUS for help with reagents and procedures for microscopy and gene expression analyses.

My thanks to Dr. Marie-Odile Benoit-Biancamano (Univ. of Montreal), Dr. Wayne A. Vogl (Univ. of British Columbia), and Dr. Joseph Hill (Univ of Texas) for their expert help in assessing the results for histopathology and electron microscopy.

I wish to thank my colleagues Nemat Mansour, Rejean Lebel, Julie Chouinard and the group from clinics, especially Oscar Esteban Espinosa, Jorge Rijo and Eric Lavallée. My dear friend Anthony Remillard, and the group of janitors with whom I shared a lot of time when working after hours and who always had a friendly word of encouragement for me. Special thanks to the personnel of the FMSS library, Martha Brideau, Diane Croteau, Collette Aubert, Huguette Vezina, Karen Doyon, Daniel Guy Boisvert, Julie Dubois and

Louise Benoit, who adopted me and have been my family here in Sherbrooke for all these years. Their love and support made the difference for me.

I would like to thank the Université de Sherbrooke for financial help through institutional scholarships. This project was supported by the Canadian Institutes of Health Research and the Medical Imaging Axis of the CRCHUS.

Finally, I want to express my gratitude to my partner in life for all his help, encouragement and support, and to my dear family, my parents and brother and all my loved ones that are not longer with us; this is dedicated to them.

9. REFERENCES

Abdel-Aziz KK (2011) Current Perspectives on Sunitinib Targeted Therapy for Tumors. *Journal of Cancer Therapy* **2**:535-541.

Abel ED (2011) A new twist in the function of the cardiac lipid droplet. *Nature medicine* **17**(9):1045-1046.

Albini A, Pennesi G, Donatelli F, Cammarota R, De Flora S and Noonan DM (2010) Cardiotoxicity of anticancer drugs: the need for cardio-oncology and cardio-oncological prevention. *Journal of the National Cancer Institute* **102**(1):14-25.

Amanzada A, Moriconi F, Mansuroglu T, Cameron S, Ramadori G and Malik IA (2014) Induction of chemokines and cytokines before neutrophils and macrophage recruitment in different regions of rat liver after TAA administration. *Lab Invest* **94**(2):235-247.

Anagnostopoulos C, Georgakopoulos A, Pianou N and Nekolla SG (2013) Assessment of myocardial perfusion and viability by positron emission tomography. *International journal of cardiology* **167**(5):1737-1749.

Ao L, Zou N, Cleveland JC, Jr., Fullerton DA and Meng X (2009) Myocardial TLR4 is a determinant of neutrophil infiltration after global myocardial ischemia: mediating KC and MCP-1 expression induced by extracellular HSC70. *American journal of physiology Heart and circulatory physiology* **297**(1):H21-28.

Aoyagi T and Matsui T (2011) The Cardiomyocyte as a Source of Cytokines in Cardiac Injury. *J Cell Sci Ther* **2012**(S5).

Aparicio-Gallego G, Blanco M, Figueroa A, Garcia-Campelo R, Valladares-Ayerbes M, Grande-Pulido E and Anton-Aparicio L (2011) New insights into molecular mechanisms of sunitinib-associated side effects. *Mol Cancer Ther* **10**(12):2215-2223.

Arakawa K, Kudo T, Ikawa M, Morikawa N, Kawai Y, Sahashi K, Lee JD, Kuriyama M, Miyamori I, Okazawa H and Yoneda M (2010) Abnormal myocardial energy-production state in mitochondrial cardiomyopathy and acute response to L-arginine infusion. C-11 acetate kinetics revealed by positron emission tomography. *Circulation journal* **74**(12):2702-2711.

Ardehali H, Sabbah HN, Burke MA, Sarma S, Liu PP, Cleland JG, Maggioni A, Fonarow GC, Abel ED, Campia U and Gheorghiade M (2012) Targeting myocardial substrate metabolism in heart failure: potential for new therapies. *European journal of heart failure* **14**(2):120-129.

Aubert G, Vega RB and Kelly DP (2013) Perturbations in the gene regulatory pathways controlling mitochondrial energy production in the failing heart. *Biochimica et biophysica acta* **1833**(4):840-847.

Authier S, Tremblay S, Dumulon V, Dubuc C, Ouellet R, Lecomte R, Cunnane SC and Benard F (2008) [11C] acetoacetate utilization by breast and prostate tumors: a PET and biodistribution study in mice. *Molecular imaging and biology* **10**(4):217-223.

Ballinger SW (2005) Mitochondrial dysfunction in cardiovascular disease. *Free radical biology & medicine* **38**(10):1278-1295.

Barba I, Chavarria L, Ruiz-Meana M, Mirabet M, Agullo E and Garcia-Dorado D (2009) Effect of intracellular lipid droplets on cytosolic Ca2+ and cell death during ischaemia-reperfusion injury in cardiomyocytes. *The Journal of physiology* **587**(Pt 6):1331-1341.

Bello CL, Mulay M, Huang X, Patyna S, Dinolfo M, Levine S, Van Vugt A, Toh M, Baum C and Rosen L (2009) Electrocardiographic characterization of the QTc interval in patients with advanced solid tumors: pharmacokinetic- pharmacodynamic evaluation of sunitinib. *Clinical cancer research* **15**(22):7045-7052.

Bengel FM, Higuchi T, Javadi MS and Lautamaki R (2009) Cardiac positron emission tomography. *Journal of the American College of Cardiology* **54**(1):1-15.

Bentourkia M, Croteau E, Langlois R, Aliaga A, Cadorette J, Bernard F, Lesur O and Lecomte R (2002) Cardiac studies in rats with 11C-acetate and PET: a comparison with 13N-ammonia. *IEEE Trans Nucl Sci* **49**:2322-2327.

Berg J, Lindgren P, Kahan T, Schill O, Persson H, Edner M and Mejhert M (2014) Health-related quality of life and long-term morbidity and mortality in patients hospitalised with systolic heart failure. *Journal of the royal society of medicine cardiovascular disease* **3**:2048004014548735 (printed online Aug 28 2014).

Bergeron M, Cadorette J, Beaudoin JF, Lepage MD, Robert G, Selivanov V, Tetrault MA, Viscogliosi N, Norenberg JP, Fontaine R and Lecomte R (2009) Performance evaluation of the LabPET APD-based digital PET scanner. *Transactions on Nuclear Science* **56**:10-16.

Bergeron M, Cadorette J, Tetrault MA, Beaudoin JF, Leroux JD, Fontaine R and Lecomte R (2014) Imaging performance of LabPET APD-based digital PET scanners for pre-clinical research. *Physics in medicine and biology* **59**(3):661-678.

Berridge BR, van Vleet JF and Herman E (2013) Cardiac, vascular and skeletal muscle system. In *Haschek and Rousseaux's Handbook of Toxicologic Pathology* (Haschek WM, Rousseaux CG, Wallig MA, Bolon B and Ochoa R eds) pp 1567-1665, Elsevier.

Biondi B (2007) Cardiovascular effects of mild hypothyroidism. *Thyroid* **17**(7):625-630.

Blasi E, Heyen J, Patyna S, Hemkens M, Ramirez D, John-Baptiste A, Steidl-Nichols J and McHarg A (2012) Sunitinib, a receptor tyrosine kinase inhibitor, increases blood pressure in rats without associated changes in cardiac structure and function. *Cardiovascular therapeutics* **30**(5):287-294.

Bolli R and Marban E (1999) Molecular and cellular mechanisms of myocardial stunning. *Physiological reviews* **79**(2):609-634.

Borde C, Kand P and Basu S (2012) Enhanced myocardial fluorodeoxyglucose uptake following Adriamycin-based therapy: Evidence of early chemotherapeutic cardiotoxicity? *World journal of radiology* **4**(5):220-223.

Bracey NA, Beck PL, Muruve DA, Hirota SA, Guo J, Jabagi H, Wright JR, Jr., Macdonald JA, Lees-Miller JP, Roach D, Semeniuk LM and Duff HJ (2013) The Nlrp3 inflammasome promotes myocardial dysfunction in structural cardiomyopathy through interleukin-1beta. *Experimental physiology* **98**(2):462-472.

Brown MA, Myears DW and Bergmann SR (1989) Validity of estimates of myocardial oxidative metabolism with carbon-11 acetate and positron emission tomography despite altered patterns of substrate utilization. *Journal of nuclear medicine* **30**(2):187-193.

Carvajal K and Moreno-Sanchez R (2003) Heart metabolic disturbances in cardiovascular diseases. *Archives of medical research* **34**(2):89-99.

Cella D, Michaelson MD, Bushmakin AG, Cappelleri JC, Charbonneau C, Kim ST, Li JZ and Motzer RJ (2010) Health-related quality of life in patients with metastatic renal cell carcinoma treated with sunitinib vs interferon-alpha in a phase III trial: final results and geographical analysis. *British journal of cancer* **102**(4):658-664.

Chacko AM and Divgi CR (2011) Radiopharmaceutical chemistry with iodine-124: a non-standard radiohalogen for positron emission tomography. *Medicinal chemistry* **7**(5):395-412.

Chatziioannou AF (2002) Molecular imaging of small animals with dedicated PET tomographs. *European journal of nuclear medicine and molecular imaging* **29**(1):98-114.

Cherry SR (2001) Fundamentals of positron emission tomography and applications in preclinical drug development. *Journal of clinical pharmacology* **41**(5):482-491.

Chintalgattu V, Rees ML, Culver JC, Goel A, Jiffar T, Zhang J, Dunner K, Jr., Pati S, Bankson JA, Pasqualini R, Arap W, Bryan NS, Taegtmeyer H, Langley RR, Yao H, Kupferman ME, Entman ML, Dickinson ME and Khakoo AY (2013) Coronary microvascular pericytes are the cellular target of sunitinib malate-induced cardiotoxicity. *Sci Transl Med* **5**(187):187ra169.

Chovatiya R and Medzhitov R (2014) Stress, inflammation, and defense of homeostasis. *Molecular cell* **54**(2):281-288.

Chu TF, Rupnick MA, Kerkela R, Dallabrida SM, Zurakowski D, Nguyen L, Woulfe K, Pravda E, Cassiola F, Desai J, George S, Morgan JA, Harris DM, Ismail NS, Chen JH, Schoen FJ, Van den Abbeele AD, Demetri GD, Force T and Chen MH (2007) Cardiotoxicity associated with tyrosine kinase inhibitor sunitinib. *Lancet* **370**(9604):2011-2019.

Cohen JD, Babiarz JE, Abrams RM, Guo L, Kameoka S, Chiao E, Taunton J and Kolaja KL (2011) Use of human stem cell derived cardiomyocytes to examine sunitinib mediated cardiotoxicity and electrophysiological alterations. *Toxicology and applied pharmacology* **257**(1):74-83.

Collinson FJ, Vasudev NS, Berkin L, Khan MM, Selby PJ and Brown JE (2011) Sunitinib-induced severe hypothyroidism with cardiac compromise. *Medical oncology* **28 Suppl 1**:S699-701.

Croteau E, Benard F, Cadorette J, Gauthier ME, Aliaga A, Bentourkia M and Lecomte R (2003) Quantitative gated PET for the assessment of left ventricular function in small animals. *Journal of nuclear medicine* **44**(10):1655-1661.

Croteau E, Gascon S, Bentourkia M, Langlois R, Rousseau JA, Lecomte R and Benard F (2012) [11C]Acetate rest-stress protocol to assess myocardial perfusion and oxygen consumption reserve in a model of congestive heart failure in rats. *Nuclear medicine and biology* **39**(2):287-294.

Dasanu CA, Padmanabhan P, Clark BA, 3rd and Do C (2012) Cardiovascular toxicity associated with small molecule tyrosine kinase inhibitors currently in clinical use. *Expert Opin Drug Saf* **11**(3):445-457.

Daugherty A, Rateri D, Hong L and Balakrishnan A (2009) Measuring blood pressure in mice using volume pressure recording, a tail-cuff method. *Journal of visualized experiments : JoVE*(27).

Davies CH, Harding SE and Poole-Wilson PA (1996) Cellular mechanisms of contractile dysfunction in human heart failure. *European heart journal* **17**(2):189-198.

de Boer MP, van der Veldt AA, Lankheet NA, Wijnstok NJ, van den Eertwegh AJ, Boven E and Serne EH (2010) Sunitinib-induced reduction in skin microvascular density is a reversible phenomenon. *Annals of oncology* **21**(9):1923-1924.

Di Carli MF, Prcevski P, Singh TP, Janisse J, Ager J, Muzik O and Vander Heide R (2000) Myocardial blood flow, function, and metabolism in repetitive stunning. *Journal of nuclear medicine* **41**(7):1227-1234.

Di Lorenzo G, Autorino R, Bruni G, Carteni G, Ricevuto E, Tudini M, Ficorella C, Romano C, Aieta M, Giordano A, Giuliano M, Gonnella A, De Nunzio C, Rizzo M, Montesarchio V, Ewer M and De Placido S (2009) Cardiovascular toxicity following sunitinib therapy in metastatic renal cell carcinoma: a multicenter analysis. *Annals of oncology* **20**(9):1535-1542.

Dilsizian V, Bacharach SL, Beanlands RS, Bergmann SR, Delbeke D, Gropler RJ, Knuuti J, Schelbert HR and Travin MI (2009) ASNC Imaging guidelines for nuclear cardiology procedures: PET myocardial perfusion and metabolism clinical imaging. *Jpournal of Nuclear Cardiology* **16**:651.

Divgi CR (2009) Molecular imaging of pulmonary cancer and inflammation. *Proceedings of the American Thoracic Society* **6**(5):464-468

Doenst T, Pytel G, Schrepper A, Amorim P, Farber G, Shingu Y, Mohr FW and Schwarzer M (2010) Decreased rates of substrate oxidation ex vivo predict the onset of heart failure and contractile dysfunction in rats with pressure overload. *Cardiovascular research* **86**(3):461-470.

Duncan CJ and Shamsadeen N (1991) Ultrastructural changes in mitochondria during rapid damage triggered by calcium, in *Calcium, Oxygen Radicals and Cellular Damage* pp 149-164, Cambridge University Press.

Dyck JR and Lopaschuk GD (2006) AMPK alterations in cardiac physiology and pathology: enemy or ally? *The Journal of physiology* **574**(Pt 1):95-112.

Ebos JM, Lee CR, Christensen JG, Mutsaers AJ and Kerbel RS (2007) Multiple circulating proangiogenic factors induced by sunitinib malate are tumor-independent and correlate with antitumor efficacy. *Proceedings of the National Academy of Sciences of the United States of America* **104**(43):17069-17074.

Eckstein N, Roper L, Haas B, Potthast H, Hermes U, Unkrig C, Naumann-Winter F and Enzmann H (2014) Clinical pharmacology of tyrosine kinase inhibitors becoming generic drugs: the regulatory perspective. *Journal of experimental & clinical cancer research : CR* **33**:15.

Egert S, Nguyen N, Brosius FC, 3rd and Schwaiger M (1997) Effects of wortmannin on insulin- and ischemia-induced stimulation of GLUT4 translocation and FDG uptake in perfused rat hearts. *Cardiovascular research* **35**(2):283-293.

Eisen T, Sternberg CN, Robert C, Mulders P, Pyle L, Zbinden S, Izzedine H and Escudier B (2012) Targeted therapies for renal cell carcinoma: review of adverse event management strategies. *Journal of the National Cancer Institute* **104**(2):93-113.

Eschenhagen T, Force T, Ewer MS, de Keulenaer GW, Suter TM, Anker SD, Avkiran M, de Azambuja E, Balligand JL, Brutsaert DL, Condorelli G, Hansen A, Heymans S, Hill JA, Hirsch E, Hilfiker-Kleiner D, Janssens S, de Jong S, Neubauer G, Pieske B, Ponikowski P, Pirmohamed M, Rauchhaus M, Sawyer D, Sugden PH, Wojta J,

Zannad F and Shah AM (2011) Cardiovascular side effects of cancer therapies: a position statement from the Heart Failure Association of the European Society of Cardiology. *European journal of heart failure* **13**(1):1-10.

Essop MF, Razeghi P, McLeod C, Young ME, Taegtmeyer H and Sack MN (2004) Hypoxia-induced decrease of UCP3 gene expression in rat heart parallels metabolic gene switching but fails to affect mitochondrial respiratory coupling. *Biochemical and biophysical research communications* **314**(2):561-564.

Evans RD and Clarke K (2012) Myocardial substrate metabolism in heart disease. *Frontiers in bioscience* **4**:556-580.

Fabian MA, Biggs WH, 3rd, Treiber DK, Atteridge CE, Azimioara MD, Benedetti MG, Carter TA, Ciceri P, Edeen PT, Floyd M, Ford JM, Galvin M, Gerlach JL, Grotzfeld RM, Herrgard S, Insko DE, Insko MA, Lai AG, Lelias JM, Mehta SA, Milanov ZV, Velasco AM, Wodicka LM, Patel HK, Zarrinkar PP and Lockhart DJ (2005) A small molecule-kinase interaction map for clinical kinase inhibitors. *Nature biotechnology* **23**(3):329-336.

Faivre S, Delbaldo C, Vera K, Robert C, Lozahic S, Lassau N, Bello C, Deprimo S, Brega N, Massimini G, Armand JP, Scigalla P and Raymond E (2006) Safety, pharmacokinetic, and antitumor activity of SU11248, a novel oral multitarget tyrosine kinase inhibitor, in patients with cancer. *Journal of clinical oncology* **24**(1):25-35.

Faivre S, Demetri G, Sargent W and Raymond E (2007) Molecular basis for sunitinib efficacy and future clinical development. *Nature reviews Drug discovery* **6**(9):734-745.

Fan D, Takawale A, Lee J and Kassiri Z (2012) Cardiac fibroblasts, fibrosis and extracellular matrix remodeling in heart disease. *Fibrogenesis Tissue Repair* **5**(1):15.

Finck BN (2007) The PPAR regulatory system in cardiac physiology and disease. *Cardiovascular research* **73**(2):269-277.

Finn RD (1999) The search for consistency in the manufacture of PET radiopharmaceuticals. *Annals of nuclear medicine* **13**(6):379-382.

Fliegner D, Schubert C, Penkalla A, Witt H, Kararigas G, Dworatzek E, Staub E, Martus P, Ruiz Noppinger P, Kintscher U, Gustafsson JA and Regitz-Zagrosek V (2010) Female sex and estrogen receptor-beta attenuate cardiac remodeling and apoptosis in pressure overload. *Am J Physiol Regul Integr Comp Physiol* **298**(6):R1597-1606.

Force T and Kolaja KL (2011) Cardiotoxicity of kinase inhibitors: the prediction and translation of preclinical models to clinical outcomes. *Nature reviews Drug discovery* **10**(2):111-126.

Fountoulakis M, Soumaka E, Rapti K, Mavroidis M, Tsangaris G, Maris A, Weisleder N and Capetanaki Y (2005) Alterations in the heart mitochondrial proteome in a desmin null heart failure model. *Journal of molecular and cellular cardiology* **38**(3):461-474.

French KJ, Coatney RW, Renninger JP, Hu CX, Gales TL, Zhao S, Storck LM, Davis CB, McSurdy-Freed J, Chen E and Frazier KS (2010) Differences in effects on myocardium and mitochondria by angiogenic inhibitors suggest separate mechanisms of cardiotoxicity. *Toxicologic pathology* **38**(5):691-702.

Frey N, Katus HA, Olson EN and Hill JA (2004) Hypertrophy of the heart: a new therapeutic target? *Circulation* **109**(13):1580-1589.

Garcia-Alvarez A, Garcia-Albeniz X, Esteve J, Rovira M and Bosch X (2010) Cardiotoxicity of tyrosine-kinase-targeting drugs. *Cardiovascular & hematological agents in medicinal chemistry* **8**(1):11-21.

Gargiulo S, Greco A, Gramanzini M, Petretta MP, Ferro A, Larobina M, Panico M, Brunetti A and Cuocolo A (2012) PET/CT imaging in mouse models of myocardial ischemia. *Journal of biomedicine & biotechnology* **2012**:541872.

Ge F, Hu C, Hyodo E, Arai K, Zhou S, Lobdell Ht, Walewski JL, Homma S and Berk PD (2012) Cardiomyocyte triglyceride accumulation and reduced ventricular function in mice with obesity reflect increased long chain Fatty Acid uptake and de novo Fatty Acid synthesis. *Journal of obesity* **2012**:205648.

Ghosh N, Rimoldi OE, Beanlands RS and Camici PG (2010) Assessment of myocardial ischaemia and viability: role of positron emission tomography. *European heart journal* **31**(24):2984-2995.

Gillespie HS, McGann CJ and Wilson BD (2011) Noninvasive diagnosis of chemotherapy related cardiotoxicity. *Current cardiology reviews* **7**(4):234-244.

Giordano FJ (2005) Oxygen, oxidative stress, hypoxia, and heart failure. *The Journal of clinical investigation* **115**(3):500-508.

Girardi F, Franceschi E and Brandes AA (2010) Cardiovascular safety of VEGF-targeting therapies: current evidence and handling strategies. *The oncologist* **15**(7):683-694.

Goldberg IJ, Trent CM and Schulze PC (2012) Lipid metabolism and toxicity in the heart. *Cell metabolism* **15**(6):805-812.

Goodman VL, Rock EP, Dagher R, Ramchandani RP, Abraham S, Gobburu JV, Booth BP, Verbois SL, Morse DE, Liang CY, Chidambaram N, Jiang JX, Tang S, Mahjoob K, Justice R and Pazdur R (2007) Approval summary: sunitinib for the treatment of imatinib refractory or intolerant gastrointestinal stromal tumors and advanced renal cell carcinoma. *Clinical cancer research* **13**(5):1367-1373.

Grassi I, Nanni C, Allegri V, Morigi JJ, Montini GC, Castellucci P and Fanti S (2012) The clinical use of PET with (11)C-acetate. *American journal of nuclear medicine and molecular imaging* **2**(1):33-47.

Greineder CF, Kohnstamm S and Ky B (2011) Heart failure associated with sunitinib: lessons learned from animal models. *Current hypertension reports* **13**(6):436-441.

Gropler RJ (2013) Recent advances in metabolic imaging. *Journal of nuclear cardiology* **20**(6):1147-1172.

Guitierrez JA and Theodorou AA (2012) Oxygen delivery and oxygen consumption in pediatric critical care, in *Pediatric Critical Care Study Guide-Text and Review* (Lucking SE, Maffei FA, Tamburro RF and Thomas NJ eds), Springer.

Gurgen D, Hegner B, Kusch A, Catar R, Chaykovska L, Hoff U, Gross V, Slowinski T, da Costa Goncalves AC, Kintscher U, Gustafsson JA, Luft FC and Dragun D (2011) Estrogen receptor-beta signals left ventricular hypertrophy sex differences in normotensive deoxycorticosterone acetate-salt mice. *Hypertension* **57**(3):648-654.

Guttman JA, Samji FN, Li Y, Vogl AW and Finlay BB (2006) Evidence that tight junctions are disrupted due to intimate bacterial contact and not inflammation during attaching and effacing pathogen infection in vivo. *Infect Immun* **74**(11):6075-6084.

Guzzardi MA and Iozzo P (2011) Fatty heart, cardiac damage, and inflammation. *Rev Diabet Stud* **8**(3):403-417.

Hall PS, Harshman LC, Srinivas S and Witteles RM (2013) The frequency and severity of cardiovascular toxicity from targeted therapy in advanced renal cell carcinoma patients. *JACC Heart failure* **1**(1):72-78.

Hamblin M, Chang L, Fan Y, Zhang J and Chen YE (2009) PPARs and the cardiovascular system. *Antioxidants & redox signaling* **11**(6):1415-1452.

Handa N, Magata Y, Mukai T, Nishina T, Konishi J and Komeda M (2007) Quantitative FDG-uptake by positron emission tomography in progressive hypertrophy of rat hearts in vivo. *Annals of nuclear medicine* **21**(10):569-576.

Hare JM and Stamler JS (2005) NO/redox disequilibrium in the failing heart and cardiovascular system. *The Journal of clinical investigation* **115**(3):509-517.

Hasinoff BB, Patel D and O'Hara KA (2008) Mechanisms of myocyte cytotoxicity induced by the multiple receptor tyrosine kinase inhibitor sunitinib. *Molecular pharmacology* **74**(6):1722-1728.

Haznedar JO, Patyna S, Bello CL, Peng GW, Speed W, Yu X, Zhang Q, Sukbuntherng J, Sweeny DJ, Antonian L and Wu EY (2009) Single- and multiple-dose disposition kinetics of sunitinib malate, a multitargeted receptor tyrosine kinase inhibitor:

comparative plasma kinetics in non-clinical species. *Cancer Chemother Pharmacol* **64**(4):691-706.

He L, Kim T, Long Q, Liu J, Wang P, Zhou Y, Ding Y, Prasain J, Wood PA and Yang Q (2012) Carnitine palmitoyltransferase-1b deficiency aggravates pressure overload-induced cardiac hypertrophy caused by lipotoxicity. *Circulation* **126**(14):1705-1716.

Health Canada (2007) Summary Basis of Decision (SBD) [Pr]Sutent, Sunitinib malate, 12.5 mg, 25 mg, 50 mg capsules, Pfizer Canada Inc. *Submission Control No. 101319*.

Heather LC, Cole MA, Lygate CA, Evans RD, Stuckey DJ, Murray AJ, Neubauer S and Clarke K (2006) Fatty acid transporter levels and palmitate oxidation rate correlate with ejection fraction in the infarcted rat heart. *Cardiovascular research* **72**(3):430-437.

Heather LC, Pates KM, Atherton HJ, Cole MA, Ball DR, Evans RD, Glatz JF, Luiken JJ, Griffin JL and Clarke K (2013) Differential translocation of the fatty acid transporter, FAT/CD36, and the glucose transporter, GLUT4, coordinates changes in cardiac substrate metabolism during ischemia and reperfusion. *Circulation Heart failure* **6**(5):1058-1066.

Hedayat M, Mahmoudi MJ, Rose NR and Rezaei N (2010) Proinflammatory cytokines in heart failure: double-edged swords. *Heart Fail Rev* **15**(6):543-562.

Herrero P, Dence CS, Sharp TL, Welch MJ and Gropler RJ (2004) Impact of reversible trapping of tracer and the presence of blood metabolites on measurements of myocardial glucose utilization performed by PET and 18F-fluorodeoxyglucose using the Patlak method. *Nuclear medicine and biology* **31**(7):883-892.

Herrero P, Kisrieva-Ware Z, Dence CS, Patterson B, Coggan AR, Han DH, Ishii Y, Eisenbeis P and Gropler RJ (2007) PET measurements of myocardial glucose metabolism with 1-11C-glucose and kinetic modeling. *Journal of nuclear medicine* **48**(6):955-964.

Herrero P, Sharp TL, Dence C, Haraden BM and Gropler RJ (2002) Comparison of 1-(11)C-glucose and (18)F-FDG for quantifying myocardial glucose use with PET. *Journal of nuclear medicine* **43**(11):1530-1541.

Hesse B, Lindhardt TB, Acampa W, Anagnostopoulos C, Ballinger J, Bax JJ, Edenbrandt L, Flotats A, Germano G, Stopar TG, Franken P, Kelion A, Kjaer A, Le Guludec D, Ljungberg M, Maenhout AF, Marcassa C, Marving J, McKiddie F, Schaefer WM, Stegger L and Underwood R (2008) EANM/ESC guidelines for radionuclide imaging of cardiac function. *European journal of nuclear medicine and molecular imaging* **35**(4):851-885.

Hipp MM, Hilf N, Walter S, Werth D, Brauer KM, Radsak MP, Weinschenk T, Singh-Jasuja H and Brossart P (2008) Sorafenib, but not sunitinib, affects function of dendritic cells and induction of primary immune responses. *Blood* **111**(12):5610-5620.

Ho YY, Lagares D, Tager AM and Kapoor M (2014) Fibrosis-a lethal component of systemic sclerosis. *Nature reviews Rheumatology*.

Hohenegger M (2012) Drug induced rhabdomyolysis. *Current opinion in pharmacology* **12**(3):335-339.

Hui EP, Lui VW, Wong CS, Ma BB, Lau CP, Cheung CS, Ho K, Cheng SH, Ng MH and Chan AT (2011) Preclinical evaluation of sunitinib as single agent or in combination with chemotherapy in nasopharyngeal carcinoma. *Invest New Drugs* **29**(6):1123-1131.

Huss JM and Kelly DP (2005) Mitochondrial energy metabolism in heart failure: a question of balance. *The Journal of clinical investigation* **115**(3):547-555.

Hussain R, Kudo T, Tsujikawa T, Kobayashi M, Fujibayashi Y and Okazawa H (2009) Validation of the calculation of the clearance rate constant (k(mono)) of [(11)C]acetate using parametric k(mono) image for myocardial oxidative metabolism. *Nuclear medicine and biology* **36**(8):877-882.

Hutson TE, Figlin RA, Kuhn JG and Motzer RJ (2008) Targeted therapies for metastatic renal cell carcinoma: an overview of toxicity and dosing strategies. *The oncologist* **13**(10):1084-1096.

Inai T, Mancuso M, Hashizume H, Baffert F, Haskell A, Baluk P, Hu-Lowe DD, Shalinsky DR, Thurston G, Yancopoulos GD and McDonald DM (2004) Inhibition of vascular endothelial growth factor (VEGF) signaling in cancer causes loss of endothelial fenestrations, regression of tumor vessels, and appearance of basement membrane ghosts. *The American journal of pathology* **165**(1):35-52.

Israel O, Weiler-Sagie M, Rispler S, Bar-Shalom R, Frenkel A, Keidar Z, Bar-Shalev A and Strauss HW (2007) PET/CT quantitation of the effect of patient-related factors on cardiac ^{18}F-FDG uptake. *Journal of nuclear medicine* **48**(2):234-239.

Jaswal JS, Keung W, Wang W, Ussher JR and Lopaschuk GD (2011) Targeting fatty acid and carbohydrate oxidation--a novel therapeutic intervention in the ischemic and failing heart. *Biochimica et biophysica acta* **1813**(7):1333-1350.

Jha PK, Vankalakunti M, Siddini V, Bonu R, Prakash GK, Babu K and Ballal HS (2013) Sunitinib induced nephrotic syndrome and thrombotic microangiopathy. *Indian journal of nephrology* **23**(1):67-70.

Jiji RS, Kramer CM and Salerno M (2012) Non-invasive imaging and monitoring cardiotoxicity of cancer therapeutic drugs. *Journal of nuclear cardiology* **19**(2):377-388.

Kamitani T, Ikeda U, Muto S, Kawakami K, Nagano K, Tsuruya Y, Oguchi A, Yamamoto K, Hara Y, Kojima T and et al. (1992) Regulation of Na,K-ATPase gene expression by thyroid hormone in rat cardiocytes. *Circulation research* **71**(6):1457-1464.

Kappers MH, van Esch JH, Smedts FM, de Krijger RR, Eechoute K, Mathijssen RH, Sleijfer S, Leijten F, Danser AH, van den Meiracker AH and Visser TJ (2011) Sunitinib-induced hypothyroidism is due to induction of type 3 deiodinase activity and thyroidal capillary regression. *The Journal of clinical endocrinology and metabolism* **96**(10):3087-3094.

Karaman MW, Herrgard S, Treiber DK, Gallant P, Atteridge CE, Campbell BT, Chan KW, Ciceri P, Davis MI, Edeen PT, Faraoni R, Floyd M, Hunt JP, Lockhart DJ, Milanov ZV, Morrison MJ, Pallares G, Patel HK, Pritchard S, Wodicka LM and Zarrinkar PP (2008) A quantitative analysis of kinase inhibitor selectivity. *Nature biotechnology* **26**(1):127-132.

Kennedy JA, Kiosoglous AJ, Murphy GA, Pelle MA and Horowitz JD (2000) Effect of perhexiline and oxfenicine on myocardial function and metabolism during low-flow ischemia/reperfusion in the isolated rat heart. *Journal of cardiovascular pharmacology* **36**(6):794-801.

Kerkela R, Grazette L, Yacobi R, Iliescu C, Patten R, Beahm C, Walters B, Shevtsov S, Pesant S, Clubb FJ, Rosenzweig A, Salomon RN, Van Etten RA, Alroy J, Durand JB and Force T (2006) Cardiotoxicity of the cancer therapeutic agent imatinib mesylate. *Nature medicine* **12**(8):908-916.

Kerkela R, Woulfe KC, Durand JB, Vagnozzi R, Kramer D, Chu TF, Beahm C, Chen MH and Force T (2009) Sunitinib-induced cardiotoxicity is mediated by off-target inhibition of AMP-activated protein kinase. *Clinical and translational science* **2**(1):15-25.

Khakoo AY, Kassiotis CM, Tannir N, Plana JC, Halushka M, Bickford C, Trent J, 2nd, Champion JC, Durand JB and Lenihan DJ (2008) Heart failure associated with sunitinib malate: a multitargeted receptor tyrosine kinase inhibitor. *Cancer* **112**(11):2500-2508.

Klein I and Danzi S (2007) Thyroid disease and the heart. *Circulation* **116**(15):1725-1735.

Klein LJ, Visser FC, Knaapen P, Peters JH, Teule GJ, Visser CA and Lammertsma AA (2001) Carbon-11 acetate as a tracer of myocardial oxygen consumption. *European journal of nuclear medicine* **28**(5):651-668.

Klocek M and Czarnecka D (2013) Quality of life in patients with chronic heart failure. In *Health-related quality of life in cardiovascular patients* (Kawecka-Jaszcz K, Klocek M, Tobiasz-Adamczyk B and Bulpitt CJ eds) pp 61-73, Springer Verlag Italia.

Klocke FJ, Baird MG, Lorell BH, Bateman TM, Messer JV, Berman DS, O'Gara PT, Carabello BA, Russell RO, Jr., Cerqueira MD, St John Sutton MG, DeMaria AN, Udelson JE, Kennedy JW, Verani MS, Williams KA, Antman EM, Smith SC, Jr., Alpert JS, Gregoratos G, Anderson JL, Hiratzka LF, Faxon DP, Hunt SA, Fuster V, Jacobs AK, Gibbons RJ, Russell RO, American College of C, American Heart Association Task Force on Practice G and American Society for Nuclear C (2003) ACC/AHA/ASNC guidelines for the clinical use of cardiac radionuclide imaging--executive summary: a report of the American College of Cardiology/American Heart Association Task Force on Practice Guidelines (ACC/AHA/ASNC Committee to Revise the 1995 Guidelines for the Clinical Use of Cardiac Radionuclide Imaging). *Circulation* **108**(11):1404-1418.

Knaapen P, Germans T, Knuuti J, Paulus WJ, Dijkmans PA, Allaart CP, Lammertsma AA and Visser FC (2007) Myocardial energetics and efficiency: current status of the noninvasive approach. *Circulation* **115**(7):918-927.

Kuge Y, Inubushi M and Tamaki N (2008) Iodinated fatty acid imaging., in *Nuclear imaging principles and applications* (Iskandrian AE and Garcia EV eds) p 462, Oxfor University Press, New York.

Kumar V, Abbas AK and Aster J (2013) Cell Injury, Death and Adaptation, in *Robbin's Basic Pathology*, Elsevier.

Lancelot S and Zimmer L (2010) Small-animal positron emission tomography as a tool for neuropharmacology. *Trends in pharmacological sciences* **31**(9):411-417.

Laskowski KR and Russell RR, 3rd (2008) Uncoupling proteins in heart failure. *Curr Heart Fail Rep* **5**(2):75-79.

Lautamaki R, George RT, Kitagawa K, Higuchi T, Merrill J, Voicu C, DiPaula A, Nekolla SG, Lima JA, Lardo AC and Bengel FM (2009) Rubidium-82 PET-CT for quantitative assessment of myocardial blood flow: validation in a canine model of coronary artery stenosis. *European journal of nuclear medicine and molecular imaging* **36**(4):576-586.

Lee L, Campbell R, Scheuermann-Freestone M, Taylor R, Gunaruwan P, Williams L, Ashrafian H, Horowitz J, Fraser AG, Clarke K and Frenneaux M (2005) Metabolic modulation with perhexiline in chronic heart failure: a randomized, controlled trial of short-term use of a novel treatment. *Circulation* **112**(21):3280-3288.

Lightfoot JC, D'Agostino RB, Jr., Hamilton CA, Jordan J, Torti FM, Kock ND, Jordan J, Workman S and Hundley WG (2010) Novel approach to early detection of doxorubicin cardiotoxicity by gadolinium-enhanced cardiovascular magnetic

resonance imaging in an experimental model. *Circulation Cardiovascular imaging* **3**(5):550-558.

Lim AY, Segarra I, Chakravarthi S, Akram S and Judson JP (2010) Histopathology and biochemistry analysis of the interaction between sunitinib and paracetamol in mice. *BMC Pharmacol* **10**:14.

Lipshultz SE, Adams MJ, Colan SD, Constine LS, Herman EH, Hsu DT, Hudson MM, Kremer LC, Landy DC, Miller TL, Oeffinger KC, Rosenthal DN, Sable CA, Sallan SE, Singh GK, Steinberger J, Cochran TR, Wilkinson JD, American Heart Association Congenital Heart Defects Committee of the Council on Cardiovascular Disease in the Young CoBCSCoC and Stroke Nursing CoCR (2013) Long-term cardiovascular toxicity in children, adolescents, and young adults who receive cancer therapy: pathophysiology, course, monitoring, management, prevention, and research directions: a scientific statement from the American Heart Association. *Circulation* **128**(17):1927-1995.

Maayah ZH, Ansari MA, El Gendy MA, Al-Arifi MN and Korashy HM (2014) Development of cardiac hypertrophy by sunitinib in vivo and in vitro rat cardiomyocytes is influenced by the aryl hydrocarbon receptor signaling pathway. *Archives of toxicology* **88**(3):725-738.

Medical Advisory Secretariat (2005) Positron Emission Tomography for the Assessment of Myocardial Viability: an evidence based analysis., Ontario Health Technology Assessment Series (www.health.gov.on.ca/ohtas).

Mellor HR, Bell AR, Valentin JP and Roberts RR (2011) Cardiotoxicity associated with targeting kinase pathways in cancer. *Toxicol Sci* **120**(1):14-32.

Miele E, Spinelli GP, Tomao F, Zullo A, De Marinis F, Pasciuti G, Rossi L, Zoratto F and Tomao S (2008) Positron Emission Tomography (PET) radiotracers in oncology--utility of 18F-Fluoro-deoxy-glucose (FDG)-PET in the management of patients with non-small-cell lung cancer (NSCLC). *Journal of experimental & clinical cancer research : CR* **27**:52.

Monsuez JJ, Charniot JC, Vignat N and Artigou JY (2010) Cardiac side-effects of cancer chemotherapy. *International journal of cardiology* **144**(1):3-15.

Montaigne D, Hurt C and Neviere R (2012) Mitochondria death/survival signaling pathways in cardiotoxicity induced by anthracyclines and anticancer-targeted therapies. *Biochemistry research international* **2012**:951539.

Mori H, Ohno Y, Ito F, Funaguchi N, Yanase K, Endo J, Nakano M, Bai La BL and Minatoguchi S (2010) Massive hematuria from the bilateral upper urinary tract in a patient treated for advanced lung cancer with gefitinib. *Japanese journal of clinical oncology* **40**(3):263-266.

Motzer RJ, Hutson TE, Tomczak P, Michaelson MD, Bukowski RM, Oudard S, Negrier S, Szczylik C, Pili R, Bjarnason GA, Garcia-del-Muro X, Sosman JA, Solska E, Wilding G, Thompson JA, Kim ST, Chen I, Huang X and Figlin RA (2009) Overall survival and updated results for sunitinib compared with interferon alfa in patients with metastatic renal cell carcinoma. *Journal of clinical oncology* **27**(22):3584-3590.

Motzer RJ, Hutson TE, Tomczak P, Michaelson MD, Bukowski RM, Rixe O, Oudard S, Negrier S, Szczylik C, Kim ST, Chen I, Bycott PW, Baum CM and Figlin RA (2007) Sunitinib versus interferon alfa in metastatic renal-cell carcinoma. *The New England journal of medicine* **356**(2):115-124.

Muller FU, Lewin G, Matus M, Neumann J, Riemann B, Wistuba J, Schutz G and Schmitz W (2003) Impaired cardiac contraction and relaxation and decreased expression of sarcoplasmic Ca2+-ATPase in mice lacking the CREM gene. *FASEB journal* **17**(1):103-105.

Murray AJ, Lygate CA, Cole MA, Carr CA, Radda GK, Neubauer S and Clarke K (2006) Insulin resistance, abnormal energy metabolism and increased ischemic damage in the chronically infarcted rat heart. *Cardiovascular research* **71**(1):149-157.

Murray LJ, Abrams TJ, Long KR, Ngai TJ, Olson LM, Hong W, Keast PK, Brassard JA, O'Farrell AM, Cherrington JM and Pryer NK (2003) SU11248 inhibits tumor growth and CSF-1R-dependent osteolysis in an experimental breast cancer bone metastasis model. *Clin Exp Metastasis* **20**(8):757-766.

Neely JR, Rovetto MJ and Oram JF (1972) Myocardial utilization of carbohydrate and lipids. *Progress in cardiovascular diseases* **15**(3):289-329.

Neuhaus T, Luyken J and Stier S (2014) Discontinuation of the tyrosine kinase inhibitor sunitinib in patients with metastatic renal cell carcinoma: a case series. *Urol J* **11**(2):1494-1498.

Olofsson SO, Bostrom P, Andersson L, Rutberg M, Perman J and Boren J (2009) Lipid droplets as dynamic organelles connecting storage and efflux of lipids. *Biochimica et biophysica acta* **1791**(6):448-458.

Ong DS, Scherrer-Crosbie M, Coelho-Filho O, Francis SA and Neilan TG (2014) Imaging methods for detection of chemotherapy-associated cardiotoxicity and dysfunction. *Expert review of cardiovascular therapy* **12**(4):487-497.

Paquette M, Tremblay S, Benard F and Lecomte R (2012) Quantitative hormone therapy follow-up in an ER+/ERalphaKD mouse tumor model using FDG and [11C]-methionine PET imaging. *EJNMMI research* **2**(1):61.

Park TS, Yamashita H, Blaner WS and Goldberg IJ (2007) Lipids in the heart: a source of fuel and a source of toxins. *Current opinion in lipidology* **18**(3):277-282.

Perrino C, Schiattarella GG, Sannino A, Pironti G, Petretta MP, Cannavo A, Gargiulo G, Ilardi F, Magliulo F, Franzone A, Carotenuto G, Serino F, Altobelli GG, Cimini V, Cuocolo A, Lombardi A, Goglia F, Indolfi C, Trimarco B and Esposito G (2013) Genetic deletion of uncoupling protein 3 exaggerates apoptotic cell death in the ischemic heart leading to heart failure. *Journal of the American Heart Association* **2**(3):e000086.

Perugorria MJ, Latasa MU, Nicou A, Cartagena-Lirola H, Castillo J, Goni S, Vespasiani-Gentilucci U, Zagami MG, Lotersztajn S, Prieto J, Berasain C and Avila MA (2008) The epidermal growth factor receptor ligand amphiregulin participates in the development of mouse liver fibrosis. *Hepatology* **48**(4):1251-1261.

Peterson LR and Gropler RJ (2010) Radionuclide imaging of myocardial metabolism. *Circulation Cardiovascular imaging* **3**(2):211-222.

Pfaffl MW (2001) A new mathematical model for relative quantification in real-time RT-PCR. *Nucleic Acids Res* **29**(9):e45.

Pili R, Adelaiye R, Miles KM, Ciamporcero E, Sotomayor P, Bjarnason GA and Park R (2013) Overcoming sunitinib-induced resistance by dose escalation in renal cell carcinoma: Evidence in animal models and patients. *Journal of clinical oncology* **31**(Supplement, Abstract 4582.).

Planavila A, Redondo I, Hondares E, Vinciguerra M, Munts C, Iglesias R, Gabrielli LA, Sitges M, Giralt M, van Bilsen M and Villarroya F (2013) Fibroblast growth factor 21 protects against cardiac hypertrophy in mice. *Nat Commun* **4**:2019.

Postic C, Leturque A, Printz RL, Maulard P, Loizeau M, Granner DK and Girard J (1994) Development and regulation of glucose transporter and hexokinase expression in rat. *The American journal of physiology* **266**(4 Pt 1):E548-559.

Qi WX, Shen Z, Tang LN and Yao Y (2014) Congestive heart failure risk in cancer patients treated with VEGFR-TKIs: a systematic review and meta-analysis of 36 clinical trials. *British journal of clinical pharmacology*.

Quintyne KI, Neenan1 T, Wallis F and Gupta1 RK (2013) Sustained long-term clinical and radiological response with sunitinib for metastatic renal-cell carcinoma (RCC). *Case Reports in Clinical Medicine* **2**(1):29-31.

Rainer PP, Doleschal B, Kirk JA, Sivakumaran V, Saad Z, Groschner K, Maechler H, Hoefler G, Bauernhofer T, Samonigg H, Hutterer G, Kass DA, Pieske B, von Lewinski D and Pichler M (2012) Sunitinib causes dose-dependent negative functional effects on myocardium and cardiomyocytes. *BJU international* **110**(10):1455-1462.

Raymond E, Dahan L, Raoul JL, Bang YJ, Borbath I, Lombard-Bohas C, Valle J, Metrakos P, Smith D, Vinik A, Chen JS, Horsch D, Hammel P, Wiedenmann B, Van Cutsem E, Patyna S, Lu DR, Blanckmeister C, Chao R and Ruszniewski P (2011) Sunitinib

malate for the treatment of pancreatic neuroendocrine tumors. *The New England journal of medicine* **364**(6):501-513.

Richards CJ, Je Y, Schutz FA, Heng DY, Dallabrida SM, Moslehi JJ and Choueiri TK (2011) Incidence and risk of congestive heart failure in patients with renal and nonrenal cell carcinoma treated with sunitinib. *Journal of clinical oncology* **29**(25):3450-3456.

Rimbaud S, Garnier A and Ventura-Clapier R (2009) Mitochondrial biogenesis in cardiac pathophysiology. *Pharmacol Rep* **61**(1):131-138.

Rini BI (2007) Sunitinib. *Expert opinion on pharmacotherapy* **8**(14):2359-2369.

Rios M, Foretz M, Viollet B, Prieto A, Fraga M, Costoya JA and Senaris R (2013) AMPK activation by oncogenesis is required to maintain cancer cell proliferation in astrocytic tumors. *Cancer research* **73**(8):2628-2638.

Ritskes-Hoitinga M (2004) Nutrition of Laboratory Mice., in *The Laboratory Mouse* (Hedrich HJ and Bullock G eds) pp 463-479, Elsevier, London.

Rock EP, Goodman V, Jiang JX, Mahjoob K, Verbois SL, Morse D, Dagher R, Justice R and Pazdur R (2007) Food and Drug Administration drug approval summary: Sunitinib malate for the treatment of gastrointestinal stromal tumor and advanced renal cell carcinoma. *The oncologist* **12**(1):107-113.

Russell III RR (2009) Myocardial metabolic imaging: Viability and beyond. *Current Cardiovascular Imaging Reports* **2**(3):223-229.

Safari F, Anvari Z, Moshtaghioun S, Javan M, Bayat G, Forosh SS and Hekmatimoghaddam S (2014) Differential expression of cardiac uncoupling proteins 2 and 3 in response to myocardial ischemia-reperfusion in rats. *Life sciences* **98**(2):68-74.

Santalucia T, Boheler KR, Brand NJ, Sahye U, Fandos C, Vinals F, Ferre J, Testar X, Palacin M and Zorzano A (1999) Factors involved in GLUT-1 glucose transporter gene transcription in cardiac muscle. *The Journal of biological chemistry* **274**(25):17626-17634.

Santalucia T, Camps M, Castello A, Munoz P, Nuel A, Testar X, Palacin M and Zorzano A (1992) Developmental regulation of GLUT-1 (erythroid/Hep G2) and GLUT-4 (muscle/fat) glucose transporter expression in rat heart, skeletal muscle, and brown adipose tissue. *Endocrinology* **130**(2):837-846.

Sari FR, Watanabe K, Widyantoro B, Thandavarayan RA, Harima M, Kodama M and Aizawa Y (2011) Sex differences play a role in cardiac endoplasmic reticulum stress (ERS) and ERS-initiated apoptosis induced by pressure overload and thapsigargin. *Cardiovasc Pathol* **20**(5):281-290.

Schlessinger J (2014) Receptor tyrosine kinases: legacy of the first two decades. *Cold Spring Harbor perspectives in biology* **6**(3).

Schmidinger M (2013) Understanding and managing toxicities of vascular endothelial growth factor (VEGF) inhibitors. *EJC Supplements* **11**(2):172-191.

Schmidinger M, Zielinski CC, Vogl UM, Bojic A, Bojic M, Schukro C, Ruhsam M, Hejna M and Schmidinger H (2008) Cardiac toxicity of sunitinib and sorafenib in patients with metastatic renal cell carcinoma. *Journal of clinical oncology* **26**(32):5204-5212.

Schwaiger M and Wolpers HG (1990) Advances in the assessment of myocardial metabolism by positron emission tomography. *Coronary Artery Disease* **1**(5):547-556.

Schwandt A, Wood LS, Rini B and Dreicer R (2009) Management of side effects associated with sunitinib therapy for patients with renal cell carcinoma. *Onco Targets Ther* **2**:51-61.

Scolletta S and Biagioli B (2010) Energetic myocardial metabolism and oxidative stress: let's make them our friends in the fight against heart failure. *Biomed Pharmacother* **64**(3):203-207.

Seely AJ, Pascual JL and Christou NV (2003) Science review: Cell membrane expression (connectivity) regulates neutrophil delivery, function and clearance. *Crit Care* **7**(4):291-307.

Seidman A, Hudis C, Pierri MK, Shak S, Paton V, Ashby M, Murphy M, Stewart SJ and Keefe D (2002) Cardiac dysfunction in the trastuzumab clinical trials experience. *Journal of clinical oncology* **20**(5):1215-1221.

Selivanov VV, Picard Y, Cadorette J, Rodrigue S and Lecomte R (2000) Detector response models for statistical iterative image reconstruction in high resolution PET. *IEEE Trans Nucl Sci* **47**:1168-1175.

Sen S, Kundu BK, Wu HC, Hashmi SS, Guthrie P, Locke LW, Roy RJ, Matherne GP, Berr SS, Terwelp M, Scott B, Carranza S, Frazier OH, Glover DK, Dillmann WH, Gambello MJ, Entman ML and Taegtmeyer H (2013) Glucose regulation of load-induced mTOR signaling and ER stress in mammalian heart. *Journal of the American Heart Association* **2**(3):e004796.

Seta Y, Shan K, Bozkurt B, Oral H and Mann DL (1996) Basic mechanisms in heart failure: the cytokine hypothesis. *Journal of cardiac failure* **2**(3):243-249.

Shah RR, Morganroth J and Shah DR (2013) Cardiovascular safety of tyrosine kinase inhibitors: with a special focus on cardiac repolarisation (QT interval). *Drug safety* **36**(5):295-316.

Shoyab M, Plowman GD, McDonald VL, Bradley JG and Todaro GJ (1989) Structure and function of human amphiregulin: a member of the epidermal growth factor family. *Science* **243**(4894 Pt 1):1074-1076.

Spector NL, Yarden Y, Smith B, Lyass L, Trusk P, Pry K, Hill JE, Xia W, Seger R and Bacus SS (2007) Activation of AMP-activated protein kinase by human EGF receptor 2/EGF receptor tyrosine kinase inhibitor protects cardiac cells. *Proceedings of the National Academy of Sciences of the United States of America* **104**(25):10607-10612.

Speed B, Bu HZ, Pool WF, Peng GW, Wu EY, Patyna S, Bello C and Kang P (2012) Pharmacokinetics, distribution, and metabolism of [14C]sunitinib in rats, monkeys, and humans. *Drug metabolism and disposition* **40**(3):539-555.

Spiekerkoetter U and Wood PA (2010) Mitochondrial fatty acid oxidation disorders: pathophysiological studies in mouse models. *Journal of inherited metabolic disease* **33**(5):539-546.

Stanley WC, Recchia FA and Lopaschuk GD (2005) Myocardial substrate metabolism in the normal and failing heart. *Physiological reviews* **85**(3):1093-1129.

Statistics Canada (2014) Causes of death, 2010 and 2011. *The Daily, Statistics Canada*.

Stegger L, Heijman E, Schafers KP, Nicolay K, Schafers MA and Strijkers GJ (2009) Quantification of left ventricular volumes and ejection fraction in mice using PET, compared with MRI. *Journal of nuclear medicine* **50**(1):132-138.

Steingart RM, Bakris GL, Chen HX, Chen MH, Force T, Ivy SP, Leier CV, Liu G, Lenihan D, Lindenfeld J, Maitland ML, Remick SC and Tang WH (2012) Management of cardiac toxicity in patients receiving vascular endothelial growth factor signaling pathway inhibitors. *Am Heart J* **163**(2):156-163.

Strayer DS and Rubin E (2014) Cell adaptation, cell injury and cell death., in *Essentials of Rubin's Pathology* (Rubin E and Reisner HM eds), Wolters Kluwer/Lippincott Williams & Wilkins.

Takahashi D, Nagahama K, Tsuura Y, Tanaka H and Tamura T (2012) Sunitinib-induced nephrotic syndrome and irreversible renal dysfunction. *Clinical and experimental nephrology* **16**(2):310-315.

Takeuchi K and Ito F (2011) Receptor tyrosine kinases and targeted cancer therapeutics. *Biological & pharmaceutical bulletin* **34**(12):1774-1780.

Tanaka Y, Shibata MA, Morimoto J and Otsuki Y (2011) Sunitinib suppresses tumor growth and metastases in a highly metastatic mouse mammary cancer model. *Anticancer research* **31**(4):1225-1234.

Tantawy MN and Peterson TE (2010) Simplified [18F]FDG image-derived input function using the left ventricle, liver, and one venous blood sample. *Molecular imaging* **9**(2):76-86.

Tawakol A, Sims K, MacRae C, Friedman JR, Alpert NM, Fischman AJ and Gewirtz H (2003) Myocardial flow regulation in people with mitochondrial myopathy, encephalopathy, lactic acidosis, stroke-like episodes/myoclonic epilepsy and ragged red fibers and other mitochondrial syndromes. *Coron Artery Dis* **14**(3):197-205.

Telli ML, Witteles RM, Fisher GA and Srinivas S (2008) Cardiotoxicity associated with the cancer therapeutic agent sunitinib malate. *Annals of oncology* **19**(9):1613-1618.

Tillisch J, Brunken R, Marshall R, Schwaiger M, Mandelkern M, Phelps M and Schelbert H (1986) Reversibility of cardiac wall-motion abnormalities predicted by positron tomography. *The New England journal of medicine* **314**(14):884-888.

Timmer SA, Lubberink M, Germans T, Gotte MJ, ten Berg JM, ten Cate FJ, van Rossum AC, Lammertsma AA and Knaapen P (2010) Potential of [11C]acetate for measuring myocardial blood flow: Studies in normal subjects and patients with hypertrophic cardiomyopathy. *Journal of nuclear cardiology* **17**(2):264-275.

Tokarska-Schlattner M, Zaugg M, Zuppinger C, Wallimann T and Schlattner U (2006) New insights into doxorubicin-induced cardiotoxicity: the critical role of cellular energetics. *Journal of molecular and cellular cardiology* **41**(3):389-405.

Turer AT, Malloy CR, Newgard CB and Podgoreanu MV (2010) Energetics and metabolism in the failing heart: important but poorly understood. *Current opinion in clinical nutrition and metabolic care* **13**(4):458-465.

Tuunanen H, Ukkonen H and Knuuti J (2008) Myocardial fatty acid metabolism and cardiac performance in heart failure. *Current cardiology reports* **10**(2):142-148.

van Bilsen M, Smeets PJ, Gilde AJ and van der Vusse GJ (2004) Metabolic remodelling of the failing heart: the cardiac burn-out syndrome? *Cardiovascular research* **61**(2):218-226

van den Brom CE, Huisman MC, Vlasblom R, Boontje NM, Duijst S, Lubberink M, Molthoff CF, Lammertsma AA, van der Velden J, Boer C, Ouwens DM and Diamant M (2009) Altered myocardial substrate metabolism is associated with myocardial dysfunction in early diabetic cardiomyopathy in rats: studies using positron emission tomography. *Cardiovascular diabetology* **8**:39.

van den Hoff J (2005) Principles of quantitative positron emission tomography. *Amino acids* **29**(4):341-353.

van Herpen NA and Schrauwen-Hinderling VB (2008) Lipid accumulation in non-adipose tissue and lipotoxicity. *Physiology & Behavior* **94**(2):231-241.

Visser FC (2001) Imaging of cardiac metabolism using radiolabelled glucose, fatty acids and acetate. *Coron Artery Dis* **12 Suppl 1**:S12-18.

vom Dahl J, Herman WH, Hicks RJ, Ortiz-Alonso FJ, Lee KS, Allman KC, Wolfe ER, Kalif V and Schwaiger M (1993) Myocardial glucose uptake in patients with insulin-dependent diabetes mellitus assessed quantitatively by dynamic positron emission tomography. *Circulation* **88**(2):395-404.

Wells QS and Lenihan DJ (2010) Reversibility of left ventricular dysfunction resulting from chemotherapy: can this be expected? *Progress in cardiovascular diseases* **53**(2):140-148.

Welti JC, Powles T, Foo S, Gourlaouen M, Preece N, Foster J, Frentzas S, Bird D, Sharpe K, van Weverwijk A, Robertson D, Soffe J, Erler JT, Pili R, Springer CJ, Mather SJ and Reynolds AR (2012) Contrasting effects of sunitinib within in vivo models of metastasis. *Angiogenesis* **15**(4):623-641.

Witteles RM, Fowler MB and Telli ML (2011) Chemotherapy-associated cardiotoxicity: how often does it really occur and how can it be prevented? *Heart failure clinics* **7**(3):333-344.

Witteles RM and Telli M (2012) Underestimating cardiac toxicity in cancer trials: lessons learned? *Journal of clinical oncology* **30**(16):1916-1918.

Wolter P, Stefan C, Decallonne B, Dumez H, Bex M, Carmeliet P and Schoffski P (2008) The clinical implications of sunitinib-induced hypothyroidism: a prospective evaluation. *British journal of cancer* **99**(3):448-454.

Yang B and Papoian T (2012) Tyrosine kinase inhibitor (TKI)-induced cardiotoxicity: approaches to narrow the gaps between preclinical safety evaluation and clinical outcome. *Journal of applied toxicology : JAT* **32**(12):945-951.

Yang CM, Lee IT, Hsu RC, Chi PL and Hsiao LD (2013) NADPH oxidase/ROS-dependent PYK2 activation is involved in TNF-alpha-induced matrix metalloproteinase-9 expression in rat heart-derived H9c2 cells. *Toxicology and applied pharmacology* **272**(2):431-442.

Ye F, Yuan F, Li X, Cooper N, Tinney JP and Keller BB (2013) Gene expression profiles in engineered cardiac tissues respond to mechanical loading and inhibition of tyrosine kinases. *Physiological reports* **1**(5):e00078.

Yokoyama I, Yonekura K, Ohtake T, Kawamura H, Matsumoto A, Inoue Y, Aoyagi T, Sugiura S, Omata M, Ohtomo K and Nagai R (2000) Role of insulin resistance in heart and skeletal muscleF-18 fluorodeoxyglucose uptake in patients with noninsulin-dependent diabetes mellitus. *Journal of nuclear cardiology* **7**(3):242-248.

Young LH, Russell RR, 3rd, Yin R, Caplan MJ, Ren J, Bergeron R, Shulman GI and Sinusas AJ (1999) Regulation of myocardial glucose uptake and transport during ischemia and energetic stress. *The American journal of cardiology* **83**(12A):25H-30H.

Zambelli A, Della Porta MG, Eleuteri E, De Giuli L, Catalano O, Tondini C and Riccardi A (2011) Predicting and preventing cardiotoxicity in the era of breast cancer targeted therapies. Novel molecular tools for clinical issues. *Breast* **20**(2):176-183.

Zhang J, Yang PL and Gray NS (2009) Targeting cancer with small molecule kinase inhibitors. *Nature reviews Cancer* **9**(1):28-39.

Zhong M, Alonso CE, Taegtmeyer H and Kundu BK (2013) Quantitative PET imaging detects early metabolic remodeling in a mouse model of pressure-overload left ventricular hypertrophy in vivo. *Journal of nuclear medicine* **54**(4):609-615.

Zhou Y, Lee JY, Lee CM, Cho WK, Kang MJ, Koff JL, Yoon PO, Chae J, Park HO, Elias JA and Lee CG (2012) Amphiregulin, an epidermal growth factor receptor ligand, plays an essential role in the pathogenesis of transforming growth factor-beta-induced pulmonary fibrosis. *The Journal of biological chemistry* **287**(50):41991-42000.

Zhou YQ, Zhu Y, Bishop J, Davidson L, Henkelman RM, Bruneau BG and Foster FS (2005) Abnormal cardiac inflow patterns during postnatal development in a mouse model of Holt-Oram syndrome. *American journal of physiology Heart and circulatory physiology* **289**(3):H992-H1001.

Zhu X, Stergiopoulos K and Wu S (2009) Risk of hypertension and renal dysfunction with an angiogenesis inhibitor sunitinib: systematic review and meta-analysis. *Acta oncologica* **48**(1):9-17.